PERFORMANCE OPTIMIZATION OF A THERMOSYPHON FLAT PLATE SOLAR WATER HEATER

NG'ETHE JOHN

MASTER OF SCIENCE
(Mechanical Engineering)

JOMO KENYATTA UNIVERSITY OF AGRICULTURE AND TECHNOLOGY

2019

Performance Optimization of a Thermosyphon Flat Plate Solar Water Heater

Ng'ethe John

A thesis submitted in partial fulfillment for the degree of Master of Science in Mechanical Engineering in the Jomo Kenyatta University of Agriculture and Technology

2019

DECLARATION

This thesis is my original work and has not been presented for a degree in any other university.

Signature ..... Date .....

Ng'ethe John

This thesis has been submitted for examination with our approval as the University Supervisors:

Signature ..... Date .....

Dr. (Eng) Hiram M. Ndiritu

JKUAT, Kenya

Signature ..... Date .....

Dr. Stephen Wanjii

JKUAT, Kenya

DEDICATION

I dedicate this work to my loving family. A special feeling of gratitude to my wife Christabel, our daughter, Sofie and son, Flynn. They have been a source of inspiration to work harder in this research. Above all I dedicate this work to God Almighty for the gift of good health and peace of mind which were crucial in completing this research.

ACKNOWLEDGEMENTS

I thank God the Almighty, first and foremost, for giving me the opportunity to undertake this research successfully. I sincerely thank my supervisors Dr. Eng. Hiram Ndiritu and Dr. Stephen Wanjii who guided and supported me throughout this research period. I am also very grateful to the Mr. David Chitayi, Mr. Erick Waiyaki, Mr. Wahinya, Mr. Muigai and other staff of J.K.U.A.T. Engineering Workshops for their guidance and immense help during fabrication and testing process.

Finally, I want to extend my gratitude to the staff members, technicians and technologists of the department of mechanical engineering and Engineering workshops (JKUAT) for their assistance during this period.

TABLE OF CONTENTS

DECLARATION ii

DEDICATION iii

ACKNOWLEDGEMENTS iv

LIST OF TABLES x

LIST OF FIGURES xi

ABBREVIATIONS xiv

NOMENCLATURE xv

ABSTRACT xvii

CHAPTER ONE 1

INTRODUCTION 1

1.1 Background 1

1.1.1 Energy Source Used to Heat Water 1

1.1.2 Energy Scenario in Kenya 3

1.2 Problem Statement 5

1.3 Objectives 7

1.4 Justification 7

1.5 Thesis Outline 8

CHAPTER TWO **10**

LITERATURE REVIEW **10**

2.1 Overview 10

2.2 Solar Energy 10

2.3 Distribution of Solar Energy in Juja Area Kenya 11

2.4 Configurations of Solar Water Heaters 12

2.4.1 Flat Plate Solar Water Heater 12

2.4.2 Evacuated Tube Solar Water Heater 15

2.5 Review of Research Studies Done on Performance of FPSWH 17

2.5.1 Heat Flow in Solar Water Heaters 17

2.5.2 Reduction of Convectional Heat Loss 18

2.5.3 Reduction of Radiative Heat Loss 20

2.5.4 Reduction of Conductive Heat Loss 22

2.5.5 Improvement of Rate of Heat Transfer 22

2.6 Summary of Gaps 25

CHAPTER THREE **26**

EXPERIMENTAL DESIGN AND METHODOLOGY **26**

3.1 Introduction 26

3.2 Design Parameters for the Water Heater 26

3.2.1 Determination of Top Heat Loss Coefficient 28

3.2.2 Determination of Bottom Heat Loss Coefficient 35
3.2.3 Determination of Side Heat Loss Coefficient 36
3.2.4 Determination of Effective Design Absorber Plate Area 36
3.2.4.1 Performance Analysis Equations 38
3.2.5 Determination of Optimal V-groove Angle 39
3.2.6 Determination of Optimal Air Gap 41
3.2.7 Determination of Effective Tilt Angle 42
3.2.8 Determination of Effective Number of Glazing 44
3.2.9 Determination of Critical Pressure of Partial Air Evacuation . 45
3.3 Fabrication of the FPSWH 46
3.3.1 Fabrication of The Absorber Plate 47
3.3.2 Housing. 48
3.3.3 Insulation. 48
3.3.4 Glazing. 49
3.3.5 Stratification Tank 49
3.3.6 Piping 50
3.3.7 Support Frame 50
3.4 Experimental Set-Up 50
3.5 Experimental Procedure 52
3.5.1 Procedure for Varying Number of Glazing Glass 54
3.5.2 Procedure for Varying the Air Gap 54

3.5.3 Procedure for Varying The Air Pressure Inside the FPSWH . 54
3.5.4 Procedure for Varying the Tilt Angle 54
3.6 Uncertainty Analysis 54
3.6.1 Instrumental Uncertainty 55
3.6.2 Experimental Uncertainty 58

CHAPTER FOUR **61**

RESULTS AND DISCUSSION **61**

4.1 Background 61
4.1.1 Influence of Flow Rates on Performance 61
4.1.2 Influence of Number of Glazing on Performance 65
4.1.3 Influence of Varying Air Pressure Inside the FPSWH 67
4.1.4 Influence of Tilt Angles on Performance 70
4.1.5 Influence of Air Gap on Performance 71
4.1.6 Effects of Outer Glass Temperatures on FPSWH Efficiency . . 74
4.2 Optimization of FPSWH 76
4.3 Comparison of performance of optimized FPSWH to the Contemporary SWHs in the Market 80

CHAPTER FIVE **82**

CONCLUSION AND RECOMMENDATIONS **82**

5.1 CONCLUSION 82

5.2 RECCOMMENDATIONS 83

REFERENCES **85**

LIST OF TABLES

Table 3.1: Critical angle of inclination depending on aspect ratio 32

Table 3.2: Design parameters for calculation of A_{ap} 37

Table 3.3: Designed parameters 38

Table 3.4: Materials commonly used on absorber plate 47

Table 3.5: Standard Deviation of thermal efficiencies of FPSWH 59

Table 3.6: Standard Deviation of experimental parametric values 59

Table 4.1: Summary of parameters that gave high efficiency 78

Table 1: Materials used for FPSWH fabrication 104

Table 2: Design parameters for calculation of A_{ap} 105

LIST OF FIGURES

Figure 1.1: Insolation intensity distribution in Kenya 4

Figure 1.2: Main heat losses and setbacks of conventional FPSWH 6

Figure 2.1: Components of a Flat Plate Solar Water Heater [51] 13

Figure 2.2: FPSWH connected to storage tank in thermosyphonic flow [51] 14

Figure 2.3: Evacuated Tube Solar Water Heater on roof top in China [54] 15

Figure 2.4: Cross-sectional view of Evacuated Tube Solar Water Heater [54] 16

Figure 2.5: Solar radiation absorption and heat-loss in FPSWH [62] . . . 17

Figure 2.6: Solar radiation absorption and heat-loss in FPSWH [63] . . . 18

Figure 2.7: ETFE film in a flat plate solar collector [64] 19

Figure 2.8: An evacuated flat plate solar collector [65] 20

Figure 2.9: Testing a FPSWH with Aero profile wings on the sides [67] . 21

Figure 2.10: Flat plate and v-grooved absorber plate air heaters [72] . . . 23

Figure 2.11: Diagram showing point of sun ray strike and shading portion [74] 24

Figure 3.1: V-groove angle θ 30

Figure 3.2: Diagram showing point of sun ray strike and shading portion [74] 39

Figure 3.3: Graph showing optimal V groove angle at $\phi = 60^0$ 40

Figure 3.4: Graph showing optimal air gap 41

Figure 3.5: Illustration of solar angles [93] 42

Figure 3.6: Graph of Optimal tilt angle for FPSWH in Juja 43

Figure 3.7: Graph of Optimal number of glazing for a FPSWH 44

Figure 3.8: Graph of critical evacuating pressure for a FPSWH 46

Figure 3.9: Inventor Autodesk illustration of the designed absorber plate 47

Figure 3.10: Absorber plate showing water channels and the V-Groove plate 48

Figure 3.11: Schematic illustration of the designed housing 49

Figure 3.12: Illustration of fiber glass and lower air gap insulation 50

Figure 3.13: Cross-Sectional view of the storage tank and insulation . . . 51

Figure 3.14:A sketch of experimental set up 52

Figure 3.15: Preliminary experimental set-up for the FPSWH 53

Figure 4.1: Temperatures versus time for 5 Litres/Hour flow rates 62

Figure 4.2: Efficiency versus time for 5 Litres/Hour flow rates 63

Figure 4.3: Temperatures versus time for varying flow rates 64

Figure 4.4: Efficiency at varying Volumetric Flow Rates 64

Figure 4.5: Influence of Volumetric Flow Rate on collector efficiency . . . 65

Figure 4.6: Temperatures versus time for varying number of glazing . . . 66

Figure 4.7: Efficiencies of different glazing against Time 67

Figure 4.8: Temperatures for un-evacuated and partially evacuated FP-SWH 68

Figure 4.9: Efficiency for both un-evacuated and evacuated FPSWH . . . 69

Figure 4.10: Temperature curves for different tilt angles 70

Figure 4.11: Effect of tilt angles on efficiency 71

Figure 4.12: Temperatures attained at different air gaps 72

Figure 4.13: Efficiency graph summarizing effects of air gaps 73

Figure 4.14: Glazing temperatures and efficiency curves for a SG-FPSWH at 1 atmosphere 75

Figure 4.15: Glazing temperatures versus efficiency for a SG-FPSWH at 1 atmosphere 76

Figure 4.16: Glazing temperatures and efficiency versus time for a SG-FPSWH partially evacuated at 2500 pa 77

Figure 4.17: Temperatures on an optimized FPSWH 78

Figure 4.18: Efficiency of the optimized FPSWH 79

Figure 4.19: Performance of an optimized FPSWH compared to other SWHs 80

Figure 1: Data Logger 110

Figure 2: Plain welded tip K-Type thermocouple 110

Figure 3: K-Type thermocouple with 6mm threaded probe 111

Figure 4: K-Type thermocouple with 100mm screwed probe 111

Figure 5: Infra red thermometer used to measure casing temperatures 112

Figure 6: Digital Irradiance Meter used for this experiment 112

Figure 7: 0.1-3.0L/Min Hall Effect water flow rate sensor with LCD read out 113

ABBREVIATIONS

SWH	Solar water heater
ETSWH	Evacuated tube solar water heater
FPSWH	Flat plate solar water heater
SG-FPSWH	Single glazed flat plate solar water heater
DG-SWH	Double glazed flat plate solar water heater

SYMBOLS

A_{ap}	Absorber plate area
α	Solar Absorptance
β	Tilt angle
β_t	Thermal expansion coefficient of gases in K^{-1}
δ	Declination angle of the earth at a particular time of the year
F_{12}	Shape factor
ϕ	Insolation's angle of incidence
φ	Latitude or inclination angle of a particular location on earth's surface
γ	Azimuth angle
h_w	Convective heat transfer coefficient from outer glass cover of the FPSWH to the atmosphere in $Watts/m^2$
h_{ap-g}	Convective heat transfer coefficient from absorber plate to the glass cover of the FPSWH in $Watts/m^2$
h_{g1-g2}	Convective heat transfer coefficient from first glass cover to the second glass cover of a double glazed FPSWH in $Watts/m^2$
λ	Side shading factor
θ_z	Zenith angle
ρ	Density
$\dot{m}$	Mass flow rate, in grams/sec
ϵ	Emissivity
Δ	Change
η	Efficiency
σ	Stefan Boltzmann constant
Q	Heat
C_w	Specific heat capacity of water
I	Incident insolation
k	Thermal conductivity in k/m

L	Distance between the absorber plate and the glass cover for a single glazed FPSWH in metres
L_1	Distance between the absorber plate and the first glass cover for a double glazed FPSWH in metres
L_2	Distance between the first glass cover and the second glass cover for a double glazed FPSWH in metres
L_3	Length of FPSWH in metres
L_4	Width of FPSWH in metres
N	Number
τ	Glazing transmittance
T_{ap}	Temperature of absorber plate in K
T_{out}	Temperature of water at the outlet of FPSWH in K
T_{in}	Temperature of at the inlet of FPSWH in K
T_a	Amient temperature within the vicinity of the FPSWH in K
T_g	Temperature of cover glass for a single glazed FPSWH in K
T_{g1}	Temperature of first cover glass for a double glazed FPSWH in K
T_{g2}	Temperature of second cover glass for a double glazed FPSWH in K
t_g	Thickness of cover glass in metres
ω	Hour angle

Subscripts

a	Atmospheric for temperatures
ap	Absorber plate
c	Critical
g	Glass
L	Air gap
o	Atmospheric for pressure

ABSTRACT

Conventional flat plate solar water heaters which are widely used to convert solar energy to thermal energy and transfer that heat to circulating water have low efficiency of less than 60%. In addition, they require high manufacturing cost, they utilize expensive copper material and selective surface coatings.

Flat plate solar water heater (FPSWH) lose 30-50% of the total harnessed heat through the top glazing glass via convection, radiation and conduction. Convection heat loss accounts for the bigger percentage of this heat loss due to the presence of air in between the absorber plate and the top glass. Radiative heat loss is a function of emissivity and shape factor of the absorber plate. In addition, the total heat loss is enhanced by poor heat transfer between the circulating water and the absorber plate. Poor heat transfer is contributed by tube pitch, type of bond between the tubes and the absorber plate as well as the thickness of the absorber plate.

The aim of this research was to reduce the heat losses in flat plate solar water heaters through re-design and material selection. Hence a partially evacuated, V-grooved corrugated collector was fabricated and its performance tested under various conditions, air gaps, different number of glazing, flow rates etc in order to obtain its optimal performance. Its absorber plate was made of galvanized iron with v-groove channels of 70^0 and painted black using carbon black matte paint. Optimizing performance of Flat Plate Solar Water Heater,(FPSWH), was realized through a v-groove redesign and partial evacuation of air at 300-2500 pa. The new design improved heat transfer ability, reduced heat loss and eliminated need for laser beam welding but still maintained the merits of FPSWH of being cheap, easy to fabricate and easy to maintain. With partial evacuation of air at 2.5×10^3 pa, efficiency of 80-85% and operating temperatures of 80-100^0C were obtained.

The findings of this research work are applicable in FPSWH manufacturing industry and Jua Kali sector whereby efficient and affordable FPSWH can be produced and availed to households, institutions and industries. Since optimized FPSWH

have high efficiency, their application can go beyond heating water to producing processing steam for businesses and industries.

CHAPTER ONE

INTRODUCTION

1.1 Background

Global energy demand is increasing continuously despite negative effect of green house gases on the environment mainly from usage of fossil fuels [1]. This is attributed to rise in population, economic growth of developing countries as well as technological advances which create more demand for power [2]. Coal and Petroleum are currently the main sources of energy leading to the concerns of further environmental degradation and future exhaustion of fossil fuel resources [3, 4], though some researchers think otherwise [5]. Faced with a reality of global warming and little or no fuel in future, scientists have come up with novel ways of conserving available energy resources through use of lean manufacturing, use of LED light bulbs, design of more efficient engines as well as harnessing renewable energy sources [4].

Solar energy is very attractive worldwide due to its availability and ease of conversion into either thermal, electrical or biomass forms of energy [6]. Many households prefer solar water heaters due to high conversion efficiency associated with solar energy to thermal energy coupled with high demand of hot water in households [7]. The available FPSWH in the market rarely exceed water outlet temperatures of 65^0C and efficiency of 60% [8–10]. Their main setback being high coefficient of convection heat transfer from the absorber plate to the glazing glass [11–14].

1.1.1 Energy Source Used to Heat Water

Hot water is required in households for cooking, washing and most importantly for bathing/showering. The more the people in a household the more the energy required to heat water which is mostly obtained from burning fossil fuels, biomass or electricity and accounts up to $\frac{1}{3}$ of the total energy use in a household [15]. It is difficult to predict the hot water demand due to its high dependence on end-user behavior, but for bathing and showering, a lot of research indicate that it accounts

for upto 50% of the total domestic hot water demand [16]. In developed countries such as USA, Europe, Russia natural gas dominate the energy used to heat water by 52% due to its low cost with electricity accounting for 25% [17]. In Sub-Sahara Africa, the main source of energy for water heating is biomass (firewood, charcoal, agricultural waste) which account for 60-70% [18–20]. In urban areas like Nairobi, demand for hot water stands at 70% for bathing/showering, 20% for cooking and 10% for drinking [21], while the commonly used energy sources for heating water in Nairobi stands at 37% electricity and 24% LPG since they have fast heating capability despite their high cost per unit [21]. Demand for hot water is expected to increase in future as many nations (such as India, China and most of African Nations) develop economically [22]. Prior research has shown that demand for hot water does not necessarily depend on increase in number of people in a household but on economical ability of such a household [15].

Hotels, learning institution and hospitals all require more hot water especially for use in showers, washing and cooking which account for 60% of their energy use [15, 17]. Most hotels and game lodges in Kenya use instant hot water shower heads to provide bathing water to their guests. This creates peak demand on national electric grid hence Solar Water Heating (SWH) Regulations 2012 were put into place. These regulations state that all business premises and institutions using more than 100 litres of hot water per day should install a SWH [21, 23]. These regulations were expected to be effective from 2018, implying that nearly all institutions of learning, hotels and hospitals will install SWH systems. Hotels and institutions have an advantage over households since they have reduced payback time of 4-5 years [24]. Hotels which have installed SWH and have hot water consumption of 10×10^3 to 25×10^3 litres per day have 49-70% of their total hot water needs covered by SWH [25].

SWH has a bright future in Kenya due to the following favorable conditions; high insolation intensities since kenya receives 4-7KW/h/day [26], high cost of electric-

ity at USD 0.197/Kwh compared to its neighbors Ethiopia at USD 0.030/Kwh and Tanzania at USD 0.09/Kwh [27] and enforcement of Government Policies such as SWH Regulations 2012 as enshrined under The Energy Act 2006 [23]. These regulations were developed to enhance uptake of solar energy and reduce reliance on fossil fuel and wood biomass. If households, restaurants and institutions utilize solar energy for heating of water, a reduction in deforestation and carbon foot print would be realized. In addition, SWH market is expected to grow at 6.78-8.0% annually worldwide from 2017 to 2021 [28]

1.1.2 Energy Scenario in Kenya

Domestic water heating in Kenya can be categorized into Urban and Rural residents. Urban households use electric kettles, instant hot water shower heads, LPG cookers, kerosene stoves and charcoal stoves for heating water depending on water usage as well as economic ability [21]. Rural residents use charcoal and firewood since most of them are off the the national power grid [20]. Kenya receives an estimated solar insolation of 4-6 kWh/m^2 with 5-7 peak hours [26]. As the map in Figure1.1.2 shows, most of the country receives solar insolation above 4-7 kWh/m^2 per day. On the contrary, most Kenyan households prefer converting it into electricity using PV panels rather than thermal energy . This is witnessed by installation of over 600,000 PV related solar home systems as compared to just 40,000 SWH systems since 1990 to 2010 [21, 29]. The main drive being low penetration of electricity into rural area hence many households install PV systems for lighting [20]. Kenya has high unemployment level of over 45% coupled with high poverty level where 40% of Kenyans live below USD 1.9 per day [30]. In addition high costs of power per kWh has left 69% of Kenyans relying on biomass for fuel [30], a factor that has contributed to the present annual deforestation rate of 0.34-0.50% [31] and destruction of water catchment areas leading to reduction in river volumes and hydro-power. Furthermore, burning of biomass is not only harmful to the people as they inhale CO and CO_2 gases but also contributes to release of greenhouse gases

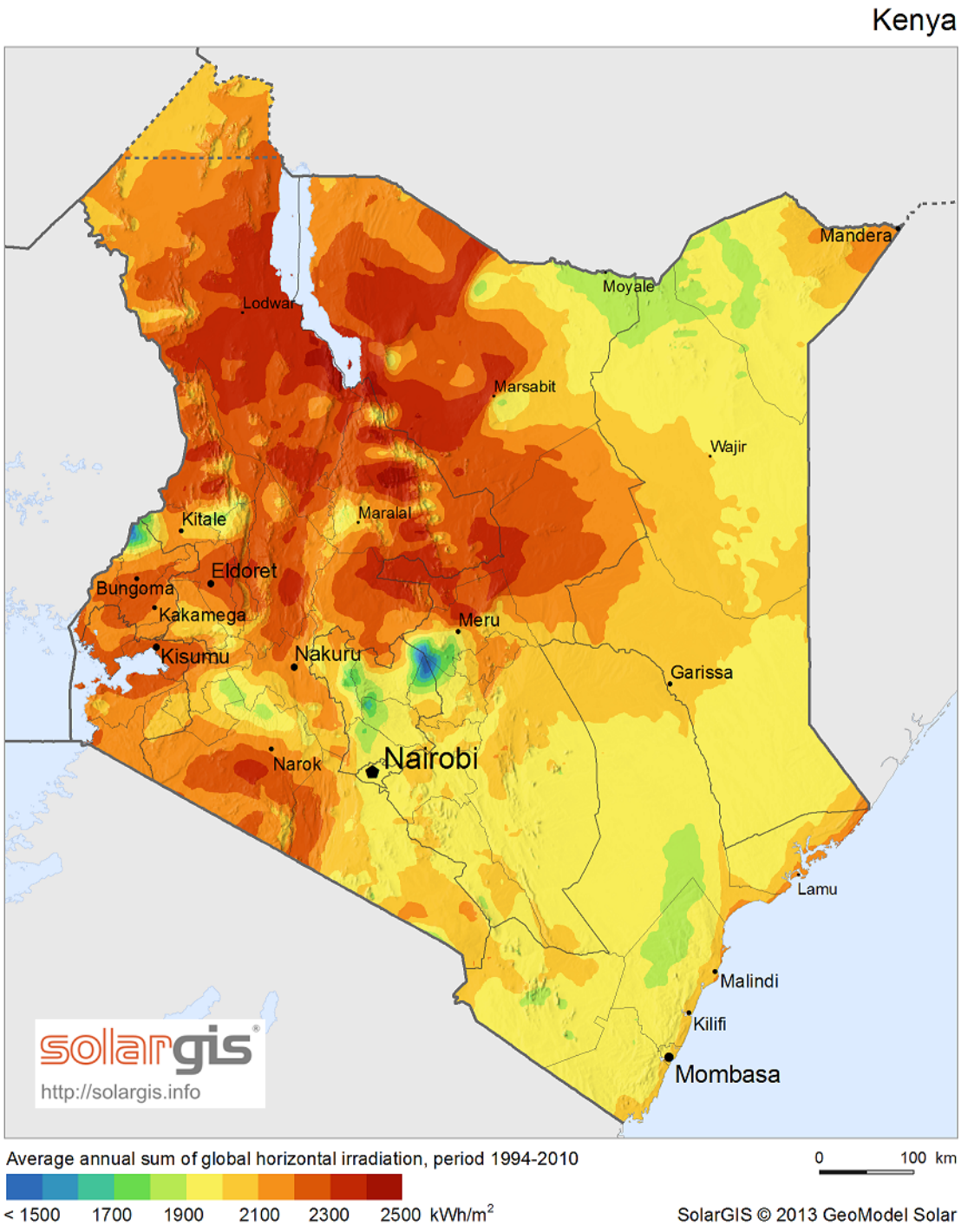

Figure 1.1: Insolation intensity distribution in Kenya

to the atmosphere [19]. According to Kenya National Bureau of Statistics forecasts, Kenyan population has an annual growth rate of 2.5% and annual economic growth rate of 5-7% implying that demand for energy is going to increase in future [30]. More so, by using electricity to heat water puts a strain on the power infrastructure, especially in the morning and the evening since it creates power demand peaks that require back up generators most of which use fossil fuels [21]. It is estimated that Kenya uses 2,246 MWh of electricity for water heating daily [32]. Solar energy is a perfect candidate for replacing fossil fuels and this calls for more efficient solar water heaters.

1.2 Problem Statement

Solar water heater systems are an environmental friendly way of providing domestic hot water [33]. The flat plate solar water heaters (FPSWH) which are cheaper than Evacuated Tube Solar Water Heaters (ETSWH) have very low conversion efficiency of 60% or less. This is because FPSWH lose 18% of heat through convection, 13% through radiation and 9% through conduction [34]. Prior research has shown that less efficient SWH systems take longer to break even and realize longer carbon pay back time due to the reduced energy harnessed from the sun [25, 35, 36]. Subjecting a FPSWH of initial cost of USD 1700 to Kenyan daily insolation of 4-7 KWh/m^2 results in a payback of 6 years if the FPSWH operates at an efficiency of 40% [37]. A FPSWH operating at 80% efficiency will pay back initial investment in 3 years for when costing is compared between solar water heating to electric water heating [35, 36]. Life-cycle assessment approach considers energy and carbon payback time as an environmental performance of SWH systems [33].

The useful energy obtained from a FPSWH depends on thermal and optical losses occurring within it. Thus, the performance of the entire solar water heater can be optimized if the losses are reduced to a minimum. The air contained between glass cover and absorber plate, as illustrated by Figure 1.2, transfers heat via convection and conduction from the absorber plate to the glass cover and consequently the cover

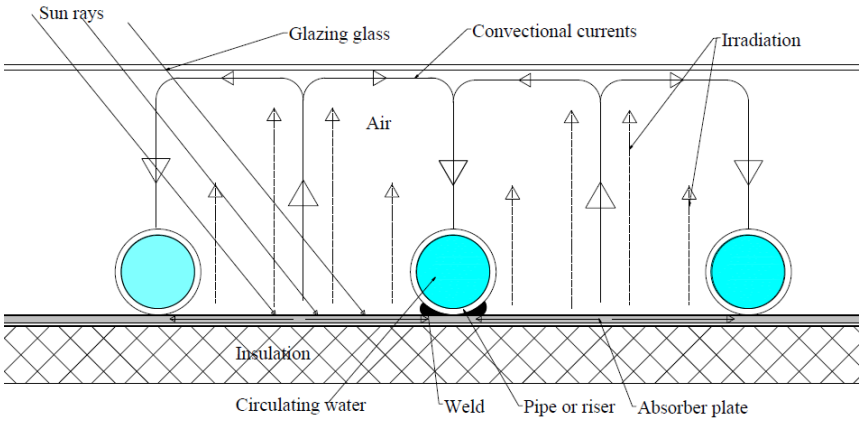

Figure 1.2: Main heat losses and setbacks of conventional FPSWH

loses heat to the environment [38, 39]. Radiative heat loses are are contributed by sections of the absorber plate that lie in between the water tubes where temperatures are higher than those near the water tubes [40]. This is because the black painted surfaces located away from the water tubes have lower temperature gradients to facilitate effective conduction, hence they radiate heat away as long wave infrared radiation. In addition, both types of heat losses are enhanced by low heat transfer rates from the absorber plate to the water in the tubes depending on the type of bonding method used. Heat travels through the absorber plate to the water tube via joining welds, therefore a higher heat transfer rate would require the absorber plate be as thick as possible or water tubes be close together [41]. However the unit cost of copper is high, USD 6/Kg compared to aluminum at USD 2.15/Kg or galvanized iron at USD 0.92/Kg, and therefore plates of 0.5mm thickness or less and tube pitch distances of 80-100 mm are commonly used in fabrication of FPSWH thus compromising on heat transfer rate. Low heat removal factor of the FPSWH makes absorber plate hotter increasing radiative and convective heat losses [42]. In addition, though solar water heating is very attractive and can save household's power bills by almost 1/3, the initial installation cost is quite high, from USD 1700 to USD 3000 [21]. Study done in India on viability of SWH systems showed that

only a few of high income families owned SWH [15]. There is a need to design and fabricate a reliable, efficient and affordable FPSWH.

1.3 Objectives

The main objective of this research is to design, develop and optimize the performance of thermosyphon flat plate solar water heater by reducing heat loss. This was to be achieved via the following specific objectives;

(i) To design a model flat plate solar heater for domestic heating application.

(ii) Test of performance of the flat plate solar water heater based on variation of flow parameters such as pressure of air inside the FPSWH and water flow rates.

(iii) To test the influence of variation in geometric parameters such as number of glazing glass, air gap and tilt angle on water outlet temperatures and FPSWH efficiency.

1.4 Justification

Cleaner and affordable sources of energy are paramount if a nation needs to expand economically and still conserve environment by producing less greenhouse gases. Solar energy satisfies these two needs although it has low energy density of (80-1367w/m^2). Therefore, thermal conversion devices such as FPSWHs need to have high efficiency if they are to tap a significant amount of energy from solar radiation. High efficiency of FPSWHs could expand their applications from domestic water heating to industrial use for production of low grade steam. According to research done in Thika-Nairobi area by Nahashon Wanyonyi (2015) [26], most Kenyan regions receive abundant solar insolation with an average annual daily insolation of 4-7 kWh/m^2/day with a very low variation coefficient of less than 1%. Although the beam variation is much reduced in the month of June to August, the rest of the

year has a good clearness index of greater than 0.4 indicating that the available insolation is able to sustain a smooth running of thermal systems.

Optimization of performance of FPSWH systems have been carried out extensively by researchers worldwide. It was proved that an evacuated FPSWH out-performs evacuated tube solar water heaters (ETSWH) and could be used to provide process steam for industries of up to 6 bars at 150^0C [43]. Incorporation of cheaper materials such as aluminum, galvanized steel, stainless steel and semi-selective paint in place of copper and selective surface coatings has enabled construction of cheaper and efficient FPSWH systems [42, 44].

In addition, manufacture of FPSWH within the country they are sold in creates both jobs and economic growth. This research work has looked at design of FPSWH and how various flow conditions and geometric parameters affect performance. The results of this research work prove that the FPSWH can be optimized to achieve temperatures above 80^0C and efficiencies above 80%.

1.5 Thesis Outline

This thesis has five chapters described as follows; The current chapter is introduction which explores importance of this research and constitutes formulation of problem statement, objectives of the research work and justification of fulfilling those objectives. The second chapter is literature review. This chapter explores other studies and researches done on improvement and optimization of FPSWH systems, their successes and the gaps that were left. Different SWH systems and setbacks of FPSWH were studied in order to understand the opportunities available for improvements. Journals on convectional, radiative and conductive heat transfer in FPSWH and inclined rectangular enclosures were extensively reviewed and relevant equations adopted or modified for design purposes.

The third chapter is methodology in which the design equations and drawings are presented. The setup and methods used for testing and collection of data are presented as well as the equipment used. This chapter also includes analysis equations

and error analysis (uncertainty) for both measurement equipment and experiment. The fourth chapter is results and discussion where the collected data is analyzed, presented and discussed. The fifth chapter is conclusion and recommendations. This chapter summaries the whole thesis and looks how the objectives were achieved and recommends what could be done in future.

CHAPTER TWO

LITERATURE REVIEW

2.1 Overview

Many studies and theories have been proposed and conducted to explain how to convert solar energy efficiently and still keep conversion cost low. The available literature covers many types of solar collectors, this review is going to concentrate on conversion of solar radiation into thermal energy for domestic water heating. The focus of this study is to understand the nature of solar energy, its distribution in Juja, Kenya and how best to capture it for heating water using Flat Plate Solar Water Heaters (FPSWH). Previous researches on different flat plate solar waters heaters have been reviewed and their contributions to the present work captured and discussed briefly.

2.2 Solar Energy

Solar energy is readily available everywhere either as beam or diffuse radiation. Its appeal emanates from the many ways it might be converted to other forms of energy in addition to its availability. Its use also depends on its local distribution as well as efficiency in the conversion process. All these factors are dependent on the nature of solar energy thus making it important to understand it first.

Solar energy is electromagnetic radiation in a wavelength range of 0.25-3.0 μ. The earth's outer atmosphere receives a Solar Constant, G_{sc}, of 1367W/m^2 and is defined as energy from the sun per unit time received on an unit area of a surface perpendicular to the direction of propagation of the radiation at mean earth distance outside the atmosphere [45]. This is, Solar Constant, the total energy in the solar spectrum but when broken down to components based on wavelengths, it is composed of 6.4% UV, 48% visible light and 45.6% infrared as adopted by World Radiation Centre (WRC). Extraterrestrial Solar Constant varies from 1410w/m^2 in January to 1320w/m^2 in June and July due to sunspots(temporary dark, cooler

areas on the surface of the sun caused by concentrations of magnetic field flux that inhibit convection). The average solar constant has a variation of 1.3-1.5kW/m^2 since 1976 to 2010 [46]. This explains why solar energy is not the major source of worlds energy as it is a low grade heat source, compared to fossil fuels and nuclear which give more energy from a very small amount.

On the earth's surface, two types of radiation reach the surface, beam and diffuse. Beam radiation is insolation received from the sun without being scattered by the molecules and particulate matter in the atmosphere. Diffuse radiation, which accounts for 40-52% of worlds irradiation, is insolation received from the sun after its direction has been changed by scattering by the atmosphere. Cloud cover and air pollution by dust and smoke play a major role in distorting direction of beam as well as altering wavelength distribution. 13% of Solar Constant is reflected and absorbed by the atmosphere, 10% or more is scattered by the atmosphere and 75% or less is received as beam radiation [47]. In summary, the beam radiation on earth's surface is rarely above 1100 W/m^2 and is received mostly by countries which lie along the equator and within the tropics. These are the areas which flat plate solar water heaters function with good efficiencies while evacuated tube solar water heaters would work efficiently in both tropical and temperate regions. Other factors such as latitude, topography, surface inclination and shading by tall objects affect the amount of insolation received on a surface. Flat plate and evacuated solar water heaters are reviewed below.

2.3 Distribution of Solar Energy in Juja Area Kenya

Oloo et al. [48] developed a model of monthly and annual solar energy distribution in Kenya. They processed publicly available meteorological data and combined the same with estimated global radiation surfaces which were modelled within a GIS environment. From the study, they estimated that approximately 70% of the land area of Kenya has an annual solar energy potential above 5 kWh/m^2/day. Specifically 32.4% of the land has an average annual solar potential ranging between

5.0-5.5 kWh/m^2/day. Additionally, approximately 26.5% of the countrys land area has the average annual solar energy potential in the range of 5.5-6.0 kWh/m^2/day. Further still, above 10.8% of the land area in Kenya has the potential of receiving more than 6 kWh/m^2/day of solar energy. The areas which were estimated to receive solar radiation above 6 kWh/m^2/day were mainly located in the high altitude ridges of rift valley and also in the regions to the east of Lake Turkana and specifically around Marsabit.

Wanyonyi et al. [26] validated the above model by experimentally conducting studies on solar radiation distribution in Juja area and from the findings and results, it is clear that Kenya receives plenty of beam radiation making it very economical to convert solar energy into thermal energy. The findings concluded that Juja and Kenya in general receives annual daily insolation range from 4-6 kWh/m^2/day and the average monthly daily insolation range from 3-7 kWh/m^2/day with intensity of 1000-1100W/m^2 .

2.4 Configurations of Solar Water Heaters

Solar water heating is a process where solar radiation is harnessed and converted into heat by an appropriate device to heat water for various purposes. The harnessing device can take various shapes but the principle of operation is always the same; a black surface is used to absorb solar radiation and pass the heat to the adjacent circulating fluid. There are two most common types of solar water heaters for domestic water heating; flat plate and evacuated tube solar water heaters.

2.4.1 Flat Plate Solar Water Heater

FPSWH have been in existence for the last 50 years without any real significant changes in their design and operational principles [49]. The first efficient and economical FPSWH were made by William Bailey and in 1909 he began selling solar water heaters under the brand name "'Day and Night". They were provided with an insulated indoor water storage tank, supplied by a separate a south facing solar

collector located outside the house. The collector consisted of a coiled pipe inside a glass covered box which had to be mounted below the storage tank. This allowed the hot water to circulate from the collector to the storage tank by natural convection [50]. The impact of his innovation was to open up FPSWH to different design innovations in order to achieve better performance. A FPSWH consists of light transmitting glazing material and a black surface responsible for absorbing solar energy and converting it to heat which is removed by circulating fluid contained in channels adjacent to the black surface. An insulation layer is positioned below the black surface (absorber plate) to reduce heat loss via conduction. Figure 2.1 illustrates basic components of a FPSWH. The glazing material is normally glass and it allows shortwave solar radiation to pass through into FPSWH but is opaque to long-wave infrared radiation from FPSWH, a phenomenon called greenhouse effect.

FPSWH are further classified into two major groups; active and passive. Ac-

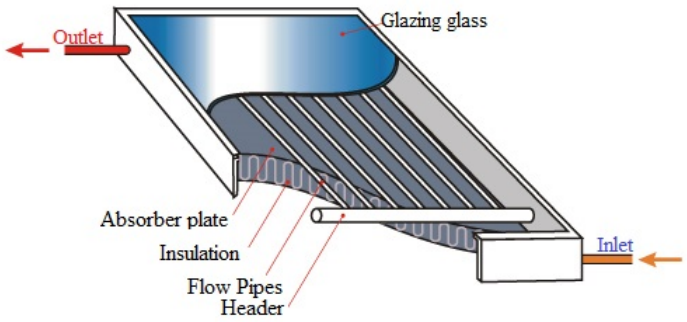

Figure 2.1: **Components of a Flat Plate Solar Water Heater [51]**

tive FPSWH uses a pump to actively circulate water through the system. Passive FPSWH use thermosyphonic flow where hot water becomes less dense and rises above the colder, denser water hence creating net pressure, a process referred to as stratification due to buoyancy forces that forces flow of water through the system. Thermosyphonic flow is not uniform since it depends on insolation. It is common to place the cold water tank above the solar collector for passive FPSWH in order

to allow gravity to aid in flow.

Flat plate solar water heaters dominate the market for SWH by 65-80% [52]. This

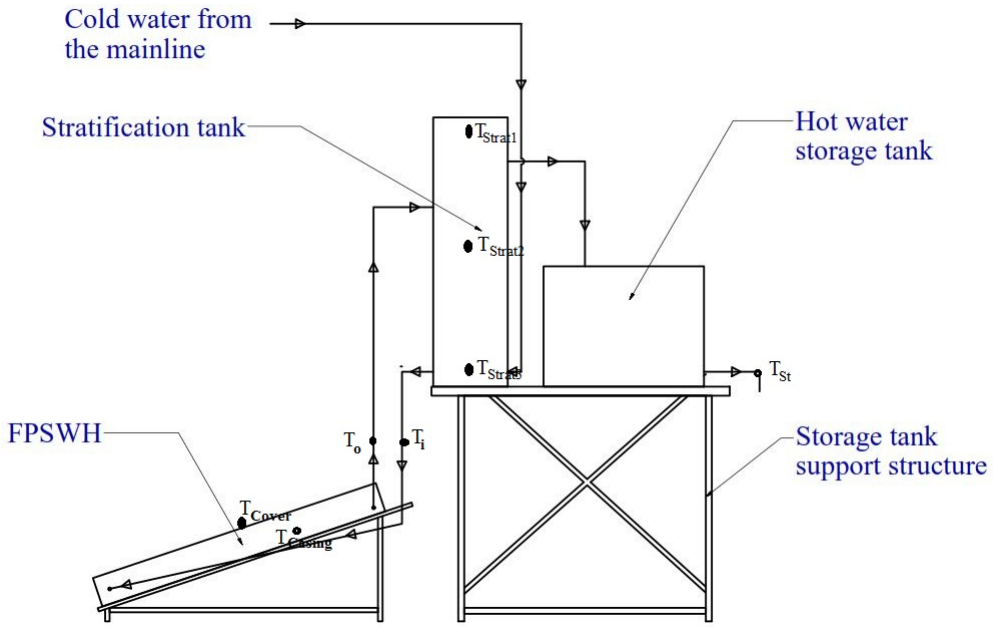

Figure 2.2: FPSWH connected to storage tank in thermosyphonic flow [51]

could be attributed to the merits of FPSWH such as;

(i) Simplicity in construction and low initial & operating cost [53],

(ii) They utilize both beam and diffuse radiation [54],

(iii) FPSWH do not require tracking systems [42].

The main setback of FPSWH is the air present in the space between absorber plate and glass which carries out convectional heat transfer. They also have a solar harnessing aperture of equal area to absorber plate thus experience greater heat losses through radiation [50]. Consequently they rarely heat water above 80^0C and if they do, the efficiency is rarely above 60%.

As a result of low performance, FPSWH have in the recent past lost their market

foothold to evacuated tube solar water heaters (ETSWHs), described below, which are more efficient but expensive [55]. This research is aimed at redesigning a FP-SWH in order to improve its efficiency. A 300litres ETSWH costs USD 150 while a FPSWH of similar capacity costs USD 100-120 [56].

2.4.2 Evacuated Tube Solar Water Heater

Evacuated glass tube solar water heaters (EGTSWHs) are the recent innovation in domestic solar thermal collectors. Figures 2.4.2 and 2.4.2 illustrate how EGTSWH are mounted and their principle of operation respectively. Evacuated tube tech-

Figure 2.3: Evacuated Tube Solar Water Heater on roof top in China [54]

nology was first developed by Quing Hua University in Beijing, China in the early 1980s [57]. But their commercial manufacture begun in 1985. By 1998, EGTSWH from Quing had a dominance of over 70% of the Chinese SWH market. However, soon afterward, the group behind the innovation disbanded and the patent lost legal enforcement thus opening the technology to the rest of the world [57].

EGSWH consist of 12 tubes per solar collector, and are widely marketed as the most efficient. This is because they are able to hold most of the heat they absorb, as the vacuum in them inhibits both conductive and convective heat losses present in FP-SWH. However, the high vacuum sealing present in EGTSWH requires sophisticated thermal and chemical evacuation as well as the complicated matched glass-to-metal

sealing technique necessary to achieve a hermetic high vacuum seal [58]. They also require high level of vacuum, -1000Pa, which can only be sustained by high precision in welding and fabrication. Hence they are less affordable compared to FPSWH and are mainly imported from china [59].

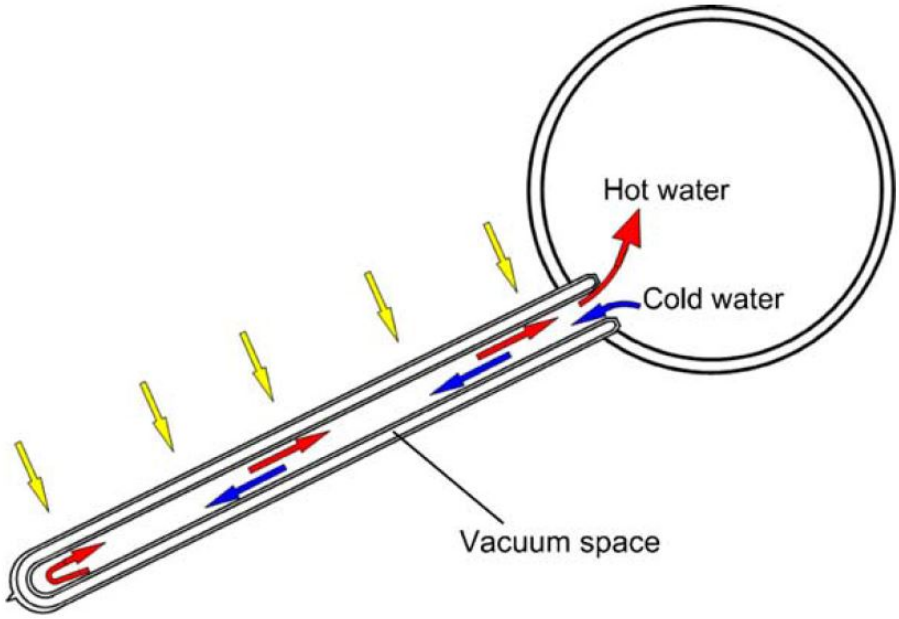

Figure 2.4: Cross-sectional view of Evacuated Tube Solar Water Heater [54]

EGTSWH are manufactured using highly tempered glass called borosilicate glass folded to make two concentric tubes. They are then heated to over 900^oC to evacuate all the air in-between the tubes before sealing in the vacuum space. The inner tube acts as the solar absorbing surface, and is therefore coated with selective absorbing coatings that raise its absorptance for solar radiation (α) to 95% and reduce its infrared emittance (ε) to 5% [60].

In the recent past, many different designs of ETSWH have emerged in the market some incorporating absorber plates and others using low pressure heat pipes. The idea of incorporating vacuum to curb heat loss is adopted in FPSWH for this research

in a bid to improve performance.

2.5 Review of Research Studies Done on Performance of FPSWH

2.5.1 Heat Flow in Solar Water Heaters

Promparn et al. [61] studied performance of FPSWH in Thailand and from their findings, efficiency of FPSWH had an average value of 56.43% and average output temperatures were found to be 68.62^0C. This confirms that FPSWH lose more than 30% of converted energy through various means as portrayed by the Figure 2.5.1. The extent of heat loss are as indicated in Figure 2.5.1, in which radiative and convective losses constitute approximately 35%.

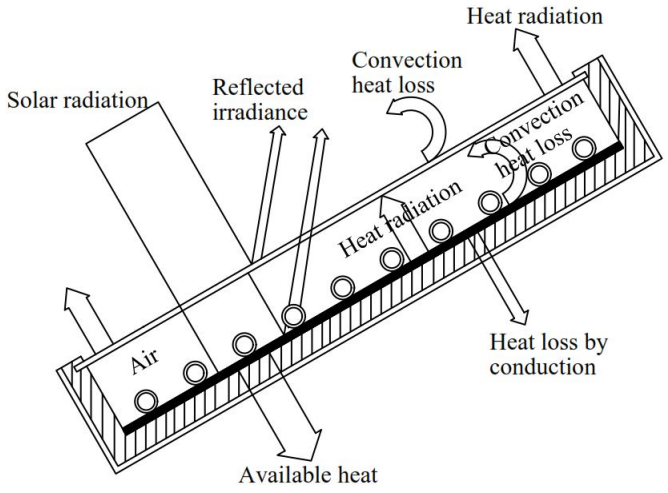

Figure 2.5: Solar radiation absorption and heat-loss in FPSWH [62]

The principal goal of this research work is to redesign the FPSWH so as to reduce the percentage of total heat loss and hence improve performance of FPSWH.
Many researches have endeavored to improve and optimize performance of FPSWH. More often, the improvements done on FPSWH for instance, selective surface electroplating, end up increasing production cost due to high cost of electroplating chemicals. On the other hand, research aimed at reducing production cost compro-

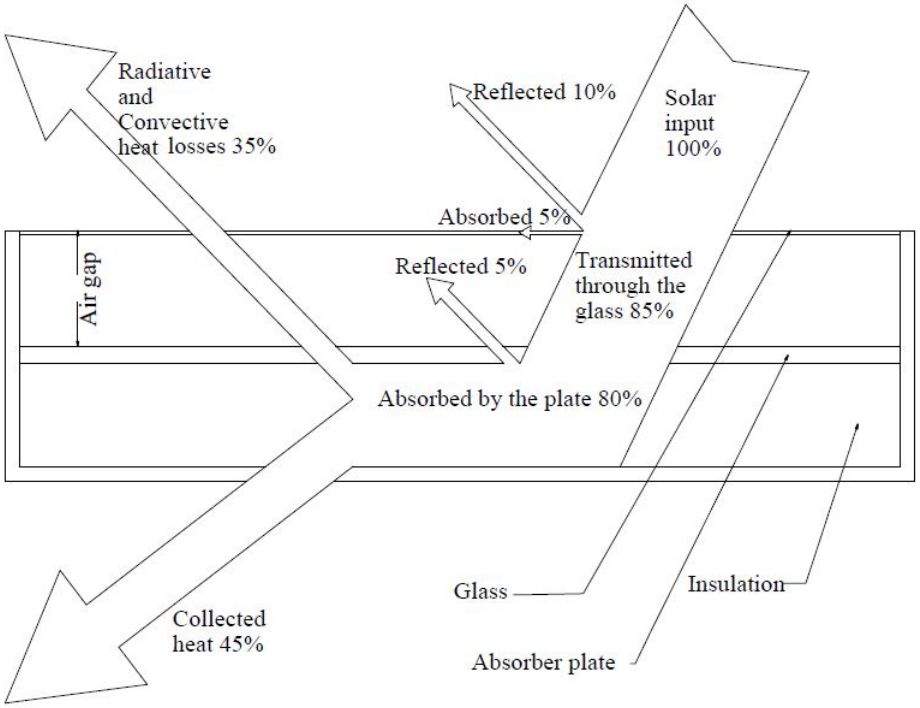

Figure 2.6: Solar radiation absorption and heat-loss in FPSWH [63]

mise efficiency, for instance use of PVC pipes and recycled PET bottles, reduce heat transfer rate due to poor thermal conductivities of plastics. The real challenge to solar energy researcher has been how to optimize performance without making the SWH too expensive. It is only affordability and efficiency of SWH that will encourage people to adopt clean and environment friendly solar energy, although reduction of global warming is an appeal to some. Below is a review of various researchers and authors who have explored different ways of optimizing performance of low cost SWH.

2.5.2 Reduction of Convectional Heat Loss

Beikircher et al. [64] together with BINE Informationsdienst Group suggested that in order to reduce convectional heat loss in the space between the glass cover and the absorber plate can be fitted with a plastic film that will prevent air convective currents from reaching the glass cover. The researchers used Ethylene Tetrafluo-

roethylene (ETFE) that has a transmittance of 0.94, thermal conductivity of 0.238 W/m-k and is stable up to temperatures of 225^0C. This technique confines hot air between the absorber plate and the plastic film thus transforming FPSWH into double glazed design as shown in Figure 2.5.2. It was possible to improve performance of a normal FPSWH from an efficiency of 37% to 50% at temperatures of 100^0C above ambient temperature. However ETFE film cost USD 30 per square meter compared to window glass which cost USD 8 per square metre. They are also prone to cracks, foldings, tearing and UV deterioration. For ETFE films to be straight, they need appropriate clamping mechanism and regular maintenance in order to reduce creasing and folding.

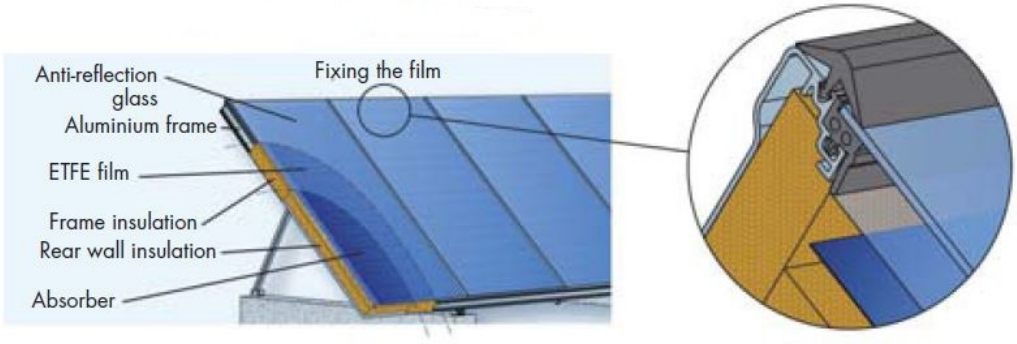

Figure 2.7: ETFE film in a flat plate solar collector [64]

Benz and Beikircher [43] evacuated a FPSWH and partially filled it with krypton at 3000 Pa (absolute pressure). This was aimed at reducing convectional and conductive heat losses. From this experiment, they established that convectional heat losses were completely eliminated at pressures below 1000 Pa. They also found out that at a pressure of 5000 Pa, conduction heat loss was reduced by 32% using argon (compared to using air), by 62% using krypton and by 77% using xenon. The FPSWH produced steam at 130-160^{o}C and steam pressure of (3-7 bars) with an efficiency of 62% at 100^{o}C. Unfortunately, they also did not vary air gap to find out the best air gap for an evacuated FPSWH since they just modified a normal FPSWH by partially evacuating it. Figure 2.8 illustrates a suspended absorber plate

inside an evacuated FPSWH.

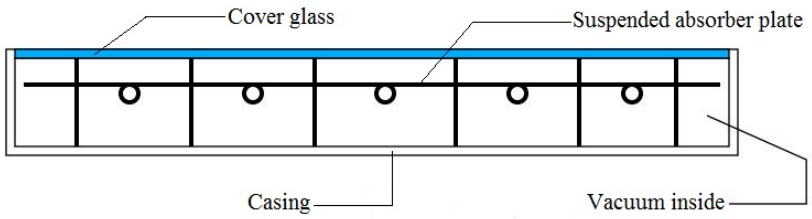

Figure 2.8: An evacuated flat plate solar collector [65]

Eaton and Blum studied use of moderate vacuum inside FPSWH and established an equation for calculating critical pressure below which convectional heat transfer is inhibited for different conditions. They also studied the effect of absorber plate emissivity on evacuated FPSWH and from findings, selective surfaces gave good results with air gaps of 50-75mm [66]. Henshall et al. validated that use of low vacuum pressures of 0.001 Pa reduced overall loss coefficient of a FPSWH to 0.86W/m^{2}k thus sustaining efficiency of 50% at temperatures of 100-120^{0}C. Jaisankar et al. [67] studied the effect of shielding the upper glass cover from wind using aero profile wings (shields) as shown in Figure 2.5.2. Aero profile wings were made up of galvanized iron-sheet metal of thickness 0.5 mm. The breadth of the wings is 6 inch. The wings were bent in curved shape and fixed onto the sides of the water heater. When collecting data, shielded FPSWH ,(shown on the right in Figure 2.5.2), was tested side by side with a convectional FPSWH ,(shown on the left in Figure 2.5.2). It was found out that, compared to conventional water heater, aeroprofile water heater had 6.32% , 13.9% and 19.4% higher mass flow rate, heat transfer and thermal performance respectively.

2.5.3 Reduction of Radiative Heat Loss

Kurzbck et al. [68] studied effect of mixing propylene random copolymer (PP-RCT), which has a melting temperature of 230^{0}C, with carbon black and measured absorption rate of solar radiation. All pigmented batches showed good absorptivity of 96

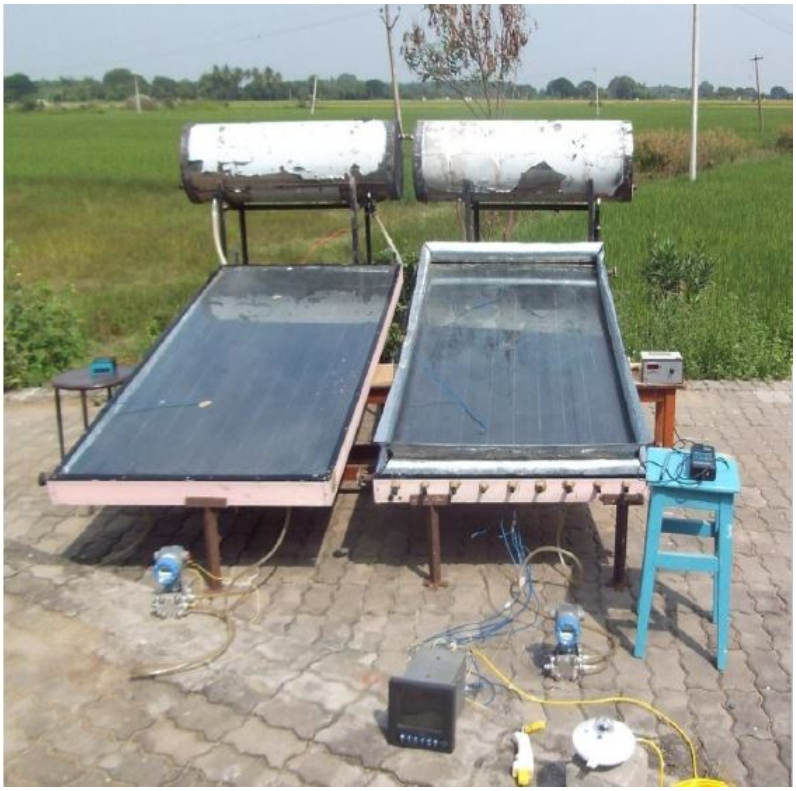

Figure 2.9: Testing a FPSWH with Aero profile wings on the sides [67]

%. Unfortunately, they did not go ahead to test emissivity and thermal conductivity of the batches. However, this gives an idea of developing cheap polymer based solar collectors. Quite a number of researchers have studied different types of selective surface coatings like electro-deposited Cr_2O_3 (Black Chrome plating), CuO or NiO (Black Nickel) and were able to achieve high absorptivity and low emissivity values. However, chemicals for electroplating technique are quite expensive and this is one of the main component that raises production cost of FPSWH. Henry et al. [] studied surface selective coatings and estimated that plating FPSWH costs about USD 28-50/m^2 while paint costs about USD 3-5/m^2. Jamaliah Idris et al. [69] studied the efficiency and production cost of Black Chrome plating copper and stainless steel. From their research, they found that Black Chromium on copper substrate gave the highest v.alue of absorption, $\alpha \geq 0.95$ and the low emittance, $\epsilon \leq 0.1$. The absorption and emittance value of stainless steel ($\alpha \geq 0.91$ and $\epsilon \leq 0.1$) were found to be

closely similar to copper when coated with black chromium. Since the two metal substrates gave almost matching results, they concluded that stainless steel could be used to replace the expensive copper metal in fabrication of FPSWH. From the work done by Sparrow et al. [70] on absorption of incident infra red light (thermal radiation) in a v-groove cavity where incident angle is smaller than half the angle of the groove ($\gamma < \theta/2$), it was proven that v-grooves could be used to reduce radiative heat loss. From their findings, absorption of incident light was higher when the surfaces were less specular (approaching black colour) and when v-groove angles were between 30^0 and 60^0 as long as $\gamma < \theta/2$. Smaller v-groove angles brought about self shading while wider angles allowed easy escape of reflected light thus lowering absorption. In case of black v-groove surfaces emitting thermal radiation at higher temperatures, angles of 30^0 or less indicated that they were more effective in reducing overall radiative heat loss due to increased absorption.

2.5.4 Reduction of Conductive Heat Loss

Beikircher et al. [71] came up with an innovation of using vacuum super insulation on the backside of the absorber plate for eliminating backside conduction of heat. They designed a stainless steel casing covered with a plastic film on top and filled it partially with low cost perlite before evacuating it to a pressure of 1 Pa. However, performance was comparable to normal glass wool insulated collector as no significant improvement was noted. This could be attributed to the perlite filling, ($k = 0.00125W/m^2$ at 1 Pa) and thermal conductivity of stainless steel casing, ($k = 54W/m^2$).

2.5.5 Improvement of Rate of Heat Transfer

Ruken Zilan et al. [42] replaced copper and aluminium plates with 1mm thick galvanized iron plate painted with 10 micron special paint. As expected, the collector exhibited low efficiency at high temperatures. However, by reducing pipe spacing from 90mm to 70mm and increasing plate thickness to 1.2mm, he was able to im-

prove heat transfer and consequently efficiency comparable to performance of copper plate SWH. However, the collector weighed above 50kg due to higher density of steel compared to copper. Since he still used copper pipes on the collector, significant cost reduction was not realized. Grigorios et al. [49] studied how metal inserts could improve heat transfer between the flow channel walls and circulating water. He found that aluminium wire mesh inserted in a water flow channel improved heat transfer to water by creating swirls and increasing surface area for conductive heat transfer. The downside effect of these inserts, was reduced flow pressure.

Basharia *et al.* [72] conducted tests on two flat plate solar air heaters, one with a flat absorber plate and the other with V-grooved absorber plate as in Fig. 2.5.5. From their research work, they concluded that the V-grooved absorber plate gave an efficiency of 15% higher than the flat absorber plate. This is because the fluid interacts with absorber plate directly compared to when the fluid is confined inside the tubes. Unfortunately the v-grooves were open towards the air gap and fluid did not flow within the triangular channels.

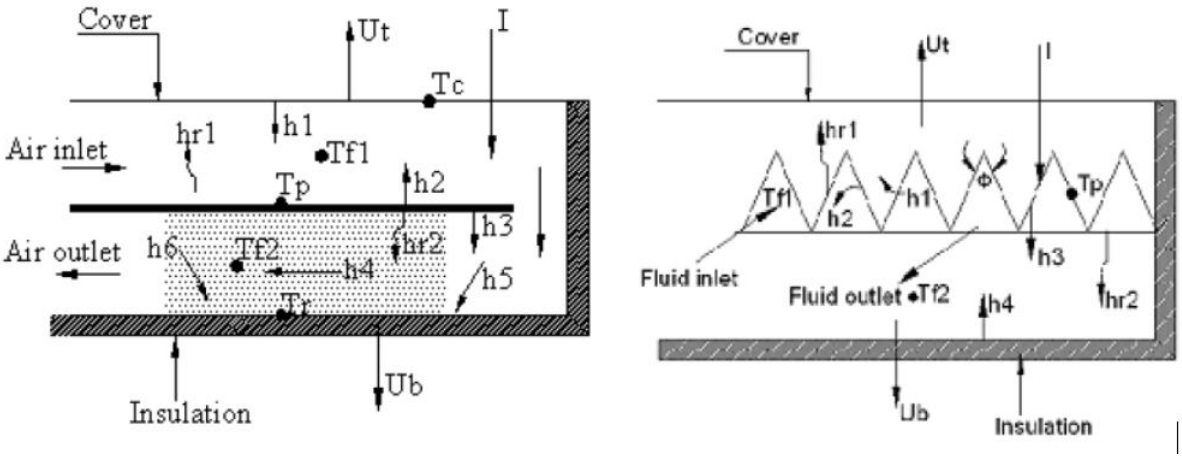

Figure 2.10: Flat plate and v-grooved absorber plate air heaters [72]

Gogol et al. [73] studied the effect of reducing riser spacing on heat transfer rates. Riser spacings were varied from from 14cm to 0cm in low mass flow rate FPSWH

as both effective and exergetic efficiencies were recorded. They found out that the most efficient collectors are those relatively long with the distance between tubes (riser spacing) as small as possible, that is collectors in which the absorber is in contact with the fluid and surface area as large as possible. Zipin *et al.* [74] studied behavior of incident light on a V-Groove with specularly reflecting walls, (surfaces behaving like a mirror). The incident angle was varied from zero to maximum and the reflections of the light beam counted before it left the v-groove as shown by Figure 2.5.5. The number of reflections the incident beam made at the walls of

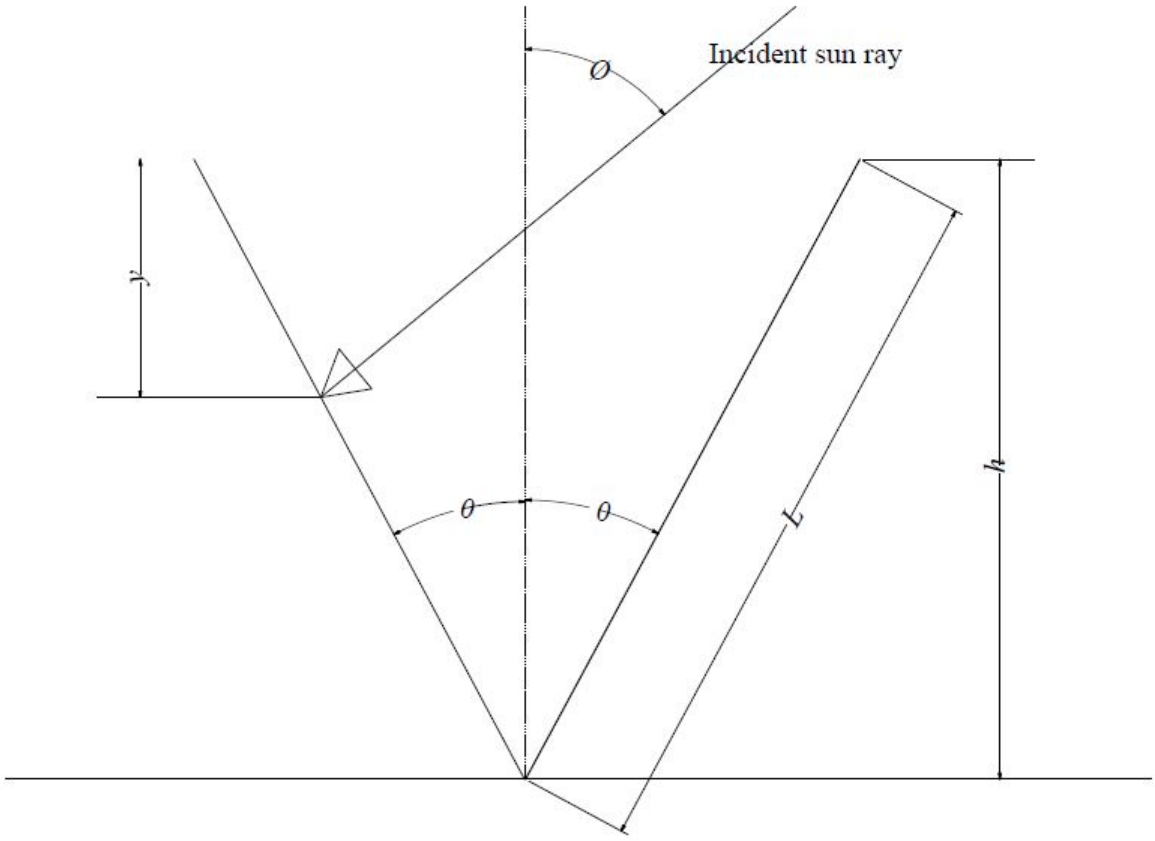

Figure 2.11: Diagram showing point of sun ray strike and shading portion [74]

the groove before it left were used to determine the apparent thermal radiation

properties exhibited by the groove. This was determined by counting the number of mirror images of the first surface that were crossed by an undeviated beam. From their findings, they concluded that effective absorption of the v-groove increased with decrease in angle of incidence. It was also noted that as long as groove angle is less than half the incident angle, the whole internal surface of the groove will be illuminated (i.e. no shading will be witnessed). The research however did not study the effect of radiation from the v-groove to the environment.

2.6 Summary of Gaps

On reviewing the past research works on flat plate solar water heaters, the following gaps have been identified.

- Research on performance of flat solar water heaters in Africa, especially Kenya, is not satisfactory. This is because FPSWH are very much dependent on ambient temperatures implying that they might be more efficient in equatorial areas as compared to temperate and colder regions.
- Research on FPSWH partially evacuated to,1-3000Pa, to reduce convective heat loss is not satisfactory.
- Though extensive work has been done on the use of V-grooved absorber plates to improve heat transfer rates on flat plate air heaters, the same has not been studied extensively on FPSWH
- FPSWH with suspended absorber plates are non existent. Suspended absorber plates take advantage of air at low pressure in reducing conductive heat loss hence eliminating the need for thicker insulating materials.
- Use of black matte paint on galvanized iron is not extensive. This technique takes advantage of low emissivity of zinc covering on steel to reduce radiative heat loss.

CHAPTER THREE

EXPERIMENTAL DESIGN AND METHODOLOGY

3.1 Introduction

In this chapter, heat loss equations for Flat Plate Solar Water Heater (FPSWH), design equations and optimization of design parameters is presented. The main aim of the research work was to reduce convection and radiation heat transfer modes which account for the larger portion of heat loss from FPSWH. Hence design equations for different parameters such as absorber plate area, air gap, evacuation pressure and number of glazing were based on this objective. The procedure used in design, material selection and fabrication of various components as well as the method and equipment used to collect experimental data are presented. Ways of analyzing the collected data and the uncertainty involved are also presented in this chapter.

Bathing water demand for a household of two occupants was taken into account when designing for capture area and storage capacity. The assumption was that, most families have a minimum of two occupants and each occupant needs 40 litres per day at a at optimal temperatures of 40^0C [75–77]. Most importantly, materials were chosen so as to improve efficiency at low-cost. After fabrication, the FPSWH was subjected to outdoor testing where parameters such as overall heat loss coefficient and efficiency were calculated and are presented in this chapter.

3.2 Design Parameters for the Water Heater

Absorber plate is the heart of a FPSWH as it captures solar radiation, converts it to thermal energy and consequently it transfers the heat to circulating water. According to the research done around Thika region by Nahashion Wanyonyi [26], Thika and Juja receive an annual average solar radiation of 5 KW/m^2/day though the values are higher in December to March (above 6 KW/m^2/day) and low in April to July (4.2-4.9 KW/m^2/day).

From research done by Rohles and Konz which aimed at establishing the right amount of water one should shower with without wastage. It was found that a person should shower or bath with about 40 liters of warm water at 40-41^{0}C [76, 78]. This implies that a household with two people require 80-100 litres/day of warm water. Hence for temperatures of 40-50^{0}C, a storage tank of 100 litres is required while a much smaller tank will suffice as long as stored water is hotter than 60^{0}C. For instance, storing solar heated water at 70^{0}C would only require a 35 litre storage tank.

Taking the aforementioned factors into consideration, the following calculations were used to determine solar capture or harnessing area based on amount of energy required to heat an equivalent amount of water from tap temperature to 41^{0}C.

Assuming that, tap water has an average temperature of 20^{0}C and density of 1000Kg/m^3. Energy required to raise 100 litres of water from 20^{0}C to 41^{0}C is calculated using Equation 3.1

$$q_{required} = mC_w\frac{\Delta T}{\Delta t}, \tag{3.1}$$

where C_w is specific heat capacity of water, ΔT is change in temperature, Δt is change in time. Energy absorbed from solar radiation by the absorber plate is given by Equation 3.2 [79]

$$q_{absorbed} = A_{ap}\alpha\tau I, \tag{3.2}$$

where A_{ap} is the area of absorber plate, τ is light transmissivity of the glass, α is the solar absorptance of the absorber plate and I is the insolation intensity in (w/m^2). Minimum $A_{ap_{min}}$ is calculated from Equation 3.3 before accounting for losses.

$$A_{ap,min} = \frac{\dot{m}C_w(T_{out} - T_{in})}{I\tau}, \tag{3.3}$$

assuming an efficiency of 40% [53],

$$A_{ap,40\%} = \frac{\dot{m}C_w(T_{out} - T_{in})}{0.4I\tau}. \tag{3.4}$$

But in real life situation, all FPSWHs are subject to varying degrees of heat losses via conduction, convection and radiation. These heat losses are largely influenced by

absorber plate area (A_{ap}), emittance of the absorber plate(ϵ), the shape of the absorber plate(shape factor) and air gap (L). Also air pressure inside the FPSWH, tilt angle, thermal conductivity of insulating material, absorber plate material, glazing material housing material are parameters which influence heat loss. Heat loss by convection and re-radiation constitute top loss while conduction constitute bottom and side loss.

By obtaining the value of top heat loss and bottom and side heat loss, efficiency of the absorber plate area estimated in Equation 3.4 can be defined clearly from theoretical point of view, thus making the design more accurate.

3.2.1 Determination of Top Heat Loss Coefficient

Heat loss from absorber plate surfaces to the glass cover and then to the environment via radiation is given by Equation 3.5 [11, 34]

$$q_{rad} = \frac{\sigma A_{ap}[(T_{ap})^4 - (T_{glass})^4](F_{1-3}^2)}{\left(\frac{1}{\epsilon_{ap}} + \frac{1}{\epsilon_{glass}} - 1\right)} = \epsilon_{glass}\sigma A_{ap}[(T_{glass})^4 - (T_{sky})^4] \tag{3.5}$$

Where F_{1-2} is the shape factor or geometric configuration factor, shown in Equation 3.7, [34,80] and its deriveation is shown in Appendix A. All temperatures are in Kelvin. σ is the Boltzmann constant taken as 5.67×10^{-8} Watts.m^{-2}.K^{-4}. ϵ_{ap} and ϵ_{glass} are emissivity constants for absorber plate material and glass cover respectively.

$$F_{1-2} = 1 - \left(\frac{1-\cos(2\theta)}{2}\right)^{1/2} = 1 - \sin\theta, \tag{3.6}$$

$$F_{1-3} = 1 - F_{1-2} = \sin\theta. \tag{3.7}$$

Psarouthakis [81] developed Equation 3.8 relating apparent emissivity to the v angle, θ, and normal emissivity, ϵ, by use of a power series, [81],

$$\epsilon_a = \left(1 + \left(\frac{1}{\epsilon} - 1\right)\sin\theta\right)^{-1}, \tag{3.8}$$

where

$$\epsilon_a = (\epsilon_{ap})_a = \left(\frac{\epsilon}{\sin\theta}\right)\left[\frac{1 - F_{1-2}}{1 - F_{1-2}(1-\epsilon)}\right]. \tag{3.9}$$

ϵ_a is defined as the ratio of energy emitted by the groove over the energy emitted by a black body of area equal to that projected by the groove [81]. Effective sky temperatures are obtained from Equation 3.10 and is calculated relative to atmospheric room temperature, T_a [34].

$$T_{sky} = T_a - 6 \tag{3.10}$$

Equation 3.7 show that for a v-grooved absorber plate configuration factor depends on v-angle only as detailed by Figure 3.2.1. A flat plate with v-angle= 180^0 has no configuration factor hence experiences maximum radiative heat loss subject to plate temperature and emissivity. However, as v-angle is reduced from π towards zero, configuration factor reduces the energy radiated outside the v-groove till a point when v-angle= 0^0 and no heat is radiated outside the v-groove. Unfortunately for solar collectors, v-angles$< 30^0$ result in self shading, whereby one surface does not receive insolation especially in the morning and evening. Hence v-angles for solar water heaters are supposed to be 30^0 or more depending on surface width [70, 74].

Heat loss from absorber plate surfaces to the environment via convection is given by Equation 3.11 [49, 82]

$$q_{convection} = h_{ap-g}(T_{ap} - T_{glass}) = h_w(T_{glass} - T_a), \tag{3.11}$$

where h_{ap-g} is the natural convective heat transfer coefficient between the absorber plate and the glass cover, h_w is the convective heat transfer coefficient between the glass cover and the atmosphere and T_{ap}, T_{glass} & T_a are the average temperatures of the absorber plate, glazing glass & atmosphere respectively in kelvin.
Convective heat transfer coefficient between the glass cover and the atmosphere,h_w is generally calculated from empirical correlation 3.12. The correlation was proposed by McAdams, 1954, and is based on experiments done by Jurges on flow of air at room temperature parallel to a heated flat plate in 1924 [34].

$$h_{w1} = 5.7 + 3.8V, \tag{3.12}$$

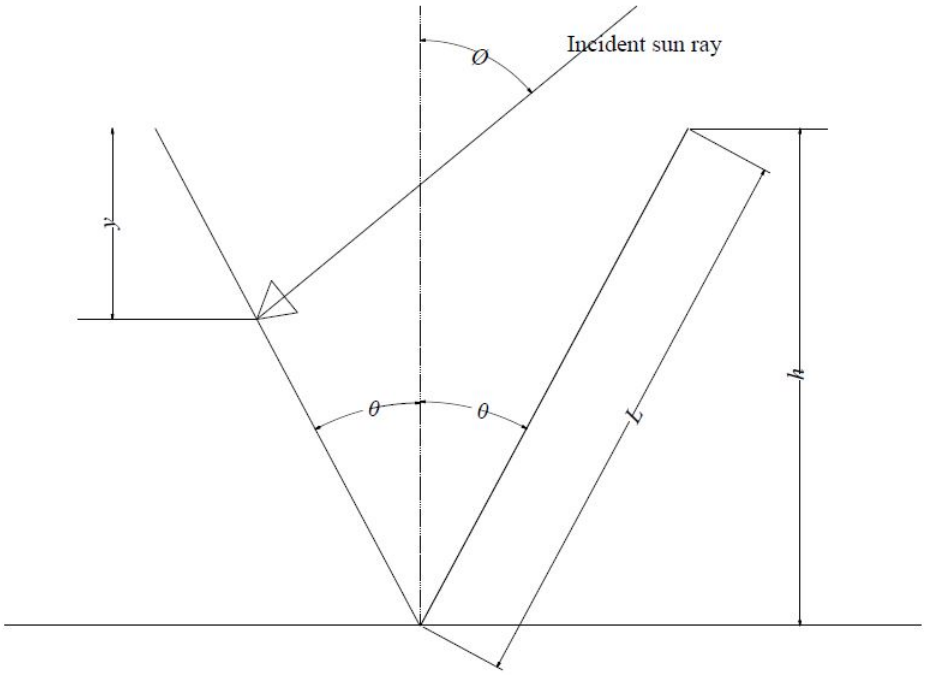

Figure 3.1: V-groove angle θ

where h_{w1} is convective heat transfer coefficient between the glass cover and the atmosphere based on assumption that wind direction is parallel to the glass cover and V is velocity of wind in m/s. However, since in reality the direction of wind is rarely parallel to the glass cover as is the case with Jurges experiments, expression 3.12 was modified by Sparrow into an accurate correlation 3.13 in order to account for any kind of wind direction [34],

$$h_w = j\rho C_p V_\infty Pr^{-2/3}, \tag{3.13}$$

where j is a dimensionless factor and is given as

$$j = \frac{0.86}{\sqrt{Re}}, \tag{3.14}$$

Re is the Reynolds number and is calculated as

$$Re = \frac{\rho u D_h}{\mu} = \frac{V_\infty L}{\sqrt{\nu}}, \tag{3.15}$$

where D_h is the hydraulic radius and,

$$L = \frac{4A_c}{C_c}, \tag{3.16}$$

where, A_c is the collector gloss area, and C_c is the circumference associated with the gross area A_c. For single glazed FPSWH, temperature of outer glass,T_g was estimated from Equation 3.17, which was proposed by Akhtar and Mullick to account for absorption of solar by glazing glasses [83].

$$T_g = \frac{fT_{ap} + T_a + \frac{\alpha_g I}{h_w+6}}{1+f}, \tag{3.17}$$

where

$$f = \frac{(12 \times 10^{-8}(0.2T_{ap} + T_a)^3 + h_w)^{-1}}{6 \times 10^{-8}(\epsilon_{ap} + 0.028)(T_{ap} + 0.5T_a)^3 + 0.6L_{ap-g}^{-0.2}(((T_{ap} - T_a)\cos\beta)^{0.25})^{-1}}.$$

While temperatures of inner and outer glasses for double glazed FPSWH were estimated from expression 3.18 for T_{g1} and expression 3.20 for T_{g2} [84].

$$T_{g1} = \frac{f_1 T_{ap} + T_{g2} + 0.11\alpha_g I}{1+f_1}, \tag{3.18}$$

$$f_1 = \frac{[3.1\sigma(T_0 + \Delta_0)^3 + 0.8(\Delta_0\beta)^{0.25}L_2^{-0.2}]^{-1} + 1.1L_{g1}}{[3.45\sigma\epsilon_{ap}(T_{ap} - \Delta_i)^3 + 0.8(\Delta_i\Delta\cos\beta)^{0.25}L_1^{-0.2})]^{-1}}, \tag{3.19}$$

where $\Delta_i = (2 - \epsilon_{ap})\frac{T_{ap}-T_2}{6}$ and $\Delta_0 = (1 + \epsilon_{ap})\frac{T_{ap}-(T_2-5(T_{ap}-T_a)L_{g2}-1.9\alpha_g I L_{g2})}{6}$. Both Δ_i and Δ_0 are obtained by regression analysis [84],

$$T_{g2} = \frac{f_2 T_{ap} + T_a + \frac{1.4\times\alpha_g I}{h_w+5}}{1+f_2}. \tag{3.20}$$

In which case,

$$f_2 = f \times (0.7 - 0.26\epsilon_{ap}). \tag{3.21}$$

Convective heat transfer coefficient between absorber plate and the glass cover ,h_{ap-g} was calculated as heat transfer coefficient of an enclosed rectangular space between inclined parallel surfaces with high aspect ratios (L_3/L) and was obtained by using one of the correlations proposed by Holland [85] and Buchberg [83] depending with Rayleigh number [34]

$$h_{ap-g} = \frac{Nu_L \times k}{L} \tag{3.22}$$

In which case the Nusselt number, Nu, is dependent on Rayleigh number and was calculated from Hollands and Buchberg correlations as

(i) Correlations by Hollands for $0^0 \leq \beta \leq \beta^*$

$$Nu_L = 1; 0 < Ra_L cos\beta < 1708$$

$$Nu_L = 1 + 1.44\left[1 - \frac{1708}{Racos\beta}\right]; 1708 < Ra_L cos\beta < 5830$$

$$Nu_L = 1 + 1.44\left[1 - \frac{1708}{Racos\beta}\right] \times \left[1 - \frac{1708(sin1.8\beta)^{1.6}}{Racos\beta}\right] + \left[\left(\frac{Racos\beta}{5830}\right)^{1/3} - 1\right];$$
$$5830 < Ra_L cos\beta < 1 \times 10^6 \tag{3.23}$$

Where

Table 3.1: Critical angle of inclination depending on aspect ratio

Aspect ratio, L_3/L	1	3	6	12	≥ 12
β^*	25^0	53^0	60^0	67^0	70^0

(ii) Correlations by Buchberg, for $0^0 \leq \beta \leq 60^0$

$$Nu_L = 1; 0 < Ra_L cos\beta < 1708$$

$$Nu_L = 1 + 1.446\left(1 - \frac{1708}{Ra_L cos\beta}\right); 1708 < Ra_L cos\beta < 5900$$

$$Nu_L = 0.229(Ra_L cos\beta)^{0.252}; 5900 < Ra_L cos\beta < 9.23 \times 10^4$$

$$Nu_L = 0.157(Ra_L cos\beta)^{0.285}; 9.23 \times 10^4 < Ra_L cos\beta < 10^6 \tag{3.24}$$

Where, $Ra_L \cos\beta = \left(\frac{g\beta_t(\Delta T)L^3}{\nu^2} \times Pr \times \cos\beta\right)$ and L in the subscript is the characteristic length and is taken as the spacing between the two surfaces. For v grooved absorber plate, the L is the distance between the glass and the mid point of crest and root of the groove. Pr is the Prandtl Number, ν is the kinematic vicosity and β_t is the thermal expansion coefficient of gases, which is equal to $1/\mathrm{T}_{Mean}$ and β is the angle the FPSWH is inclined to.

Since the Hollands correlations have a maximum of 10% error in predicting h_{ap-g} for $60^0 < \beta < 90^0$ and Buchberg et al. correlations are not applicable for $60^0 < \beta < 90^0$ [12], Elsherbiny 3.27 correlations were used to calculate $h_a g$ for inclination angles $60^0 < \beta < 90^0$, [14] [12]

i For $\beta = 90^0$, $10^3 \leq Ra_L \leq 10^7$, and $5 \leq L/H \leq 110$

$$Nu_1 = 0.0605 Ra_L^{1/3}$$

$$Nu_2 = \left[1 + \left(\frac{0.104 Ra_L^{0.293}}{1 + \left[\frac{6310}{Ra_L}\right]^{1.36}}\right)^3\right]^{1/3}$$

$$Nu_3 = 0.242 \left(\frac{Ra_L}{A.R.}\right)^{0.272}$$

$$Nu_{90} = [Nu_1, Nu_2, Nu_3]_{max} \tag{3.25}$$

ii For $\beta = 60^0$

$$Nu_1 = \left[1 + \left(\frac{0.0936 Ra_L^{0.313}}{1 + \frac{0.5}{\left[1+\left(\frac{Ra_L}{3160}\right)^{20.6}\right]^{0.1}}}\right)^7\right]^{1/7}$$

$$Nu_2 = \left(0.104 + \frac{0.175}{A.R.}\right) Ra_L^{0.283}$$

$$Nu_{60} = [Nu_1, Nu_2]_{max} \tag{3.26}$$

iii For $60^0 < \beta < 90^0$

$$Nu_\beta = \left[\frac{(90^0 - \beta)Nu_{60} + (\beta - 60^0)Nu_{90}}{30^0}\right] \tag{3.27}$$

Though Equations 3.1 to 3.27 are used to establish radiative and convective heat losses, most researchers such as Samdarshi and Mullick [11],Garg and Datta [13] and Klein as quoted by [12] have combined both convective and radiative heat loss factors and obtained a simplified empirical equation to facilitate simulation and design of solar water heaters.

For this project, the equation adopted is the one proposed by Mullick and Samdarshi in 1988 for a single glazed FPSWH with a flat absorber plate [11, 12]. After incorporating the v-groove shape factor, Equation 3.28 was used to calculate top heat loss coefficient for a single glazed FPSWH.

$$\frac{1}{U_t} = \left[h_{ap-g} + \frac{\sigma(T_{ap}^2 - T_g^2)(T_{ap} + T_g)}{\frac{1}{(\epsilon_{ap})_a} + \frac{1}{\epsilon_g} - 1}\right]^{-1} + \left[h_w + \frac{\epsilon_g \sigma(T_g^4 - T_s^4)}{(T_g - T_a)}\right]^{-1} + \frac{t_g}{K_g} \tag{3.28}$$

Where

$$h_{ap-g} = \frac{Nu_L \times k}{L}$$

Nu_L is obtained from correlations proposed by Hollands 3.23 and Buchberg 3.24 mentioned above. For double glazed FPSWH, Equation 3.29 was used to calculate top heat loss coefficient. By replacing h_{ap-g} in Equation 3.28 with design parameters (temperature, air gap tilt angle etc), and adding shape factor for V-grooved absorber plate, the design Equation 3.28 for the top loss coefficient for a double glazed absorber plate was obtained as Equation 3.29

$$\begin{aligned}\frac{1}{U_t} = & \left[h_{ap-g1} + \frac{\sigma(T_{ap}^2 - T_{g1}^2)(T_{ap} + T_{g1})}{\frac{1}{(\epsilon_{ap})_a} + \frac{1}{\epsilon_g} - 1}\right]^{-1} + \left[h_{g1-g2} + \frac{\sigma(T_{g1}^2 - T_{g2}^2)(T_{g1} + T_{g2})}{\frac{2}{\epsilon_g} - 1}\right]^{-1} \\ & + [h_w + \epsilon_g \sigma(T_{g2}^2 - T_a^2)(T_{g2} - T_a)]^{-1} + \frac{2t_g}{K_g}\end{aligned} \tag{3.29}$$

Where h_{ap-g} has been replaced by

$$h_{ap-g} = \frac{5.78[(T_{ap} - T_g)cos\beta]^{0.27}}{\left(\frac{(T_{ap}-T_g)}{2}\right)^{0.31} L_{ap-g}^{0.21}}$$

and h_{g1-g2} by

$$h_{g1-g2} = \frac{5.78[(T_{g1} - T_{g2})cos\beta]^{0.27}}{\left(\frac{(T_{g1}-T_{g2})}{2}\right)^{0.31} L_{g1-g2}^{0.21}}$$

to yield the final empirical Equation 3.30 for double glazed FPSWH [11]

$$\begin{aligned}\frac{1}{U_t} = & \left[\frac{5.78[(T_{ap} - T_{g1})cos\beta]^{0.27}}{\left(\frac{(T_{ap}-T_{g1})}{2}\right)^{0.31} L_{ap-g}^{0.21}} + \frac{\sigma(T_{ap}^2 - T_{g1}^2)(T_{ap} + T_{g1})}{\frac{1}{(\epsilon_{ap})_a} + \frac{1}{\epsilon_g} - 1}\right]^{-1} \\ & + \left[\frac{5.78[(T_{g1} - T_{g2})cos\beta]^{0.27}}{\left(\frac{(T_{g1}-T_{g2})}{2}\right)^{0.31} L_{ap-g}^{0.21}} + \frac{\sigma(T_{g1}^2 - T_{g2}^2)(T_{g1} + T_{g2})}{\frac{2}{\epsilon_g} - 1}\right]^{-1} \\ & + [h_w + \epsilon_g\sigma(T_{g2}^2 - T_a^2)(T_{g2} - T_a)]^{-1} + \frac{2t_g}{K_g}\end{aligned} \tag{3.30}$$

And for this case of a double glazed FPSWH, simplified correlations 3.31 and 3.32 were used for estimating T_{g1} and T_{g2} as [11]

$$T_{g2} = T_a + h_w^{-0.4}(0.0021T_{ap} + 0.57\epsilon_{ap} - 0.146)(T_{ap} - T_a) \tag{3.31}$$

$$T_{g1} = T_{ap} - (0.7 - 0.34\epsilon_{ap})(T_{ap} - T_{g2}) \tag{3.32}$$

3.2.2 Determination of Bottom Heat Loss Coefficient

Heat loss from absorber plate surfaces to the environment via conduction is given by Fourier's law stated in Equation 3.33 [79]

$$\frac{\Delta q}{\Delta t} = kA(-\Delta T). \tag{3.33}$$

Applying Newton's law of cooling on the absorber plate bottom , Equation 3.33 is modified to Equation 3.34

$$q_{back} = \frac{T_{ap} - T_a}{\frac{\delta_{fg}}{k_{fg}A_{ap}} + \frac{\delta_{air}}{k_{air}A_{aps}} + \frac{\delta_{wood}}{k_{wood}A_{ap}}} \tag{3.34}$$

Therefore, bottom heat loss coefficient is summarized as

$$\frac{1}{U_b} = \frac{q_{back}}{A_{ap}(T_{ap} - T_a)} = \frac{\delta_{fg}}{k_{fg}} + \frac{\delta_{air}}{k_{air}} + \frac{\delta_{wood}}{k_{wood}} \tag{3.35}$$

3.2.3 Determination of Side Heat Loss Coefficient

Side heat loss also occur through conduction and is basically a function of thermal conductivity and dimensions of the casing such as length, width and height(spacing between the bottom and the glass cover). Side heat loss is dependent on thermal conductivity of the insulation material and the housing. Calculation of U_{side} aims to reduce collector sizing since the bigger the collector, the more heat is lost through the sides.

$$q_{side} = \frac{T_{ap} - T_a}{\frac{\delta_{fg}L_3L_4}{2L(L_3+L_4)k_{fg}} + \frac{\delta_{wood}L_3L_4}{2L(L_3+L4)k_{wood}}} \tag{3.36}$$

And it follows that side heat loss coefficient can be expressed as

$$\frac{1}{U_{side}} = \frac{q_{side}}{T_{ap} - T_a} = \frac{\delta_{fg}L_3L_4}{2L(L_3 + L_4)k_{fg}} + \frac{\delta_{wood}L_3L_4}{2L(L_3 + L_4)k_{wood}} \tag{3.37}$$

$$\frac{1}{U_{side}} = \frac{q_{side}}{T_{ap} - T_aA_(ap} = \frac{\delta_{fg}}{2L(L_3 + L_4)k_{fg}} + \frac{\delta_{wood}}{2L(L_3 + L_4)k_{wood}} \tag{3.38}$$

3.2.4 Determination of Effective Design Absorber Plate Area

Carrying out energy balance, the amount of solar energy absorbed by the absorber plate is equal to the heat removed by the circulating fluid and the heat lost by the FPSWH to the atmosphere

$$I\alpha\tau = \dot{m}C_w\Delta T + [(q_{loss,convection} + q_{loss,radiation}) + q_{loss,conduction}] \tag{3.39}$$

The convective, conductive and radiative heat loss terms can be represented in a single overall heat loss term given by Equation 3.40 [49]

$$\dot{m}C_wT = A_{ap}I\alpha\tau - A_{ap}U_l(T_{map} - T_a) \tag{3.40}$$

Where T_{map} is the mean temperature of the whole FPSWH and $U_l = U_t + U_b + U_s$

Table 3.2: Design parameters for calculation of A_{ap}

Parameter	Denotation	Value
Insolation	I	1000 Watts/m^2
Absorber plate temperature	T_{ap}	100^0C
Atmospheric temperature	T_a	25^0C
Water outlet temperature	T_{out}	85^0C
Water inlet temperature	T_{in}	25^0C
Absorber plate absorptivity	α_{ap}	0.95
Absorber plate emissivity	ϵ_{ap}	0.95
Glazing glass absorptivity	α_g	0.11
Glazing glass emissivity	ϵ_g	0.91
Glazing glass transmittance	τ_g	0.90
Wind speed	w	2.5m/s
Air gap	L	60 mm
Flow rate	$\dot{m}$	$1.9444\times10^{-3}kg/s$

From above outlined equations, absorber plate area or solar harnessing area was calculated from Equation 3.41

$$A_{ap} = \frac{\dot{m}C_w(T_{out} - T_{in})}{I\alpha\tau - U_l(T_{map} - T_a)} \tag{3.41}$$

Equation 3.40 show that heat lost to the atmosphere is dependent on difference between the average temperature of the collector and atmospheric temperature, i.e. the collector loses more heat at peak absorber plate temperatures. Therefore the collector was designed based on the parameters listed on Table 3.2.4. From Equation 3.41, effective absorber plate area was calculated as 1.0 m^2 (as articulated by Appendix B) and other designed parameters are listed in the Table 3.2.4 for an average temperature of 100^0C.

Table 3.3: Designed parameters

No	Designed Parameter	Value
1	Absorber plate area	1.0 m^2
2	Average heat loss coefficient	$7.254w/(m^2k)$
3	Efficiency	0.497

3.2.4.1 Performance Analysis Equations

Equation 3.40 can also be rewritten as [86, 87]

$$\dot{m}C_w(T_{out} - T_{in}) = F_r A_{ap} I\alpha\tau - F_r A_{ap} U_l(T_{in} - T_a) \tag{3.42}$$

Where F_r is a very important parameter in solar water heaters called Heat Removal Factor [88]. It is a measure of how efficient the collector is in transferring absorbed heat to the circulating water. It is not easy to determine the value of F_r, but as the FPSWH heats up in the morning, there reaches a point when $T_{in} = T_a$. At such a point, the second term of Equation 3.42 becomes zero enabling minimum of F_{rmin} to be calculated from Equation 3.44 below. However, as the water entering the FPSWH heats up above ambient temperature,F_r increases till noon when it reaches the peak value.

$$F_{rmin} = \frac{\dot{m}C_w(T_{out} - T_{in})}{A_{ap} I\alpha\tau} \tag{3.43}$$

Instantaneous efficiency of FPSWH is calculated as a fraction of total received solar energy which is converted to useful thermal energy [89]

$$\eta = \frac{\dot{m}C_w(T_{out} - T_{in})}{I\tau A_{ap}} \tag{3.44}$$

In most cases, FPSWHs show higher efficiency when they operate at high flow rate and low T_{out}. However, the absorbed energy might not be presented at a useful temperature level thus rendering the collector exegetic inefficient. Hence Zhong Ge *et al* came up with a modification on instantaneous efficiency based on the second law of thermodynamics, Equation 3.45, in order to capture quality of heat absorbed

called exegetic efficiency [90, 91].

$$\eta_{exegetic} = \frac{\dot{m}C_w(T_{out} - T_{in})}{IA_{ap}\left(1 - \frac{T_a}{T_s}\right)} \tag{3.45}$$

3.2.5 Determination of Optimal V-groove Angle

V angle was determined on the basis of limiting surface shading especially in the morning at 10.00am when irradiation attains full intensity as well as on the basis of maximizing benefits of shape factor. Since at a point where shading factor is maximum the shape factor is minimum, a compromise was drawn at the middle in order to maximize shape factor and reduce shading factor. Using cosine rules, shading factor for various angles was calculated using Equation 3.46 as proposed by Zipin [74] with reference to Figure 3.2.5 below and shape factor using Equation 3.47 and curves drawn for angles $0^0 - 90^0$.

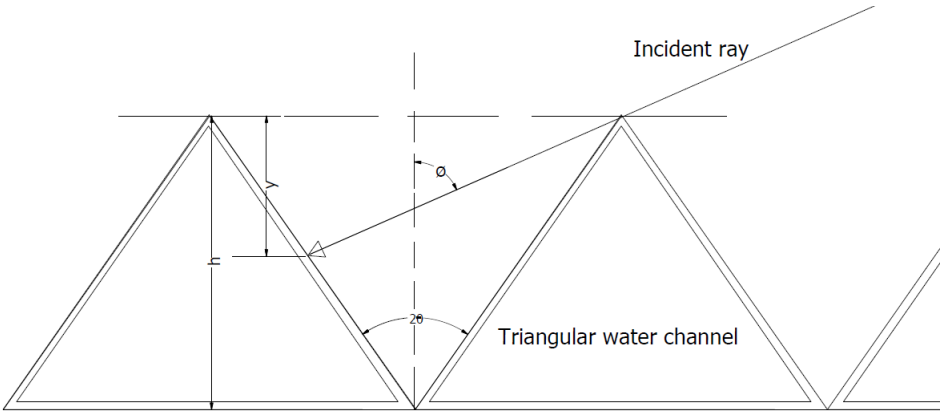

Figure 3.2: Diagram showing point of sun ray strike and shading portion [74]

$$\lambda = \frac{y_{max}}{h} = \frac{2\cos\phi\sin\theta}{\sin(\phi + \theta)}, \tag{3.46}$$

$$F_{12} = 1 - \sin\theta, \tag{3.47}$$

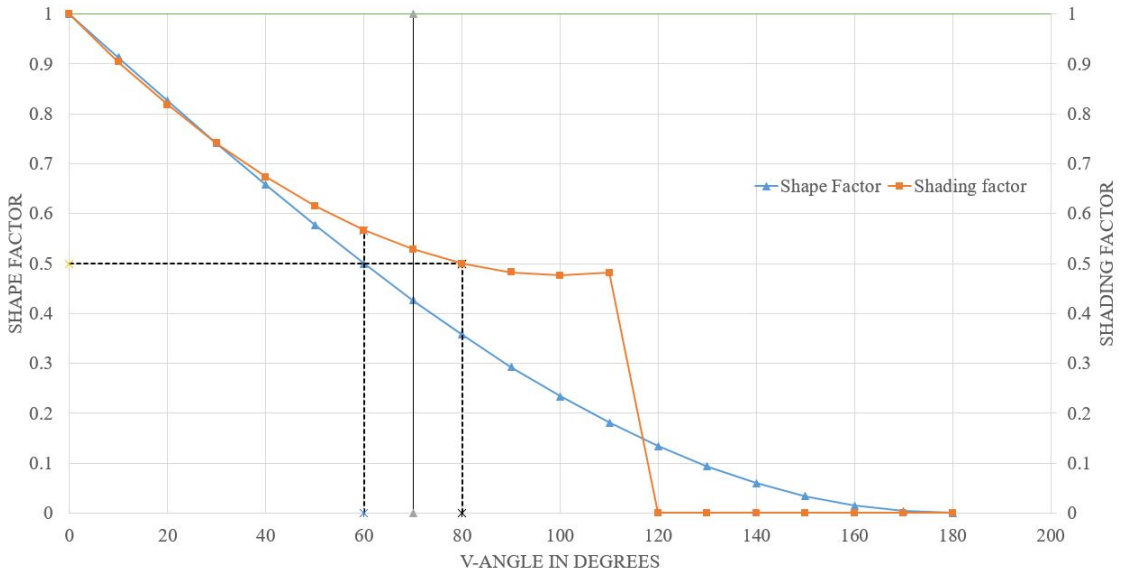

Figure 3.3: Graph showing optimal V groove angle at $\phi = 60^0$

where λ is the Shading factor and F_{12} is the Shape-factor.

Also,

$$\begin{aligned}\cos\phi = \; & \sin\varphi(\sin\delta\cos\beta + \cos\delta\cos\gamma\cos\omega\sin\beta) \\ & + \cos\varphi(\cos\delta\cos\omega\cos\beta - \sin\delta\cos\gamma\sin\beta) \\ & + \cos\delta\sin\gamma\sin\omega\sin\beta,\end{aligned} \tag{3.48}$$

$$\delta = 23.45\sin\left[\frac{360}{365}(284+n)\right]. \tag{3.49}$$

Equations 3.48 and 3.49 are used to calculate incident angle ϕ where φ is the locations latitude, δ is earth's declination angle which varies with different seasons of the year, β is the tilt angle of the FPSWH with respect to a flat ground while γ and ω are azimuth angle and hour angle of the sun respectively. n in Equation 3.49 is the day of the year. From graph in Figure 3.2.5 it can be seen that shape factor of 0.5 corresponds to a v-angle of 60^0 and shading factor of 0.5 corresponds to v angle of 80^0. A v angle of 70^0 lies in between them with a shading factor of 0.52 and

shape factor of 0.42. A v angle of 70^0 was taken as optimal since it corresponds to dimensions of a triangular chanel of height 16mm and base length of 23.5mm.

3.2.6 Determination of Optimal Air Gap

Convective currents are generated by body forces acting on the fluid in which there is density gradient due to temperature gradient [92]. The air in between the absorber plate and the cover glass in single glazed FPSWH form multi-cellular buoyancy driven flows when there is a temperature gradient between the two surfaces, resulting in heat transfer between the two surfaces. The air gap,(distance between the absorber plate and the glass cover), influences aspect ratio of the enclosed cavity which in turn affects Rayleigh number. The Figure 3.2.6 shows how natural con-

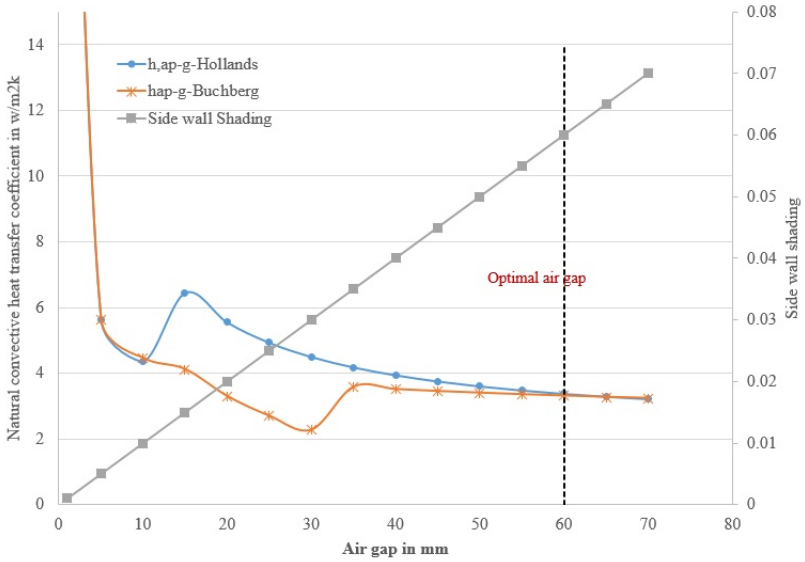

Figure 3.4: Graph showing optimal air gap

vection heat transfer coefficient varies with air gap within the laminar flow domain, $Ra_L \cos\beta < 10^6$, for inclined enclosed cavities of high aspect ratios. Large air gaps also make the FPSWH huge and cumbersome as well as creating significant side wall

shading in the morning and evening [38]. Thus choosing an optimal air gap is always a compromise between reducing both convection heat transfer coefficient and side wall shading. Although the former takes priority. Figure 3.2.6 demonstrates that optimal air gap chosen was 60mm, since it is the point where the slope in convection heat transfer coefficient begins to level meaning that $L > 60mm$ will result in slight effect on convection heat transfer coefficient but will increase side wall shading.

3.2.7 Determination of Effective Tilt Angle

Juja lies in a latitude of 1^0 11' 00" South of equator, which is the angle made by the radial line joining a given location to the center of the earth with the projection of the line on the equatorial plane. Tilt angle is the angle to which the collector is tilted towards the sun in order to receive maximum solar radiation, shown in Figure 3.2.7. Its aimed at making the FPSWH's surface be normal to the midday sun and is calculated from FPSWH azimuth angle γ and solar azimuth angle γ_s. Various

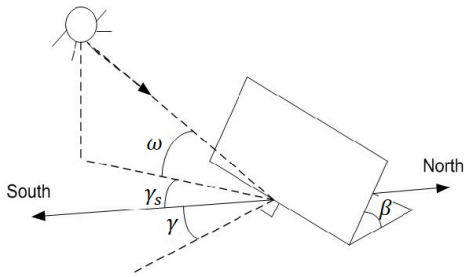

Figure 3.5: Illustration of solar angles [93]

researchers such as Morse and Czarnecki [94], Kern and Harris [95], Christensen and Barker [96] have conducted studies on how to obtain optimal tilt angles for locations with latitudes above 24^0 and all of them have found that optimal tilt angle is equal to the latitude of that location. For locations within latitude of 24^0, many theories on optimal tilt angle do exist each depending on different factors affecting a specific location [97], [98]. Camelia and Dorin Stanciu however proposed a method

of calculating optimal tilt angles of FPSWHs for different geographical locations and at different time of the year based on Hottel Woertz model of estimating incident solar radiation which is simply expressed in the equation 3.50 [99],

$$\beta_{Opt} = \varphi - \delta, \tag{3.50}$$

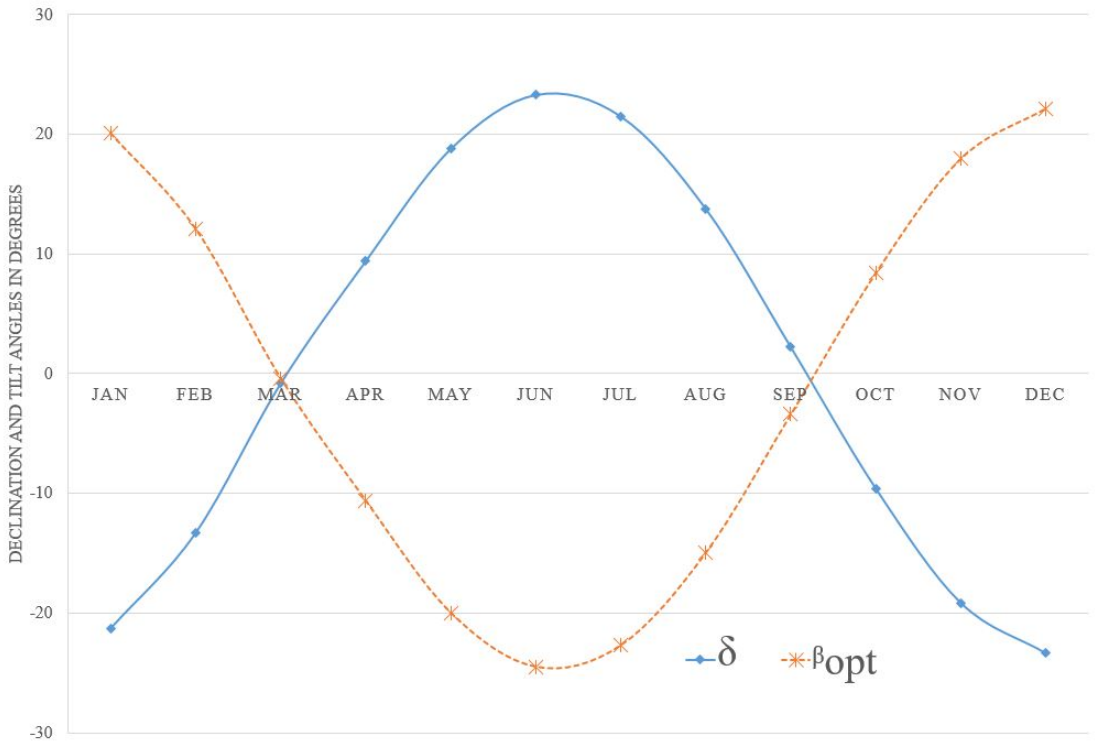

Figure 3.6: Graph of Optimal tilt angle for FPSWH in Juja

where δ is calculated as outlined by Equation 3.49 above. Thus for Juja location, optimal tilt angle varies with each month of the year as shown by Figure 3.2.7 although if the FPSWH is to be fixed for longer period of time, β_{Opt} from March to September has an average value of 14^0 facing due North and an average value of 16^0 from October to February facing due south.

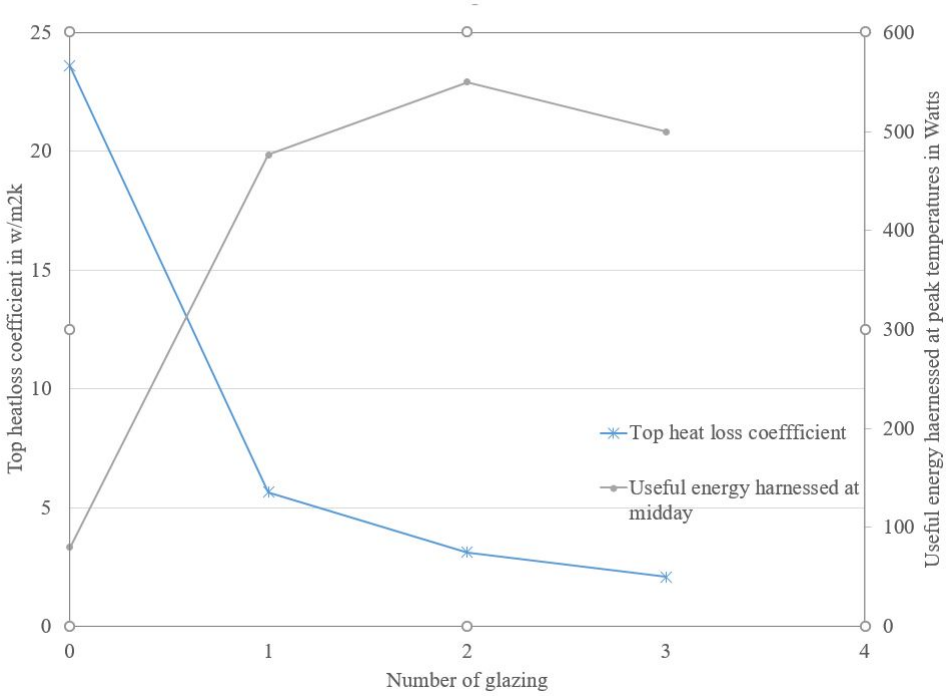

Figure 3.7: Graph of Optimal number of glazing for a FPSWH

3.2.8 Determination of Effective Number of Glazing

Glazing of FPSWHs reduces top heat loss coefficient by firstly shielding the absorber plate from winds and secondly by preventing transmission of long wavelength radiation to the atmosphere through greenhouse effect. Previous researches and studies show that use of more than one glazing reduces outer glass cover temperatures hence ultimately reducing the overall heat loss coefficient [100–102]. The setback to use of multi-glazing on FPSWHs come in form of reduced insolation reaching the absorber plate hence efficiencies start to drop when more than two glass covers are used as illustrated by Figure 3.2.8, illustrating that double glazed FPSWH are more efficient.

3.2.9 Determination of Critical Pressure of Partial Air Evacuation

Benz and Beikircher in 1999 developed an evacuated FPSWH able to produce process steam at 150^0C when partially filled with Krypton at 3000 Pa [43]. Partial evacuation means that the pressure of air in space between the absorber plate and the glass cover is reduced to a point where natural convection is inhibited, i.e. Nusselt number is a unit and the dominant mode of heat transfer is gas heat conduction [103]. Prior experiments have shown that for air gaps of less than 25mm, pressures of 10-500 Pa are required to inhibit convectional heat transfer while low pressures of 0.1 Pa are sufficient to eliminate both convectional heat transfer and gas heat conduction [104, 105]. Eaton and Blum experimented with partially evacuated FPSWHs and established the following relationship for natural convection heat transfer between the absorber plate and the glass cover

$$h_{ap-g} = (1.263 - 0.3476\beta + 0.06933\beta^2)(T_{ap} - T_g)^{0.25} \left(\frac{P}{P_0}\right)^{0.5} \tag{3.51}$$

Where P is the partial evacuation pressure, P_0 is the atmospheric pressure and β is the tilt angle. Equation 3.51 holds for the following conditions; $2.5 \times 10^4 \leq Gr \leq 11 \times 10^6, 19998.3Pa \leq P \leq 101324.72Pa, 25mm \leq L \leq 150mm, 10 \leq L_1/L \leq 40$ and $0 \leq \beta \leq \pi/3$. In this case the Grashof's number is calculated from the following modified Equation 3.52 [66]

$$Gr = \frac{(P/133.322)^2(100L)^3(T_{ap} - T_g)}{D} \tag{3.52}$$

where $D = 9.4595 \times 10^{-8}(T_{ap}+T_g)^3 + 5.0356 \times 10^{-9}(T_{ap}+T_g)^4 + 6.8267 \times 10^{-11}(T_{ap}+T_g)^5 + 3.3381 \times 10^{-14}(T_{ap}+T_g)^6 + 4.1413 \times 10^{-18}(T_{ap}+T_g)^7$. The modification is shown in Appendix A. Equation 3.52 is used to calculate critical pressures at which convection heat transfer is inhibited when a threshold value of Grashof's number is specified, say 2000 as specified by Correlations by Holland et al [66], then critical partial evacuating pressure is given as

$$P_c = \left(\frac{266644D}{[(\frac{L}{100})^3(T_{ap} - T_g)]} \right)^{1/2} \tag{3.53}$$

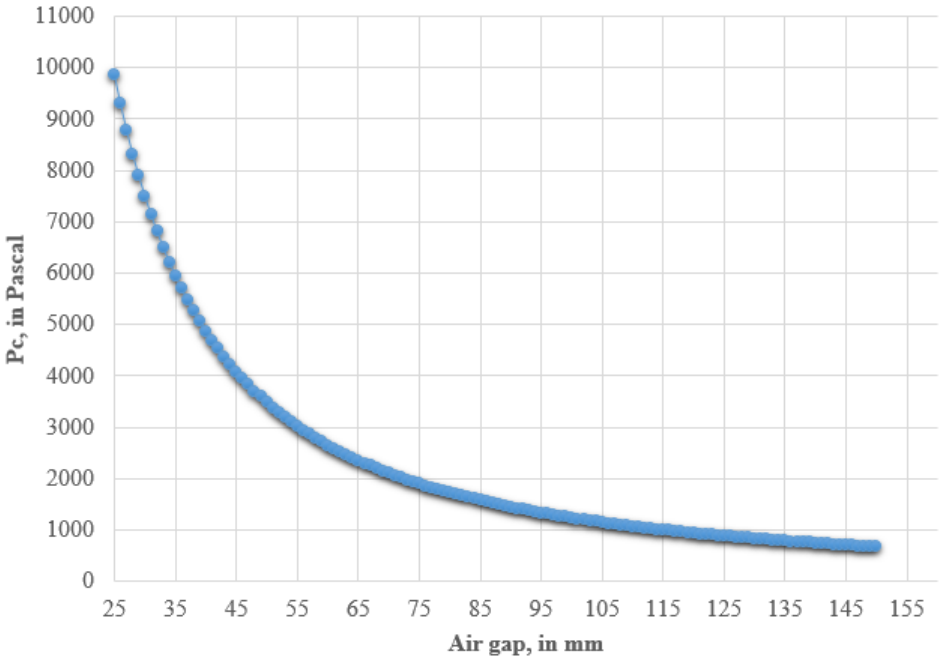

Figure 3.8: Graph of critical evacuating pressure for a FPSWH

Where L is the air gap. Equation 3.53 shows that as air gap increases, the critical partial evacuating pressure required decreases as it approaches ultra high vacuum ($<$ 0 Pa). For a FPSWH with absorber plate at 105^0C and cover glass at 35^0C, critical partial evacuating pressures depend on air gap as the Figure 3.2.9 shows.

3.3 Fabrication of the FPSWH

An absorber plate of area 1.25 m x 0.8m =1.0 m^2 was designed and fabricated with parametric value as shown by Tables 3.2.4 and 3.2.4, incorporating a V-groove angle of 70^0. The area of $1.0m^2$ is quite ideal as Ghimire et al. [8] found that efficiency of FPSWH decreased with areas larger than $1.0m^2$. The Table3.3 was used in materials selection, where galvanised iron sheet was chosen based on its pricing compared to

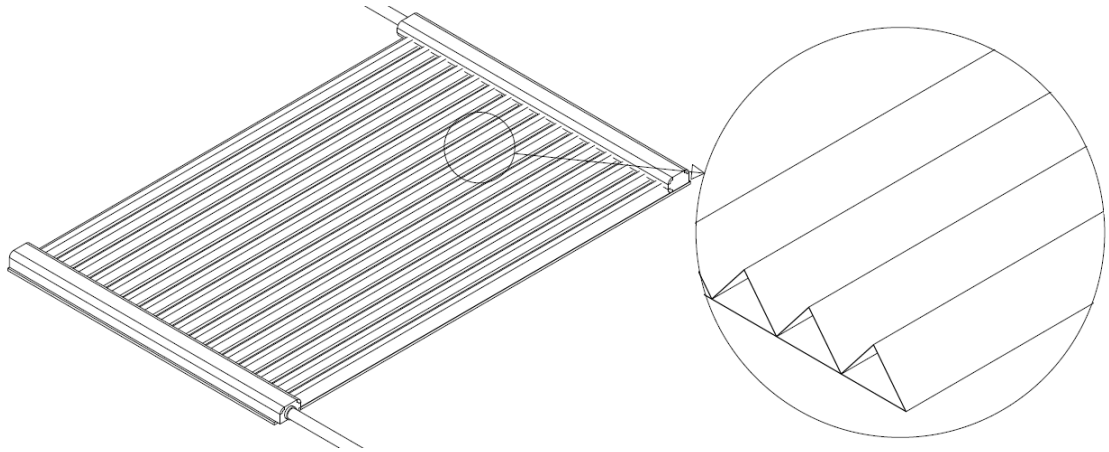

Figure 3.9: Inventor Autodesk illustration of the designed absorber plate

copper and aluminium.

Table 3.4: Materials commonly used on absorber plate

SN	Material	Size	K, Watts/m^2	Cost in Kshs
1	Copper	3ft $\times 6ft \times 1mm$	386	51,822
2	Aluminium	3ft $\times 6ft \times 1mm$	204	22,000
3	Galvanized iron	4ft $\times 8ft \times 1mm$	51	3,000

3.3.1 Fabrication of The Absorber Plate

A galvanized iron sheet of 1150mm long, 1352mm wide and 0.5mm thickness was folded into a corrugated shape using a manual sheet metal bending machine to form a total of 26 V-grooves. Each groove had a V angle of 70^0 , a vertical height of 21mm and base length of 30 mm as shown in the Figure 3.3.1 enabling the absorber plate to hold 9.418 litres of water when full. The corrugated sheet metal was then welded onto a flat galvanized iron together with end headers. The absorber plate was then washed and degreased, for good paint adherence, before it was painted black using

a special black matte spray paint.

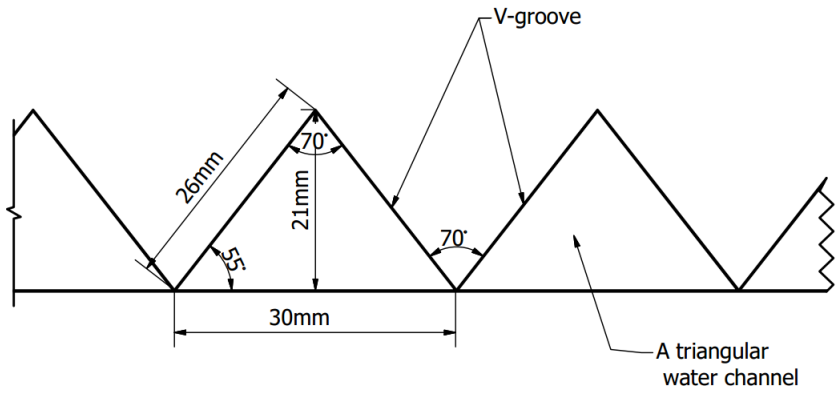

Figure 3.10: Absorber plate showing water channels and the V-Groove plate

3.3.2 Housing.

The housing for absorber plate was designed so as to suspend absorber plate and insulation at 50mm above the housing's floor to incorporate a 50mm air insulation as shown by Figure 3.3.2. It was also designed with provision for holding one or more glass glazing as well as for varying air gap. After designing, the housing was constructed with 25mm thick pieces of wooden block-boards and joined with glue in order to offer an air tight seal for ease of air evacuation. Wood is cheap and has low thermal conductivity (0.097 W/m-k) hence enabling it to act as an insulator. It was then painted white to reduce radiative heat loss.

3.3.3 Insulation.

A 50mm thick fiberglass insulation was used at the back of absorber plate [44]. To avoid use of a thicker insulation layer, absorber plate and fiber glass insulation were suspended at 50mm above the housing floor, as shown by Figure 3.3.3. Since air has very low thermal conductivity (0.025 W/m-k) and has upward rising convective

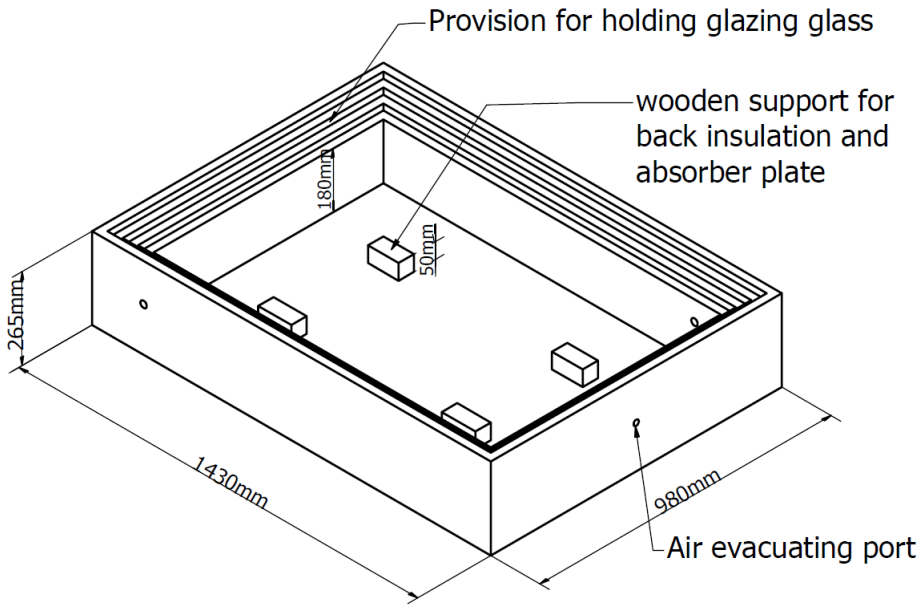

Figure 3.11: Schematic illustration of the designed housing

currents, it acts as a good insulator especially where the top surface is hotter than the bottom surface. In this scenario, the backplate is treated as a heated surface facing down whose heat transfer coefficient is negligible as shown by Equation 3.54 [106–108]

$$h_{air-cavity} = (0.27)Ra_{L-lower}^{1/4} \times \frac{L_{lower}}{k_{air}} + \frac{k_{air}}{L_{lower}} \tag{3.54}$$

where L_{lower} is the lower air gap

3.3.4 Glazing.

Window glass of thickness 3mm and transmittance of 0.9, absorptivity of 0.11 and emittance of 0.91 was used for glazing [109–111].

3.3.5 Stratification Tank

Storage tank of 80 litres capacity was constructed using 1mm thick stainless steel and wrapped in 100 mm thick fiber glass insulation. Calculation of optimal insulation

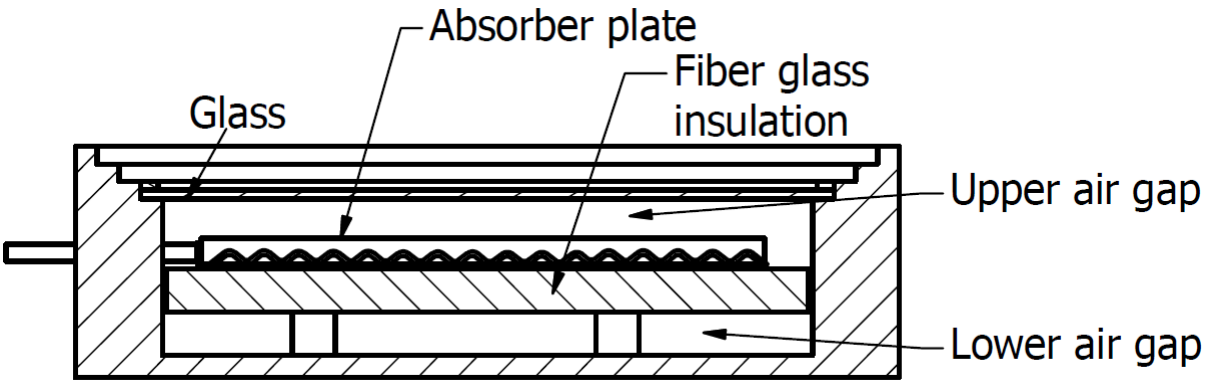

Figure 3.12: Illustration of fiber glass and lower air gap insulation

thickness is shown in Appendix C. The insulation layer was protected from moisture infiltration by a galvanized iron jacket painted white. The tank was 1000mm long and 320mm in diameter as shown in the Figure 3.3.5. It was also fitted with baffles for reducing the rates of mixing hot and cold water [112–114].

3.3.6 Piping

Flexible PVC (polyvinyl chloride) pipes of 12.7mm diameter were used to join the tank to the FPSWH due to their low thermal conductivity (0.5 W/mk). They also offer other benefits such as low cost, light weight and being non-toxic. Unfortunately they are affected by ultra violet light causing them to degrade faster [115].

3.3.7 Support Frame

The support structure was constructed using 3"X3"X0.0591" angle bars and block-boards to support a 80 litres stratification tank and the FPSWH as shown by Figures 3.4 and 3.4. Lastly it was painted shiny blue for rust protection and aesthetic appeal.

3.4 Experimental Set-Up

The experiment was to be conducted outdoors using natural light, where the FP-SWH was exposed to weather elements such as wind, dust,rain and dew. The

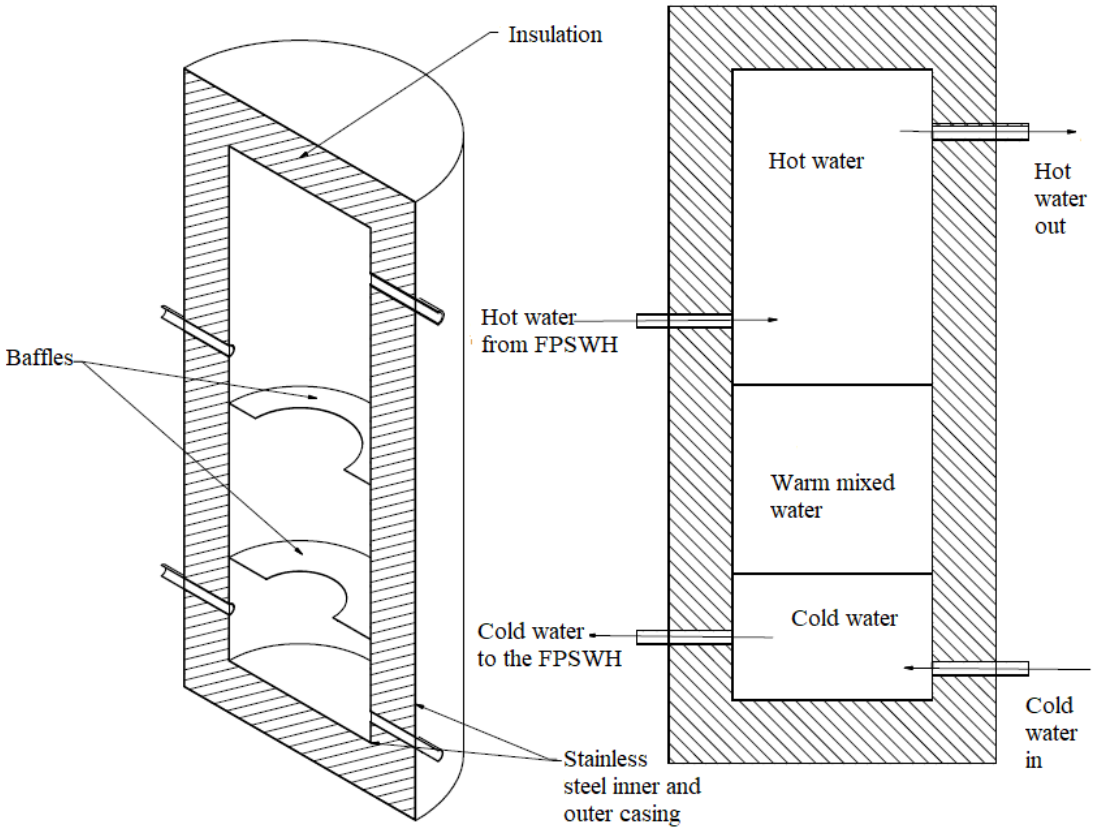

Figure 3.13: Cross-Sectional view of the storage tank and insulation

support structure was set outside away from shading structures and the FPSWH and storage (stratification) tank were mounted on it as shown by Figures 3.4 and 3.4. Using flexible PVC pipes, the tank and FPSWH were connected together. The whole system was filled with water and all the air displaced to avoid air locks and allow thermosyphonic flow to take place [116]. Measuring and data collection equipment were arranged as shown in the Figure 3.4 making the assembly ready for testing.

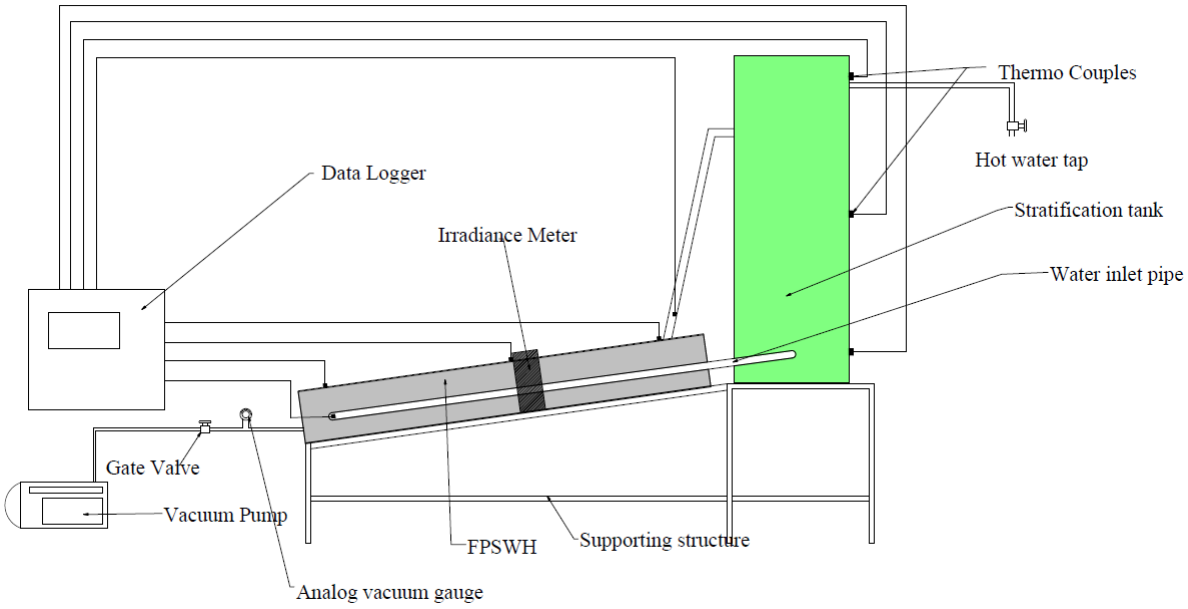

Figure 3.14: A sketch of experimental set up

3.5 Experimental Procedure

The general procedure involved setting up the equipment, taking readings from thermometers, data loggers and insolation meter after every 10 minutes interval. Conventional procedure for FPSWH testing is to collect data once the collector has attained near steady state conditions, i.e. 30-45 minutes to allow outlet temperatures to attain temperatures above inlet and room temperatures [117]. The experimental set up as detailed by Figure 3.4 was set outdoors and thermocouples connected to the data logger which was powered by electricity (240 V ac power source). In order to maximize insolation received, the collector was oriented due North and TMPV 206 Solar Irradiance Meter was used to measure incoming radiation intensity for that orientation. The tests were conducted and data collected from 9.30am to 4.30am at a uniform interval of 10 minutes and results are presented in the next chapter. One of the following parameters such as flow rate, tilt angle, air gap, air pressure inside the FPSWH and number of glazing was varied while the others were held

Figure 3.15: Preliminary experimental set-up for the FPSWH

constant in order to ascertain its effect on performance of FPSWH. The tests were done between February to June 2016. The following subsections explain how specific test for a given parameter was conducted.

3.5.1 Procedure for Varying Number of Glazing Glass

At atmospheric pressure, inclination of 8^0 and flow rates of 7 litres per hour, the FPSWH was at first tested without glazing glass from 9.00am to 4.30am. A glazing glass was added with an air gap of 50mm, then tested from 9.00am to 4.30pm the next day. A second glass was added with a first air gap of 60mm and second air gap of 20mm and then tested from 9.00am to 4.30pm on a different day.

3.5.2 Procedure for Varying the Air Gap

At atmospheric pressure, inclination of 8^0 and flow rates of 7 litres per hour, the glass pane was placed at 50mm above absorber plate (air gap of 50mm) and tested from 9.00am to 4.30pm. Then it was adjusted to 70mm above absorber plate and later to 90mm and tested the from 9.00am to 4.30pm on different days for each air gap.

3.5.3 Procedure for Varying The Air Pressure Inside the FPSWH

For this test, an air gap of 60mm, single glazing glass, inclination of 8^0 and flow rate of 7 litres/hour were maintained while the pressure of air inside the FPSWH was varied from one atmospheres to 2500 pa as indicated by Equation 3.53 for an air gap of 60mm.

3.5.4 Procedure for Varying the Tilt Angle

At atmospheric pressure,single glazing and flow rates of 7 litres per hour, the FP-SWH was oriented in a North-south direction as it was tilted from 0^0 to 60^0 in an interval of 10^0 and each tilt angle tested from 9.00am to 4.30pm.

3.6 Uncertainty Analysis

It is quite difficult to measure a physical quantity with zero uncertainty. Uncertainty is the magnitude expressing the discrepancies between the true and measured quantities [118]. Error analysis is the study and evaluation of uncertainties with an

aim to inform the researcher how large their uncertainties are and how to reduce them when necessary [119] . The instruments used to make measurements vary in quality as does the expertise of the researchers using them. Furthermore, parameters that are out of the control of the researcher may cause undesired variations in the quantities that are being measured. These measured values are used in calculations to obtain experimental results that are usually compared with the predictions of theory or with the results of other experiments [118].

In this research the performance of V-grooved FPSWH was based on measured data that utilized a number of equipment and measuring devices such as Irradiance meter, digital weighing scale, thermocouples connected to a data logger and stop watch. The overall uncertainty was obtained from a repeated number of five measurements and a brief analysis is presented with the equations used in evaluating both the instrumental and experimental uncertainties.

3.6.1 Instrumental Uncertainty

Different instruments were used for collection of data for the respective parameters determined. These devices had rated accuracies that independently contributed to the overall measurements. In this work it was possible to establish the uncertainty on dependent variables based on contributions from independent measurements, i.e. propagated uncertainty. This was done through a technique proposed by Robinson and Bevington for estimation of such uncertainties [118]. The performance of the FPSWH involved measurements of incident solar radiation, temperatures of water entering and leaving the FPSWH as well as absorber and glass temperatures, temperatures of lower, middle and upper parts of storage tank. The measured quantities were used to calculate the heat gain from insolation, heat loss from FPSWH, efficiency and stored energy. Thermal efficiency of the FPSWH is calculated from insolation, inlet and outlet temperatures of FPSW as shown by Equation (3.44), and summarized by Equation 3.55 . The uncertainty was evaluated using the general

Equation 3.56.

$$\eta = \eta(\dot{m}, T_{in}, T_{out}, I, \tau, A_{ap}) \tag{3.55}$$

$$\sigma_\eta = \sqrt{\left(\frac{\partial \eta}{\partial \dot{m}} U_{\dot{m}}\right)^2 + \left(\frac{\partial \eta}{\partial T_{in}} U_{T_{in}}\right)^2 + \left(\frac{\partial \eta}{\partial T_{out}} U_{T_{out}}\right)^2 + \left(\frac{\partial \eta}{\partial I} U_I\right)^2 + \left(\frac{\partial \eta}{\partial \tau} U_\tau\right)^2 + \left(\frac{\partial \eta}{\partial A_{ap}} U_{A_{ap}}\right)^2} \tag{3.56}$$

where $U_{\dot{m}}$, $U_{T_{in}}$, $U_{T_{out}}$, U_I and $U_{A_{ap}}$ were the uncertainties from the respective parameters (mass flow rate,inlet and outlet temperatures, insolation, glass transmittance and absorber plate area). Some parameters were measured using more than one equipment and hence propagated uncertainty was calculated as demonstrated below;

- Mass flow rate; Mass flow rate is calculated as

$$\dot{m} = \frac{mass}{time} = \frac{m}{t} \tag{3.57}$$

hence two measuring equipment were used; a stop watch with manufacturers accuracy specified as ± 0.1 seconds, ie ($\sigma_t = \pm 0.1s$) and a weighing scale with manufacturers accuracy specified as ± 0.1 grams,ie ($\sigma_m = \pm 0.1g$). Since $\dot{m} = function(m, t)$, similarly, uncertainty of mass flow rate is given as

$$\sigma_{\dot{m}} = function(\sigma_m, \sigma_t) \tag{3.58}$$

$$\sigma_{\dot{m}} = \sqrt{\left(\frac{\partial \dot{m}}{m} \sigma_m\right)^2 + \left(\frac{\partial \dot{m}}{t} \sigma_t\right)^2} \tag{3.59}$$

Partial derivative of mass flow rate with respect to mass and time is given as

$$\frac{\partial \dot{m}}{\partial m} = \frac{\partial}{\partial m}\left(\frac{m}{t}\right) = \frac{1}{t} \tag{3.60}$$

$$\frac{\partial \dot{m}}{\partial t} = \frac{\partial}{\partial t}\left(\frac{m}{t}\right) = -\frac{m}{t^2} \tag{3.61}$$

Hence

$$\sigma_{\dot{m}} = \pm\sqrt{\left(\frac{1}{t} \sigma_m\right)^2 + \left(-\frac{m}{t^2} \sigma_t\right)^2} \tag{3.62}$$

Expressing the uncertainty as relative to the values measured we get

$$\frac{\sigma_{\dot{m}}}{\dot{m}} = U_{\dot{m}} = \pm\sqrt{\left(\frac{\sigma_m}{m}\right)^2 + \left(-\frac{\sigma_t}{t}\right)^2} \tag{3.63}$$

and in percentage

$$U_{\dot{m}} = 100 \times \sqrt{\left(\frac{\sigma_m}{m}\right)^2 + \left(-\frac{\sigma_t}{t}\right)^2} \tag{3.64}$$

- Inlet and outlet Temperatures were measured using thermocouples and read out using a data logger with manufacturers specified precision of $\pm 0.1^0$C, ie ($\sigma_T = \pm 0.1^0$C). Therefore the uncertainty is expressed as quotient of data loggers accuracy with the measured value

$$U_T = \pm\frac{\sigma_T}{T} \tag{3.65}$$

- Insolation, I, and transmittance, τ, were measured using irradiance meter with manufacturers accuracy of $\pm 1 watts/m^2$, ie ($\sigma_I = \pm 1 W/m^2$) and there uncertainties expressed as

$$U_I = \pm\frac{\sigma_I}{I} \tag{3.66}$$

$$U_\tau = \pm\sqrt{\left(\frac{\sigma_\tau}{I'}\right)^2 + \left(\frac{\sigma_I}{I}\right)^2} \tag{3.67}$$

  where I is the insolation measured using irradiance meter above the cover glass while I' is the insolation measured below the cover glass.

- Absorber plate area was measured using a meter rule with an accuracy of $\pm 0.1m$ hence uncertainty in the absorber plate area was given as

$$U_{A_{ap}} = \pm\sqrt{\left(\frac{\sigma_{L_2}}{L_2}\right)^2 + \left(\frac{\sigma_{L_3}}{L_3}\right)^2} \tag{3.68}$$

Similarly, Equation (3.56) was rewritten as a percentage to give Equations (3.69 and 3.70).

$$\frac{\sigma_\eta}{\eta} = 100\sqrt{\left(\frac{\sigma_{\dot{m}}}{\dot{m}}\right)^2 + \left(\frac{\sigma_{T_{in}}}{T_{in}}\right)^2 + \left(\frac{\sigma_{T_{out}}}{T_{out}}\right)^2 + \left(\frac{\sigma_I}{I}\right)^2 + \left(\frac{\sigma_\tau}{\tau}\right)^2 + \left(\frac{\sigma_{A_{ap}}}{A_{ap}}\right)^2} \quad (3.69)$$

$$U_\eta = 100\sqrt{(U_{\dot{m}})^2 + (U_{T_{in}})^2 + (U_{T_{out}})^2 + (U_I)^2 + (U_{A_{ap}})^2 + (U_\tau)^2}, \quad (3.70)$$

From Equation (3.70), the uncertainty for thermal efficiency of the single glazed FPSWH was determined as 3.57%, while that of double glazed FPSWH and partially evacuated single glazed FPSWH were calculated as 3.92% and 4.5% respectively.

3.6.2 Experimental Uncertainty

The data collected repeatedly under a specified condition showed a spread about the mean. The deviations of these data from the mean were evaluated for a sample to determine the experimental uncertainty. The standard deviation is the most used technique as proposed by Robinson and Bevington [118], given by Equation (3.71). The coefficient of variation (COV) can also be used to measure the variability of the obtained data relative to its mean as given by Equation (3.73). Taking mass flow rate for instance,

$$\sigma_\eta = \sqrt{\frac{1}{N-1}\sum_{i=1}^{N}(\eta_i - \overline{\eta})^2}, \quad (3.71)$$

where N was the number of repeated measurements, η was the thermal efficiency and $\overline{\eta}$ was the average thermal efficiency for each experimental set up given by Equation (3.72).

$$\overline{\eta} = \frac{1}{N}\sum_{i=1}^{N}\eta. \quad (3.72)$$

$$COV = \frac{\sigma}{\overline{\eta}}, \quad (3.73)$$

where σ_η is the standard deviation and $\overline{\eta}$ is the mean of the obtained data.

$$\overline{\eta} = \frac{1}{n}(\eta_1 + \eta_2 + \eta_3 + ... + \eta_n), \tag{3.74}$$

The quotient of standard deviation over calculated thermal efficiency was taken as uncertainty which was expressed as a percentage to give Equation (3.75).

$$\frac{\sigma_\eta}{\eta} = U_\eta = 100\frac{\sqrt{\frac{1}{N-1}\sum_{i=1}^{N}(\eta_i - \overline{\eta})^2}}{\overline{\eta}}. \tag{3.75}$$

Efficiency of a FPSWH is calculated from parameters such as insolation, inlet and outlet water temperatures and flow rate. Five readings were taken repeatedly for all the parameter for five days and used in evaluation of the experimental uncertainties in thermal efficieny. The results in Tables 3.6.2 and 3.6.2 indicate the reproducibility of the data. The uncertainty was less than 5.0% and the deviation corresponds with the range of accuracy of instrumental uncertainties.

Table 3.5: Standard Deviation of thermal efficiencies of FPSWH

Type of FPSWH set up	Average value	Standard deviation (%)
Single glazed FPSWH		3.5
Double glazed FPSWH		3.8
Partially evacuated single glazed FPSWH		4.0

Table 3.6: Standard Deviation of experimental parametric values

Parameter	Average value	Standard deviation (%)
Insolation	700Watts/m^2	4.7
Flow rate	5Litres/hour	0.7
Evacuation air pressure	2500Pa	4.0
Water inlet temperature	23^{0}C	1.3
Water outlet temperature	70^{0}C	1.6

The instrumental and experimental uncertainties show that the data obtained over a repeated set of experiments depicted the performance of the FPSWH under test.

CHAPTER FOUR

RESULTS AND DISCUSSION

4.1 Background

Flat Plate Solar Water Heaters (FPSWH), lose about 40% of the absorbed energy via radiative and convective heat transfer .This limits their performance to a maximum efficiency of 60% and peak out put temperatures of 60-70^{0}C at an average flow rate of 0.003 kg/s. Radiative and convective heat transfer coefficients are dependent on design parameters such as air gap, water flow rate, air pressure inside the collector, number of glazing, tilt angle among others. In order to optimize performance of a given FPSWH, finding optimal values of these parameters is crucial and in this chapter performance of the collector is analyzed as each parameter was varied while others were held constant.

The data presented in this section was collected from exposing the collector to sunlight and weather elements outdoors. This chapter discusses how the optimal values of the parameters are chosen for reduced heat loss coefficients and increased efficiency. The tests were done from months of February to June where beam radiation varied from 150-1050 Watts/m^2 due to dynamic cloud cover. The morning hours from April to June were particularly cloudy and chilly contributing to low efficiencies in the morning and evenings. However, some days had more solar intensities than others hence the collector attained temperatures above 70^{0}C. The collector was oriented in North-South direction, to allow tilting towards sun which keeps shifting its inclination angles with different seasons, and no sun tracking mechanism was used.

4.1.1 Influence of Flow Rates on Performance

The tests were conducted for 5 litres/hour, 7.5litres/per hour, 8.5litres/hour and 23litres/hour. For each value of flow rate, the tests were conducted for three days consecutively as tabulated by Figure 4.1.1 for temperatures and Figure 4.1.1 for

efficiency.

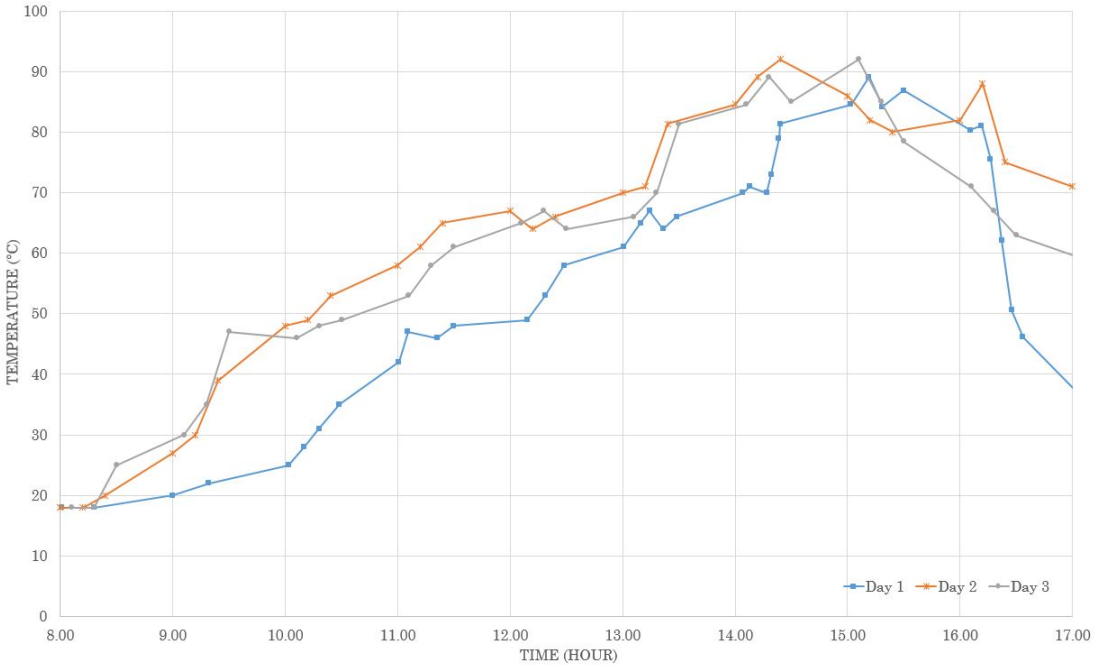

Figure 4.1: Temperatures versus time for 5 Litres/Hour flow rates

The temperature data was recorded every 20 minutes from 08.00 am to 17.00 pm as outlined in the procedure highlighted above. Then the data was averaged and tabulated together as shown by Figure 4.1.1 for ease of comparison.

From Figure 4.1.1, it can be observed that peak temperatures of hot water exiting FPSWH were higher for smaller flow rates, 0-10 litres/hour, as there was sufficient residence time resulting to more heating. It is also observed that flow rates of 5.0-7.8 litres/hour allowed water exiting the FPSWH to attain temperatures of above 50^0C thus are recommended for domestic washing and bathing activities which require water at temperatures about 40^0C. It is evident from results that flow rates of 8.5-25 litres/hour failed to achieve water outlet temperatures of above 40^0C and are therefore recommended for pool heating. As expected, instantaneous efficiencies were higher for larger flow rate values due to high heat removal factor which is

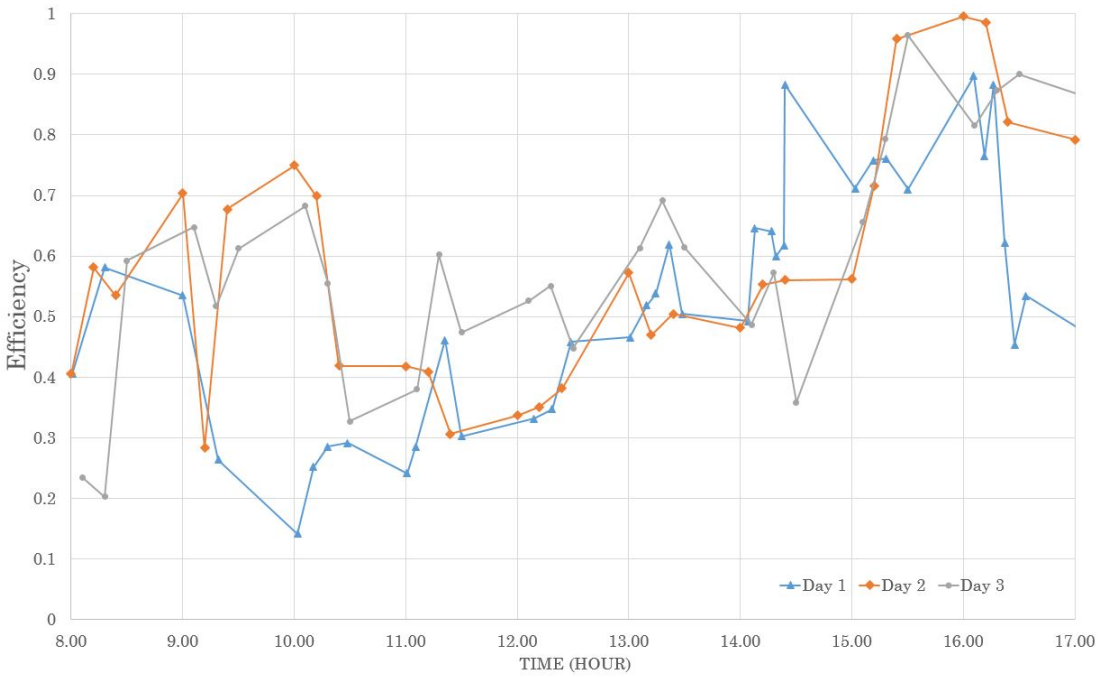

Figure 4.2: Efficiency versus time for 5 Litres/Hour flow rates

directly proportional to flow rate. This is well illustrated by lines of best fit plotted on Figure 4.1.1. Figure 4.1.1 illustrates comparison of instantaneous efficiency and exergetic efficiency for the experimental volumetric flow rates. It is observed that for this particular FPSWH, a volumetric flow rate of 7.5 litres/ hour gives the circulating water just optimal residence period to achieve temperatures of about 80^0 C at instantaneous and exergetic efficiencies of 0.54 and 0.46 respectively. Exergetic efficiency is calculated using Equation 3.45. Coincidentally, this optimal volumetric flow rate is closer to the design value of 7.0 litres/hour and a similar value was experimentally obtained by Dagdougui et al. [120] and by Ghimire and Pokhrel [8] during their analysis of Flat Plate Solar Water Heaters (FSWH).

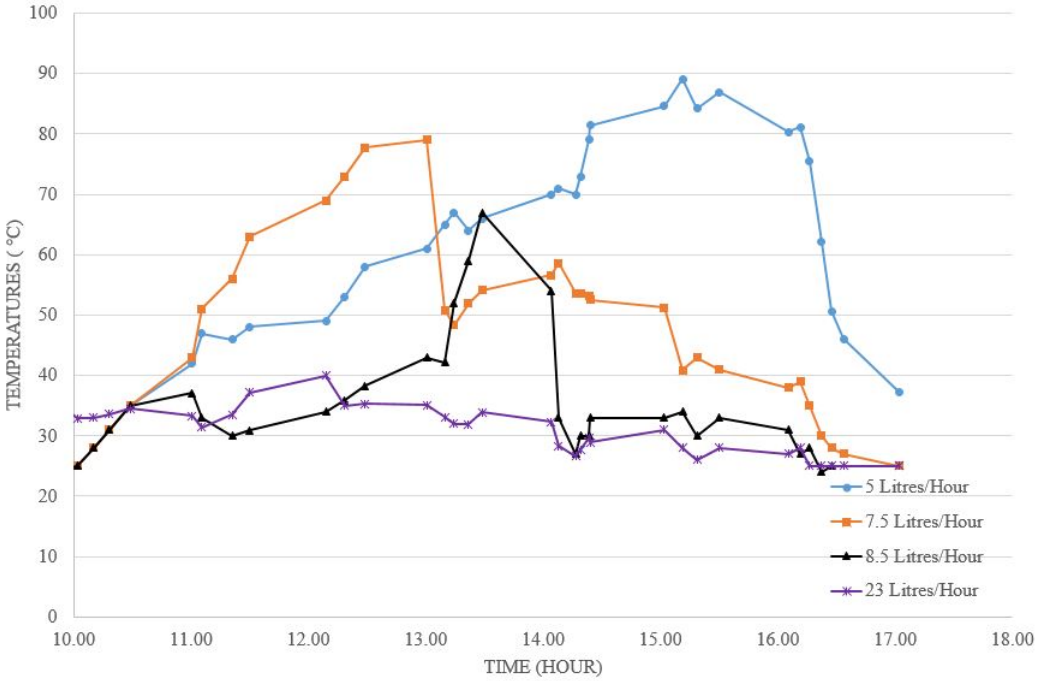

Figure 4.3: Temperatures versus time for varying flow rates

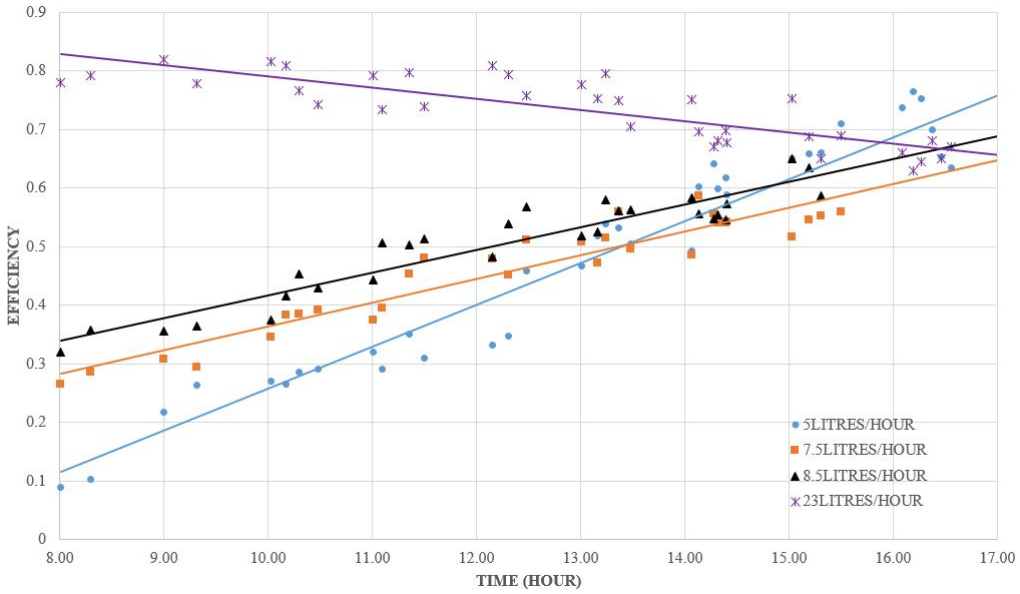

Figure 4.4: Efficiency at varying Volumetric Flow Rates

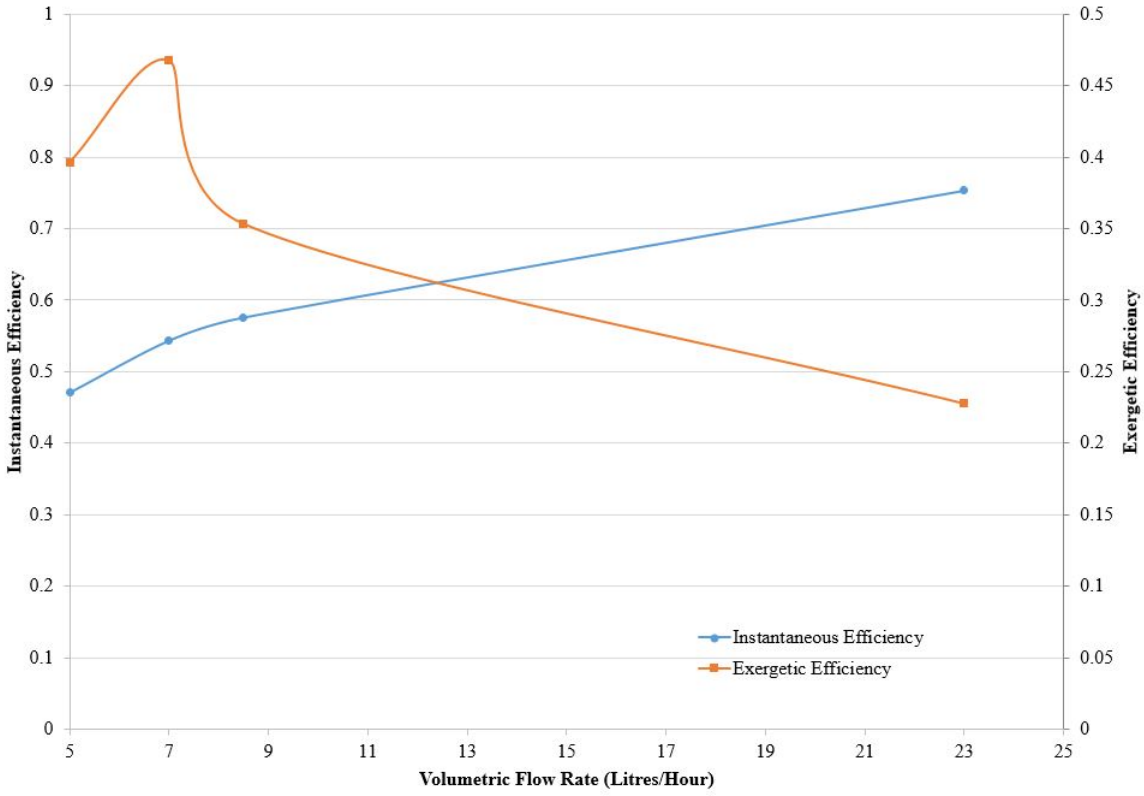

Figure 4.5: Influence of Volumetric Flow Rate on collector efficiency

4.1.2 Influence of Number of Glazing on Performance

Glazing of flat solar collectors play a crucial role of isolating the FPSWH from winds and introducing green house effect to lower radiative heat loss. For this test, design parameters such as flow rate of 7 litres/hour, 1 atmospheric pressure and tilt angle of 8^0 were held constant as number of glazing were varied and tested. For single glazing, an air gap of 60mm was used while for double glazing, air gaps of 50mm and 20mm were used, based on findings by, [121, 122], and design calculations in methodology. From Figure 4.1.2, temperatures above 85^0C were attained with a single glazing followed by double glazing, 79^0C and lastly unglazed FPSWH, 59^0C. Though double glazed FPSWH was more efficient, as illustrated by Figure 4.1.2, single glazed FPSWH attained higher temperatures. This was because of low trans-

mittance of window glass (85-90%) used as glazing, hence reducing transmittance of solar radiation to below 70% for a double glazed FPSWH. These results are in agreement with those obtained by Ihaddadene et al. [121] who also used commercial window glass as type of glazing. However, temperature changes of hot water exiting FPSWH, which are much affected by variation in insolation, were less pronounced in double glazed FPSWH as compared to unglazed FPSWH. This could be attributed to the high temperatures of air inside the first air gap as well as heat absorbed by both glasses which served as a temporary storage of heat in double glazed FPSWH. Double glazing also means double green house effect which lessens irradiation from the absorber plate.

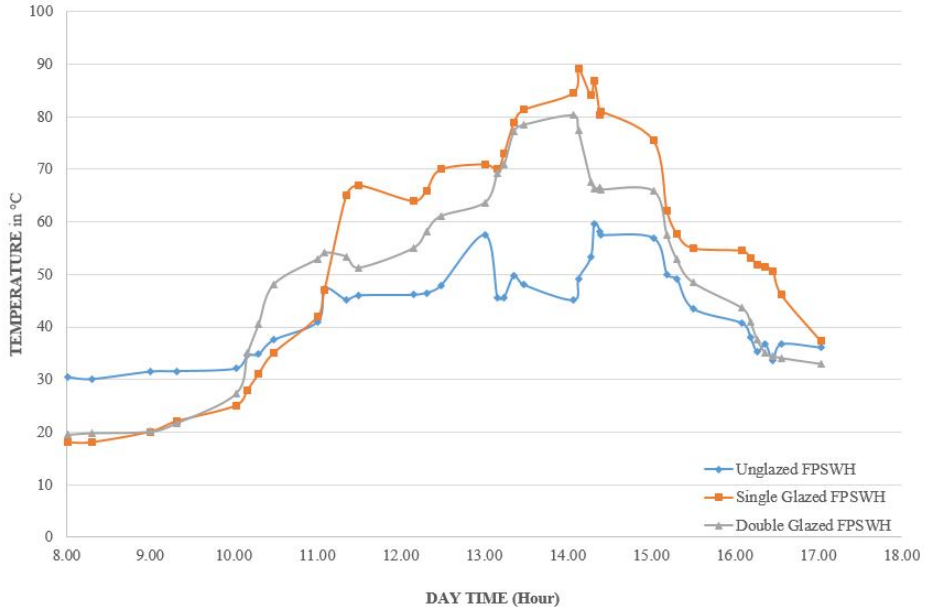

Figure 4.6: Temperatures versus time for varying number of glazing

From Figures 4.1.2 and 4.1.2, it is noted that from about 8.00 am to 10.00 am, the FPSWH warmed up in the order of glazing beginning with unglazed, single glazed and lastly double glazed FPSWH. This behavior is ascribed to cosine effect, [34], presented by morning hourly angles. Cosine Effect is reduction of radiation by the cosine of the angle between the solar radiation and a surface it is incident

on. Cosine effect is increased by the number of surfaces the solar radiation falls on, hence unglazed FPSWH was able to outperform glazed counterparts in the morning as illustrated by Figure 4.1.2 while double glazed FPSWH registered poor performance at the same time as seen in Figure 4.1.2.

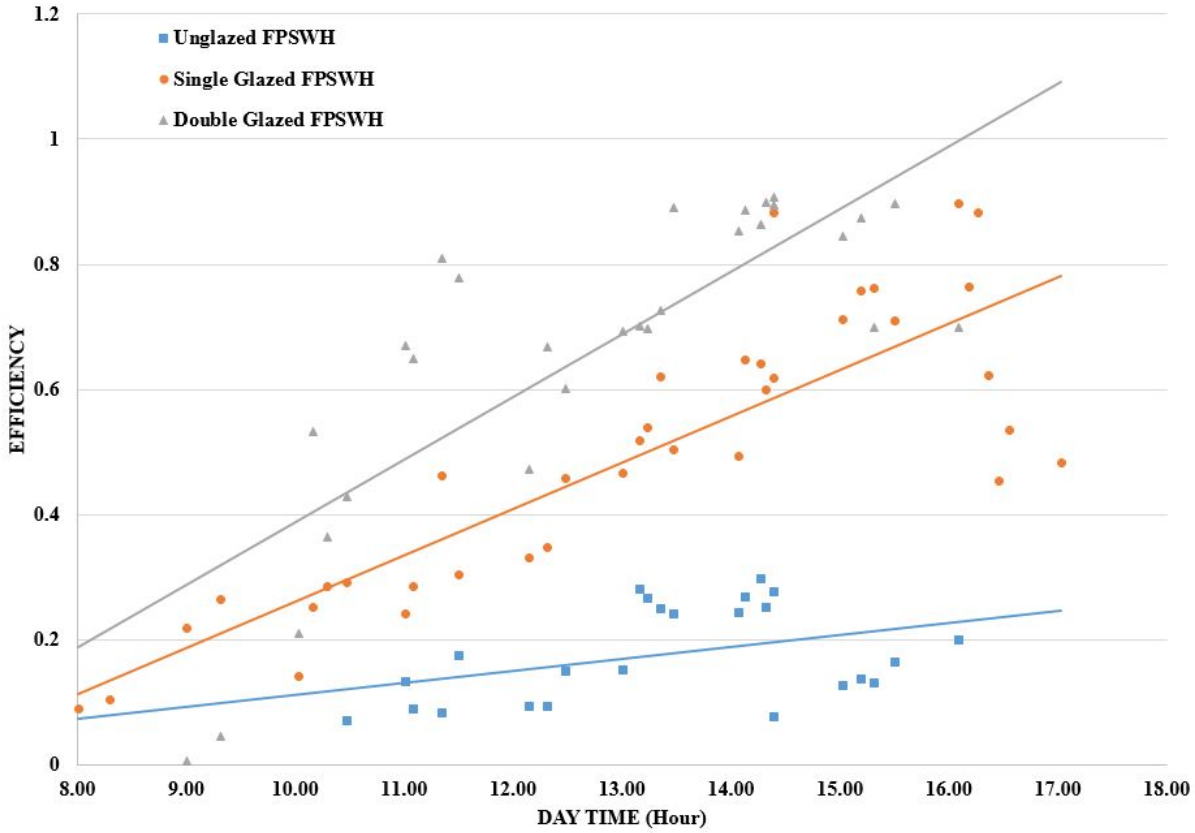

Figure 4.7: Efficiencies of different glazing against Time

4.1.3 Influence of Varying Air Pressure Inside the FPSWH

As Figure 4.1.3 shows, temperatures of above 80^0C are attained with FPSWH with air evacuated at 2500 Pa,(absolute pressure), at 12.00 noon and maintained for four hours till 4.00pm. The FPSWH with air at one atmosphere attains temperatures of 80^0C at 4.00pm and maintains it for less than 20 minutes only. It is observed

that the temperatures of the water exiting evacuated FPSWH were higher than that of un-evacuated FPSWH in the entire experimental period. It is therefore inferred that evacuated FPSWH conserved most of the absorbed energy which was in turn passed to the circulating fluid. This ability to conserve energy is accredited to reduced convectional heat transfer from the absorber plate to the glass cover since low pressure of below 2500Pa curtail buoyancy driven heat and mass transfer that is much experienced in un-evacuated FPSWH in form of buoyancy driven multi-cells [43, 71, 123].

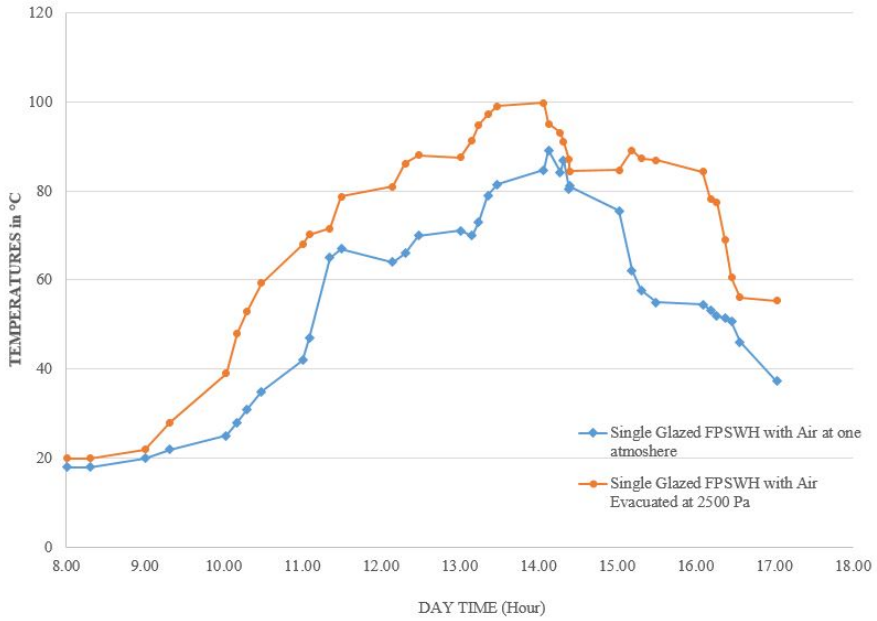

Figure 4.8: Temperatures for un-evacuated and partially evacuated FP-SWH

Reducing air pressure inside the FPSWH reduces heat loss hence making the plate more efficient as illustrated by Figure 4.1.3, where it is seen that evacuated FPSWH performed well especially in the morning hours but after mid-day, the difference in performance between un-evacuated and evacuated FPSWH was less pronounced. However, fluctuations in solar radiation intensities caused by variation in sky clearance index contributed to scatter of instantaneous efficiency below 70% and above 90% for the evacuated FPSWH, as shown in Figure 4.1.3. High instantaneous efficiency above 90% were mostly witnessed, for the evacuated case, when declines in insolation were preceded by periods with high intensity solar radiation of above 1000 Watts/m^2. This observation is consistent with research done by Hossein and

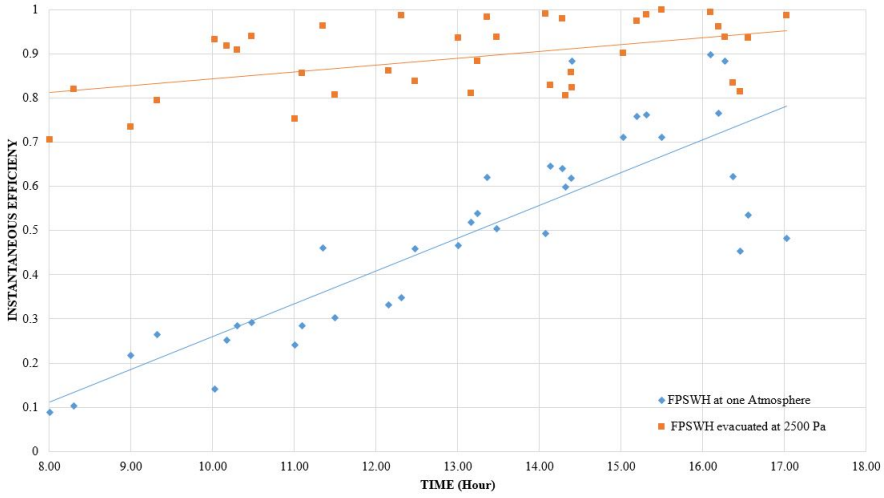

Figure 4.9: Efficiency for both un-evacuated and evacuated FPSWH

Saidi [124] on effects of air pressure on natural convectional heat transfer. From their experiment, they concluded that low pressure means low density which in turn means reduced/low Rayleigh number and Nusselt number resulting in low convection heat transfer coefficient. Benz and Beikircher [43] also conducted a similar experiment, though they used Krypton gas at a pressure of 50 Pa, and achieved an efficiency of 45% at absorber plate temperature of above 150^{0}C.

4.1.4 Influence of Tilt Angles on Performance

Tilt angle is the angle the FPSWH is inclined to in order to maximize absorbed solar radiation [125]. Due to earth's revolution around the sun, each geographical location on earth's surface experiences variation of the position of mid-day sun and this variation is significantly affected by the location's latitudinal angle [126].

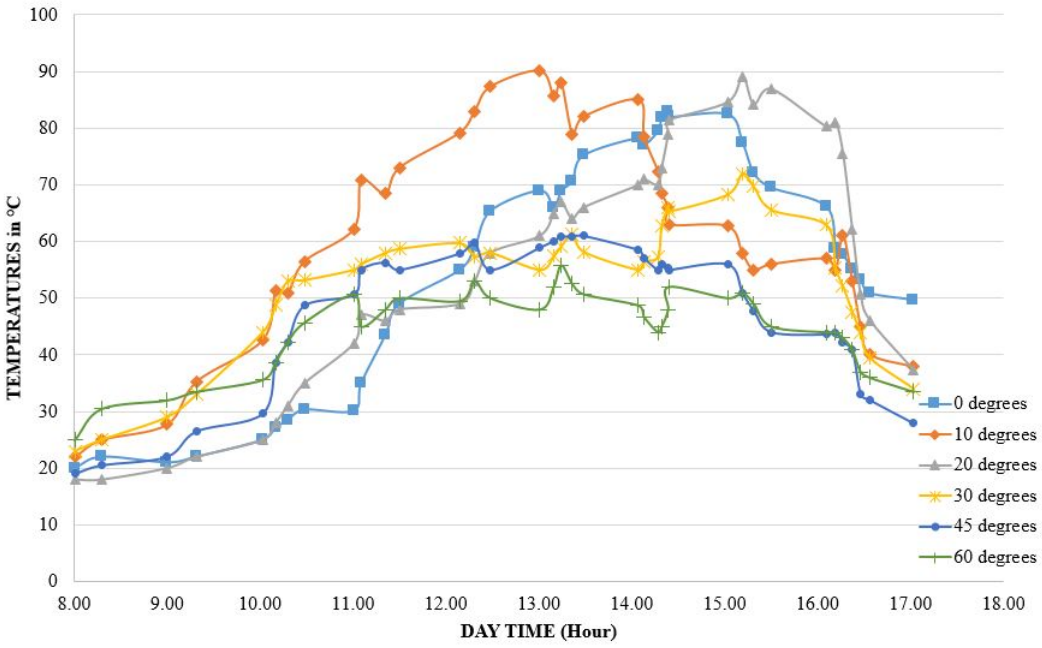

Figure 4.10: Temperature curves for different tilt angles

Hence calculation of optimal tilt angle is paramount for each month of the year. From Figure 4.1.4, it is observed that FPSWH with tilt angles of 0-20^0 discharged hot water with peak temperatures above 80^{0}C while those with tilt angles of 30-45 ^{0} obtained peak temperatures of 60-70^{0}C and lastly a FPSWH inclined to 60^0 achieved maximum peak temperatures of 50-55^{0}C. This implies that tilt angles of 0-20^0 enabled the FPSWH to absorb more energy from solar radiation incident on them. Figure 4.1.4 illustrates effect of tilt angle on instantaneous efficiency where it is observed that performance of FPSWH increases from horizontal to an inclination angle of 10^0 and decreases from an inclination of 10^0 to 60^0. Tilt angles play a crucial

role of reducing cosine effect on radiation falling on to a surface. From Figure 4.1.4, it is observed that for Juja (Kenya) on a month of March, optimal tilt angle is 10^0 and further increase in tilt angle increases cosine effect thus causing loss of energy. This data agrees with research findings of Gacuca's [127] experiments with an integrated solar collector at Juja which indicate that tilt angles of 10-15^0 absorbed more solar radiation and allowed thermosyphon action to take place earlier than in the other tilt angles.

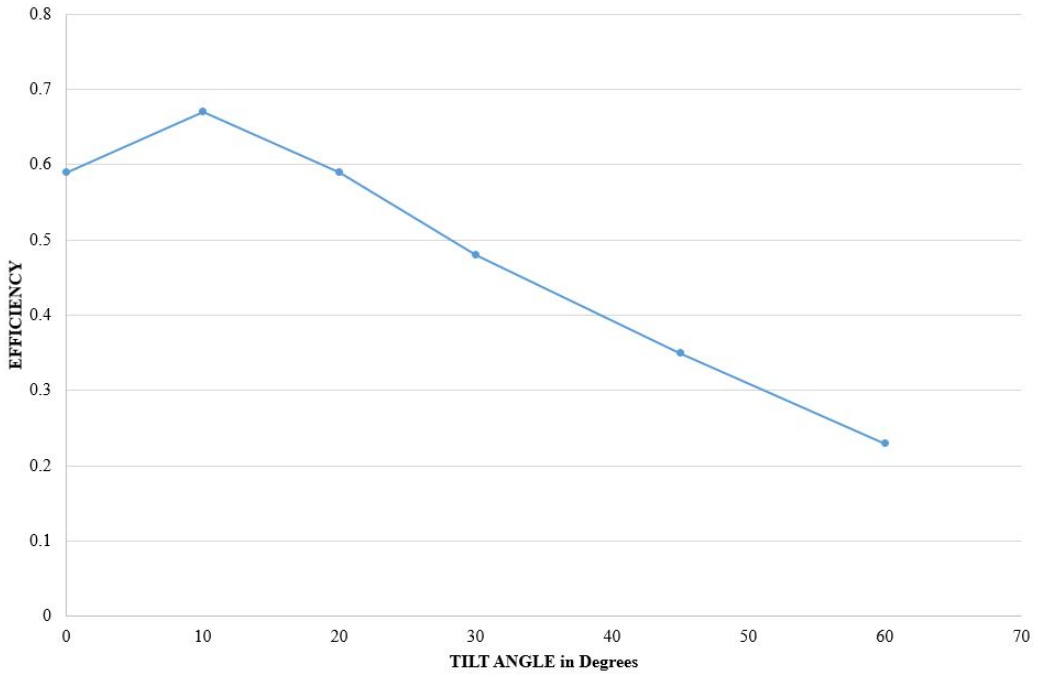

Figure 4.11: Effect of tilt angles on efficiency

4.1.5 Influence of Air Gap on Performance

Air-gap, which is the distance between absorber plate and glass cover, has significant effect on convective heat transfer from absorber plate to the glazing glass unless the space is completely evacuated of air [38]. Three air gaps were considered for this experimental test, 50mm, 60mm & 70mm and from Figure 4.1.5, it is observed that the V-grooved FPSWH performed quite well with the three air gaps by attaining temperatures above 70^0C for a constant flow rate of 7 litres/hour. Figure 4.1.5 shows

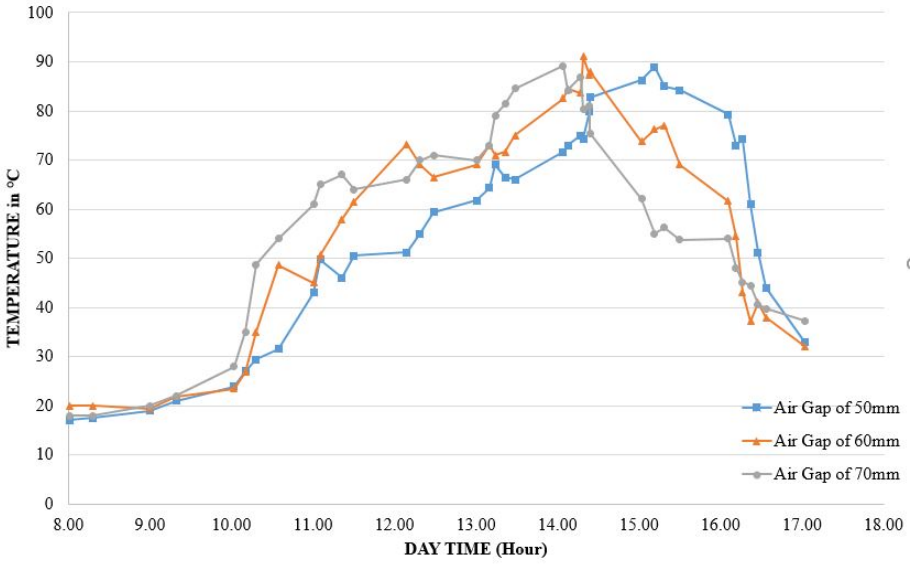

Figure 4.12: Temperatures attained at different air gaps

that air gaps of 60mm gave better performance by attaining an average efficiency of 0.6 on a day that was mostly overcast, i.e. had low sky clearance index with an average insolation of 500-600 W/m^2.

For the 50mm air gap, it is observed from Figure 4.1.5 that temperatures of above 40^{0}C and 70^{0}C were attained at 11.00am and 2.00 pm respectively, while peak temperatures are attained at 3.00pm. At 60mm air gap, temperatures of above 40^{0}C and 70^{0}C were attained at 10.30am and 12.00 pm respectively, while peak temperatures are attained at 2.00pm. At 70mm air gap, temperatures of above 40^{0}C and 70^{0}C were attained at 10.00am and 12.30 pm respectively, while peak temperatures are attained at 2.00pm. Figure 4.1.5 illustrates that FPSWH air gaps of 50mm, 60mm and 70mm discharged hot water at temperatures of above 70^{0}C for 2 hours, 3 hours and $1\frac{1}{2}$ hours in that order. This implies that air gap of 60mm was more efficient, as indicated by Figure 4.1.5 though marginally, as the three gaps 50mm 60mm and 70mm recorded an average instantaneous efficiency of 56%, 60% and 57% respectively. Performance of a v-grooved FPSWH is affected

by v-angle, air gap and depth of v-channels. 60mm air gap provided a distance of 50mm from the crest of v-channels,(hottest regions of v-channels), to the glass which confines convectional flow in laminar region thus reduced convectional heat loss due to insignificant air conduction in this air gap. However, 70mm air gap allowed both turbulent and laminar heat flows hence increased convectional heat loss. 50mm air gap allowed both air conduction and laminar convectional flow that also resulted in increased heat loss.

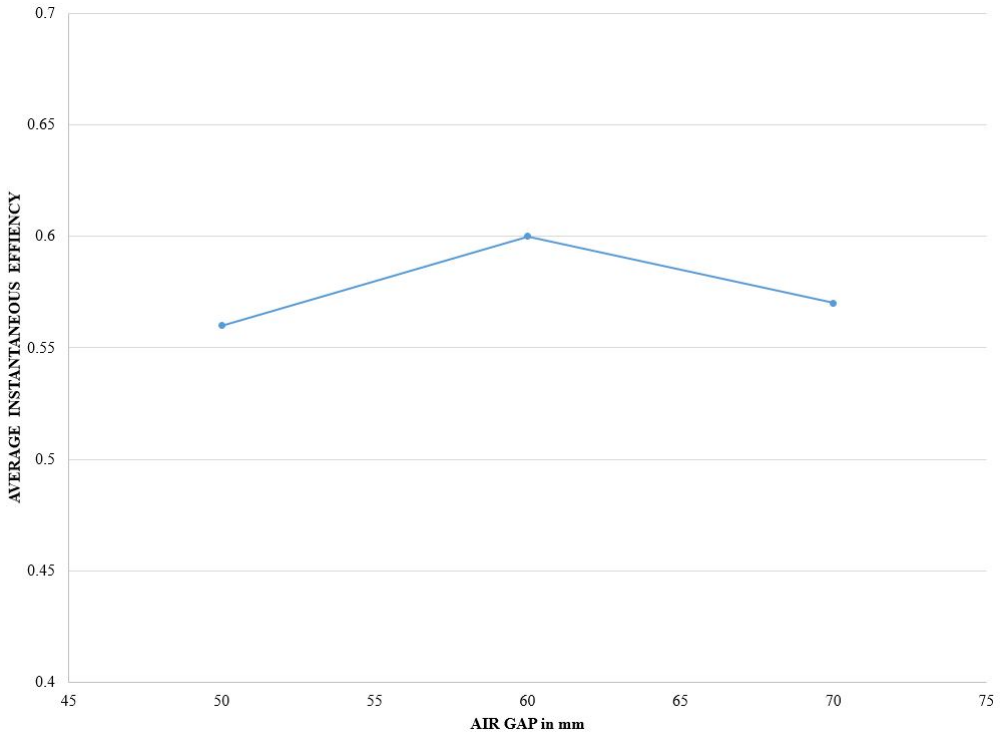

Figure 4.13: Efficiency graph summarizing effects of air gaps

From literature, free convection is inhibited at an air gap of 0-7mm although heat conduction by air dominate the heat losses [38]. Convective heat transfer coefficient for air gaps of 7-20mm exceed 5.0 kW/m^2 but increase in air gaps from 20mm to 100mm experience reduction in convection heat transfer although shading by side walls increase with increase in air gap [38, 128].

4.1.6 Effects of Outer Glass Temperatures on FPSWH Efficiency

Glazing glass (discussed in sub-section 4.1.2 above) serves many purposes such as allowing in insolation and discouraging re-radiation from absorber plate. It also insulates the hot FPSWH from winds & cooler atmospheric air outside it while at the same time heats up to above room temperature. This is illustrated by Figure 4.1.6 where it is observed that outer glass temperature rises from 20^0C at 9.00 a.m. to 62^0C at 01.00 p.m. then drops to 40^0C at 05.00 p.m.. When the air inside the FPSWH is evacuated, Figure 4.1.6, it is seen that outer glass temperature rises from 30 ^{0}C at 9.00 a.m. to 35^0C at 01.00 p.m. and then cools down to 30^0C at 05.00 p.m..

The extent to which the glazing glass heats up is a function of convective heat transfer coefficient from the absorber plate to the glass, tilt angle, absorptance of the glass, intensity of radiation, emissivity of the absorber plate and wind speed outside the FPSWH. Consequently, the temperatures of the glass affect the rate of heat transfer from absorber plate to the glazing glass. As glass temperatures increase, heat loss from the absorber plate reduce thus allowing the FPSWH to achieve peak temperatures and efficiency [84]. Figure 4.1.6 shows instantaneous efficiency increases as glazing glass temperatures rise from 20-60^0C to reach a peak efficiency of 75% and falls as glass temperatures reduce below 50^0C. From Figure 4.1.6, it is observed that efficiency of FPSWH only reaches the peak of 75% after the glass has attained a temperature of above 50^0C. This is because window glass absorbs 8% of incident insolation allowing it to heat up and when it attains temperatures of 50-60^0C, temperature difference between absorber plate and glazing are reduced to below 40^0C at afternoon, which in turn discourage convectional currents hence allowing the FPSWH to achieve high efficiency at peak insolation of about 1000 Watts/m^2.

Figure 4.1.6 illustrates how efficiency increases with increase in outer glass temperatures for a single glazed FPSWH at one atmosphere up to about 55^0C from which

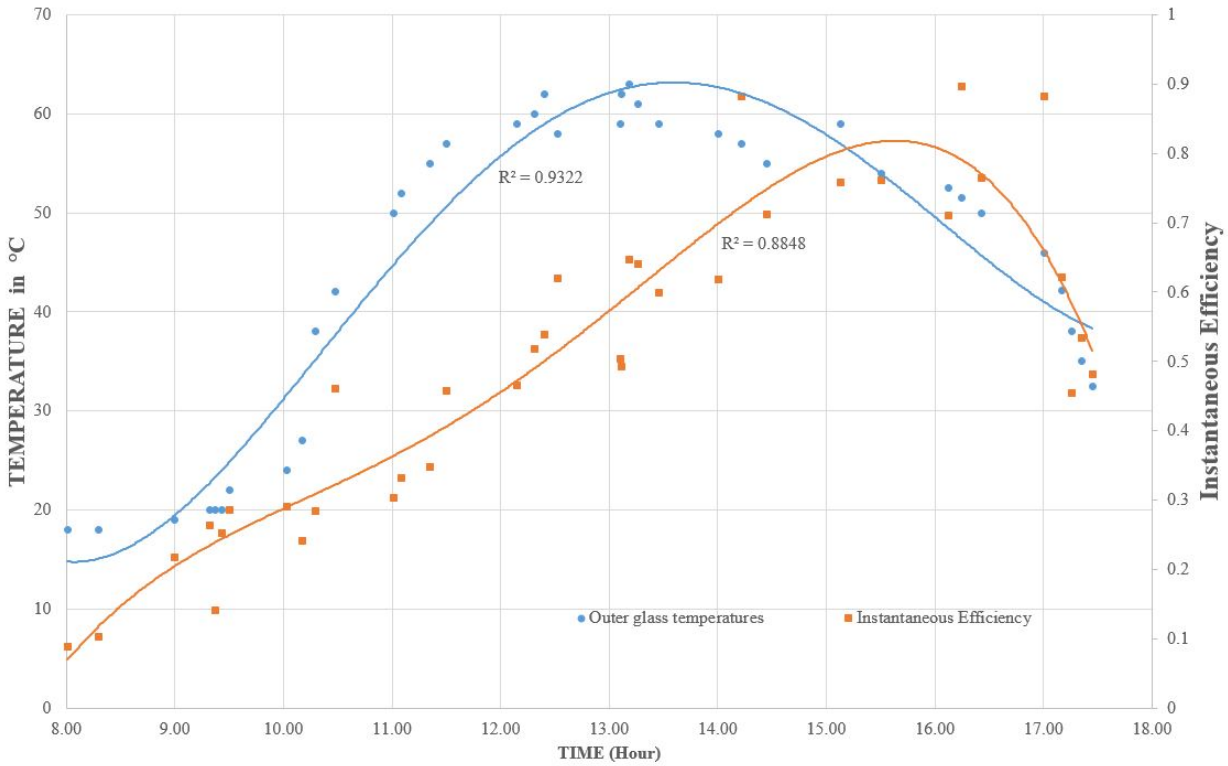

Figure 4.14: Glazing temperatures and efficiency curves for a SG-FPSWH at 1 atmosphere

further increase in glass temperatures result in a drop in efficiency. This figure show that there is an optimal outer glass temperature of 50-55^{0}C at which the collector works at an average efficiency of 70%. The scatter in instantaneous efficiency is contributed by variation in cloud cover that cause changes in intensity of solar radiation.

When the air inside FPSWH was partially evacuated to 2500 Pa, outer glass temperatures did not rise above 33^{0}C and efficiency was maintained above 70% throughout the day as illustrated by Figure 4.1.6. This implies that convection heat transfer played a major role in raising outer glass temperatures as well as contributing more than two thirds of the total top heat loss when Figures 4.1.6 and 4.1.6 are compared.

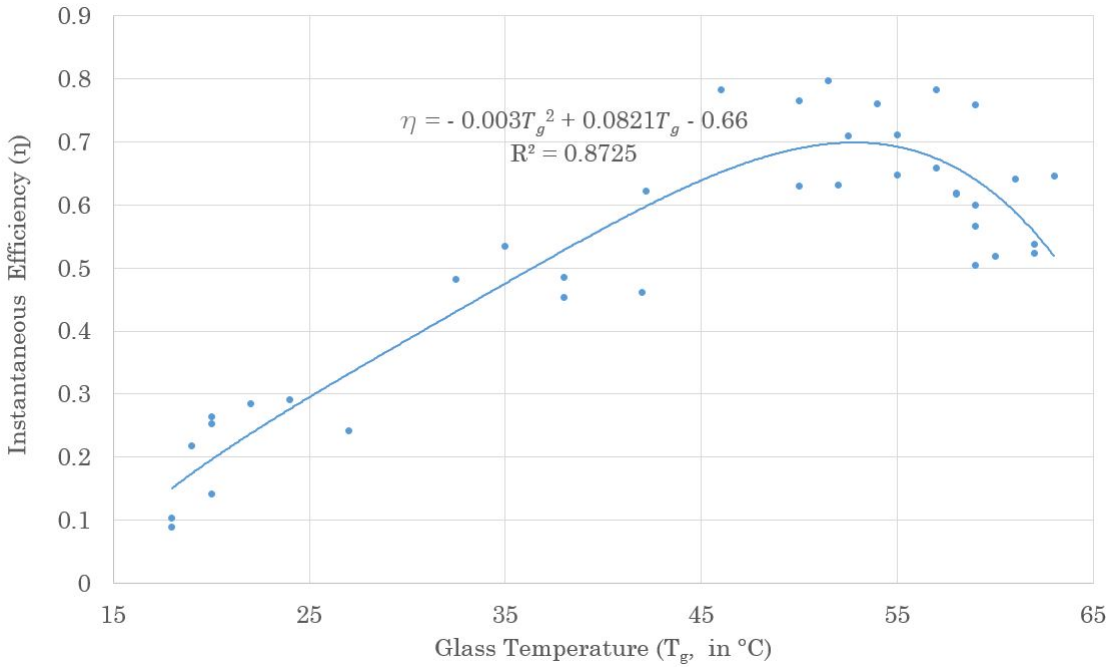

Figure 4.15: Glazing temperatures versus efficiency for a SG-FPSWH at 1 atmosphere

4.2 Optimization of FPSWH

Table 4.2 gives a summary of values of different parameters that were varied in order to ascertain the point at which the V-Grooved FPSWH performed optimally. The parametric values presented are the optimal values for a FPSWH located at Juja, Kenya. However it was noted that, flow rates of above 8litres/hour gave higher efficiency but water exiting the FPSWH failed to achieve temperatures above 40^0C. Hence for larger flow rates to achieve higher temperatures, larger solar capturing area is required as indicated by design calculations in chapter 3.

From the Table 4.2, it was observed that air evacuation allowed the collector to achieve high temperatures at high efficiencies. Similarly, double glazing gave good performance but was limited by use of window glass, which due to low solar transmittance ,($\tau = 0.85 - 0.90$), affected performance of the FPSWH. But since window glass is cheaper, (USD 6.0/m^2), and readily available, both low iron glass (crystalline

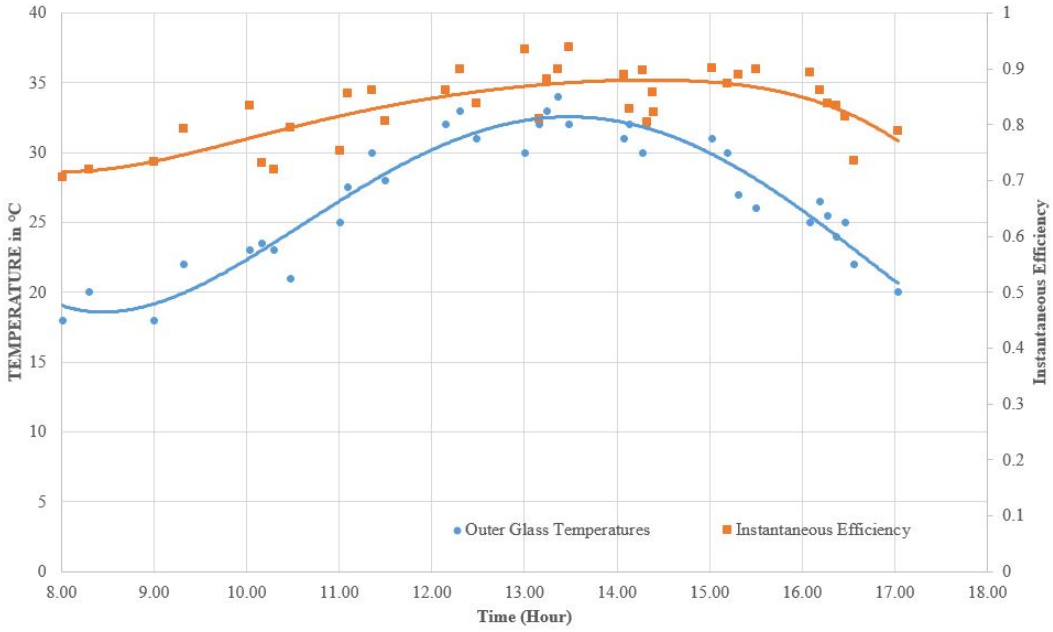

Figure 4.16: Glazing temperatures and efficiency versus time for a SG-FPSWH partially evacuated at 2500 pa

glass) and widow glass can be combined in a double glazed FPSWH to give good transmittance at lower cost. For optimization purpose, the above outlined parametric values were employed on an improved FPSWH. The first glass was maintained as high iron content window glass due to its strength against air evacuation buckling, and the second glass was 2mm low iron glass with transmittance of 95%.

The FPSWH housing was made of three layers of wooden blocks glued together for an airtight bond while the glass was fixed using water resistant adhesives and silicon. However, the FPSWH still experienced loss of vacuum due to difference in thermal expansion of glass and wood at the junctions of the two materials. This compromised the air-tight joints which allowed air into the FPSWH. Thus due to problems of sealing the vacuum, evacuation pressure could not be lowered below 1000 Pa for an air gap of 60mm hence vacuum pump was operated to average 2000-2500 Pa. A flow rate of 7 litres/hour was used instead of 23 litres/hour to allow temperatures of 70-90^{0}C to be attained. Figure 4.2 shows performance of an

textbf

Table 4.1: Summary of parameters that gave high efficiency

Parameters Varied	Value with Highest Efficiency	Highest Efficiency Attained	Peak Temperature Attained	Average Temperature Attained
Flow rate	23 litres/hour	80 %	40 ^{0}C	35 ^{0}C
Number of glazing	2 glass panes	88%	80.3 ^{0}C	51 ^{0}C
Air pressure	2000 Pa	93%	100 ^{0}C	72 ^{0}C
Tilt angle	8^0	67%	90.1 ^{0}C	61 ^{0}C
Air gap	60 mm	66%	91.1 ^{0}C	57 ^{0}C

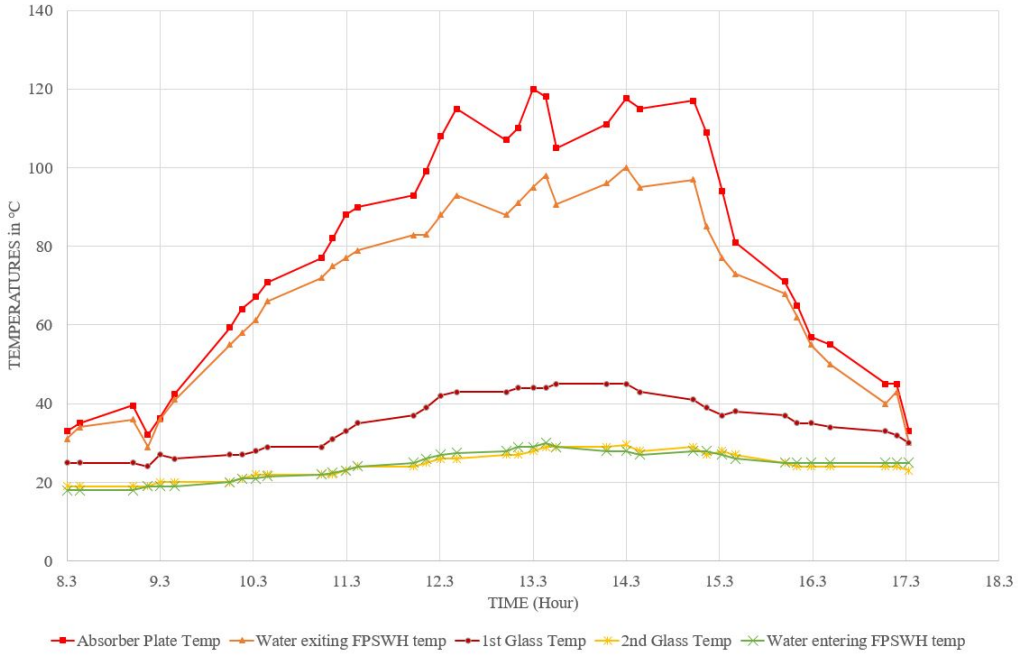

Figure 4.17: Temperatures on an optimized FPSWH

optimized FPSWH in terms of temperatures and Figure 4.2 in terms of efficiency.

It is observed that hot water temperatures of above 40^0C were attained at 10.30am while temperatures of 80^0C were attained at 11.40am and sustained till 3.30pm.

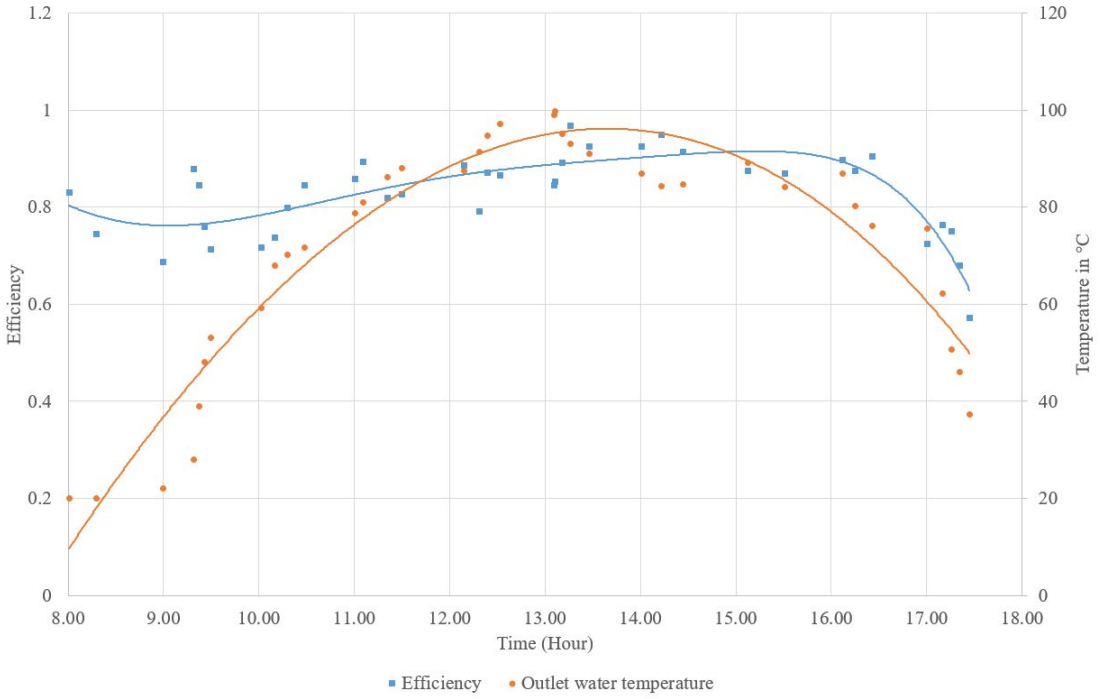

Figure 4.18: Efficiency of the optimized FPSWH

Efficiencies of 0.7-0.88 were attained and maintained throughout the day mainly due to reduced convective and radiative heat transfer. Figure 4.2 also illustrates that outer glass temperatures never exceeded 30^0C the entire experimental period despite absorber plate temperatures exceeding 100^0C and this allowed peak efficiency of 0.9 to be achieved at 2.30pm. This implies that the optimized FPSWH was able to conserve more than 80% of the energy absorbed from the incident insolation.

4.3 Comparison of performance of optimized FPSWH to the Contemporary SWHs in the Market

It was crucial to compare how the optimized v-grooved FPSWH to the existing solar water heaters in the market. This was achieved by comparing the instantaneous efficiencies against the parameter $\frac{T_{in}-T_a}{I}$. T_{in} is the temperature of water entering the FPSWH while T_a is atmospheric temperature measured by a thermometer placed outdoors in a shaded area with free circulation of air. I is the insolation measured in watts. The results were as shown by Figure 4.3.

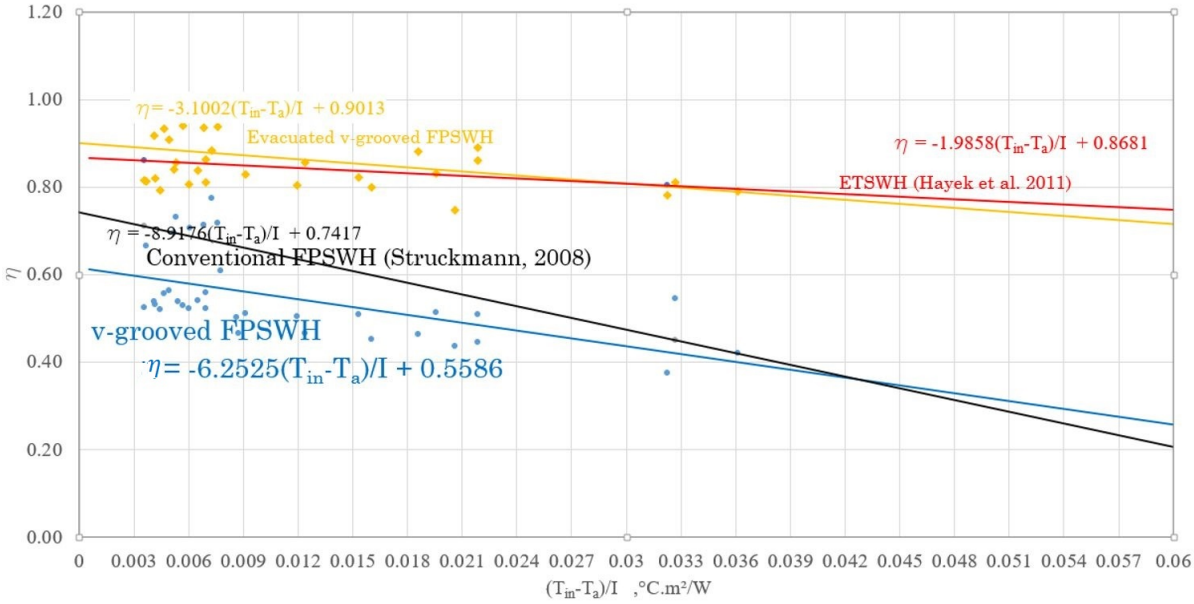

Figure 4.19: Performance of an optimized FPSWH compared to other SWHs

Hayek et al. [129] carried out extensive study of evacuated tube solar water heaters subjected to weather conditions in Beirut and found that efficiency of ETSWH varried between 0.75-0.83 depending on weather conditions. These findings were close to the performance of the optimized FPSWH under the current study as shown in Figure 4.3. The difference, though marginal, may be attributed to effects selective surface on the ETSWH that enable them to perform better for increased $\frac{T_{in}-T_a}{I}$.

Struckmann [63] studied performance of conventional FPSWHs and found out that their typical thermal efficiency ranges from 0.2-0.7. If the FPSWH has selective surface coatings and copper material, its performance ranges from 0.5-0.7 while the others have thermal efficiencies of 0.2-0.5. From Figure 4.3, a conventional FPSWH made of copper material and selective surface coating outperforms the un-evacuated v-grooved FPSWH under this study though it performs dismally compared to the ETSWH. Thus from this comparison, it is seen that partial evacuation of air fron v-grooved FPSWH improves its performance significuntly.

CHAPTER FIVE

CONCLUSION AND RECOMMENDATIONS

5.1 CONCLUSION

The v-grooved FPSWH was fabricated using locally available materials and tested outdoors. From the results obtained, v-grooved FPSWH demonstrated its ability to provide hot water for domestic washing and bathing. Due to its simplicity of construction and high efficiency of 80% (average of 85% when evacuated and 89% when optimized), the collector proved to be a viable alternative for heating water from solar energy in Kenya.

The main objective of this research was to design and fabricate an efficient flat plate solar collector with reduced convectional, conductive and radiative heat losses. From the findings of the results the following conclusions were made;-

- The v-grooved absorber plate was designed to eliminate need of laser and electro-deposition welding commonly used to improve heat transfer in conventional FPSWH. The welded seams and joints for the v-grooved absorber plate were mainly aimed at achieving zero water leakages since heat transfer was accomplished by upper surfaces of the absorber plate. This led to the conclusion that the design is suited to areas without complex welding machines and technology such as Sub-Saharan countries. The design also allowed thin sheet metal to be used with little warping.

- Heat transfer between the absorber plate and circulating water was improved. This was accomplished by reducing the distance between the absorber plate and the water since the water circulated just below the solar absorbing surface hence allowing the collector to achieve hot water temperatures of above 40^0C by 10.00 a.m. and temperatures of about 70-90^0C by 1.00-3.00 p.m.. At the same time un-evacuated FPSWH operated at an average of 70% while

evacuation of air at 2000-2500 Pa allowed it to operate at an efficiency of 80-85%. It can be concluded that v-groove design and evacuation of the FPSWH increased heat transfer.

- Since circulating water flowed beneath the solar absorbing surface, the v-grooved FPSWH exhibited a unique character where instantaneous efficiency increased with increase in solar intensity. Hence for all the experimental tests done on the FPSWH, peak efficiency was attained at mid-day, 12.00pm-3.30pm while mornings and evenings experienced low performance. It can be concluded that v-groove absorber plate design is suitable for tropical and equatorial regions which receive high percentage of direct solar radiation.

- Use of window glass, (high iron content glass), was both a limiting factor due to their low transmittance of $\tau \leq 0.90$ as well as an encouraging factor since their high solar absorptance of 0.08 allowed them to heat up and thus discourage the rate of convective heat transfer. This was illustrated by the experiment that showed instantaneous efficiency increased with rise in outer glass temperature up to 55^0C. It can be concluded that window glass augments v-groove design better than crystalline-low-iron glass thus improving efficiency of the FPSWH.

- V-groove configuration increased absorber plate surface area thus resulting in increased convectional heat losses as witnessed at times of low solar intensity such as mornings and evenings. This problem was overcame by partial air evacuation at 2000 Pa as well as by use of double glazing. It can be concluded that partial evacuation of air at 2000-2500 Pa enabled the collector to perform more efficiently even in the morning and evening hours.

5.2 RECCOMMENDATIONS

The following recommendations were outlined for further study of v-grooved FP-SWH:

- For this research, 3 layers of wooden block-boards were glued together to form FPSWH casing and establish glass seating. However, the wooden housing failed to maintain vacuum pressure of 2000 Pa for more than 1 hour thus necessitating the vacuum pump to be operated throughout the test period. More research is required to establish a better housing and viable means of mating casing and glazing glass.

- When the water temperatures approached 100^0C, the FPSWH started to produce high back pressures that reduced water flow rates through the FPSWH. This behavior required active pumping which was not anticipated. An automated system is required to monitor temperature levels to avoid temperature build up above 95^0C.

- This research utilized a v-angle of 70^0. More exploration of different v-angles is required in order to ascertain effects of v-angle on performance of FPSWH.

- Further study on selective paints or coatings should be applied on the absorber plate to reduce radiative heat loss coefficient.

REFERENCES

[1] N. Girouard, E. Konialis, C. Tam, and P. Taylor, *OECD Green Growth Studies 2012 ; Energy*, 12th ed. France, OECD Publisher.

[2] J. Darmstadter, *Energy and Population*, 4th ed. Germany, Resources for the Future.

[3] A. G. Chmielewski, "Environmental effects of fossil fuel combustion," *Interaction: Energy & Environment*, vol. 4, no. 2, pp. 56–74, 2009.

[4] M. Hoel and S. Kvemdokk, "Depletion of fossil fuels and the impacts of global warming," *Resource and Energy Economics*, vol. 18, pp. 115–136, 1996.

[5] D. Brki, "Are fossil fuels the main cause of todays global warming?" *Working and Living Environmental Protection*, vol. 6, no. 1, pp. 29 – 38, 2009.

[6] K. S. Lackner, "Comparative impacts of fossil fuels and alternative energy sources," *Issues in Environmental Science and Technology;Carbon Capture: Sequestration and Storage*, vol. 29, pp. 1–40, 2010.

[7] S. Chinnammai, "An economic analysis of solar energy," *Journal of Clean Energy Technologies*, vol. 1, no. 1, pp. 18–21, 2013.

[8] N. Ghimire and R. Pokhrel, "Analysis of parameters of locally manufactured flat tube solar water heater to increase the efficiency," *Rentech Symposium Compendium,*, vol. 3, pp. 26–29, 09 2013.

[9] N. Ogie, I. Oghogho, and J. Jesumirewhe, "Design and construction of a solar water heater based on thermosyphon principle," *Journal of fundamentals of renewable energy and applications*, vol. 3, pp. 1–8, 2013.

[10] U. K. Nayak, "Heat transfer and flow friction characteristics of solar water heater with inserted baffles inside the tube," *International journal of engineering research and science*, vol. 1, no. 4, pp. 33–38, 07 2015.

[11] S. Samdarshi and S. C. Mullick, "Analytical equation for the top heat loss factor of a flat plate collector with double glazing," *Journal of solar energy engineering*, vol. 113, pp. 117–122, 05 1991.

[12] S. Kumar and S. C. Mullick, "Glass cover temperature and top heat loss coefficient of a single glazed flat plate collector with nearly vertical configuration," *Ain Shams Engineering Journal*, 2012.

[13] H. Garg and G. Datta, "The top loss calculation for fiat plate solar collectors," *Solar Energy*, vol. 32, no. 1, pp. 141–143, 1984.

[14] S. M. Elsherbiny, G. Raithby, and K. Hollands, "Heat transfer by natural convection across vertical and inclined air layers," *ASME Journal of Heat Transfer*, vol. 104, pp. 96–102, 1982.

[15] P. Veeraboina and G. Ratnam, "Analysis of the opportunities and challenges of solar water heating system (swhs) in india: Estimates from the energy audit surveys & review," *Renewable and Sustainable Energy Reviews*, vol. 16, p. 668 676, 2012.

[16] X. Yang and B. Tysoe, "Disparate standards: Comparing standard domestic hot water modeling methods for multi-resdential buildings," *ASHRAE*, 2016.

[17] E. J. Urban, "Monitoring and modeling hot water consumption in hotels for solar thermal water heating system optimization," Master's thesis, Appalachian State University, 2011.

[18] T. Hove, B. Mubvakure, and A. Schwarzlmuller, "Survey on demand of solar water heaters in the institutional sector," Germany.

[19] United Nations; Climate Change Secretariat, "Solvatten solar safe water heater : Kenya," USA.

[20] A. Korkovelos, "Inergy modelling to support subnational sustainable planning in developing countries; case study of kakamega county in kenya," Master's thesis, KTH Industrial Engineering and Management, 08 2015.

[21] A. B. Momanyi, "Solar water heating in urban housing: A study of factors affecting adoption among households in nairobi," Master's thesis, University of Nairobi, 2015.

[22] G. Energy and Technology, *Modeling, Design, Construction, and Operation of Power Generators with Solid Oxide Fuel Cells*, 1st ed., J. Kupecki, Ed. USA, Springer International, vol. 1.

[23] Kenyan Constitution, "The energy (solar water heating) regulations, 2012."

[24] T. Frantzis, "Solar water heating systems in the tourist industry," Vesta Solar Heaters Ltd, Tech. Rep.

[25] S. Exergia, "Hot water from the sun for hotels;basic facts for the management," European Commission Directorate General for Energy and Transport, Tech. Rep., 2004.

[26] W. N. Wasike, "Assessment of the solar radiation potential of the thika-nairobi area, panel sizing and costing," Master's thesis, Jomo Kenyatta University of Agriculture and Tecchnology, 2015.

[27] Triple E Consulting , "Production of a market study in order to strengthen economic cooperation in the energy sector," Embassy of the Kingdom of the Netherlands (EKN), Nairobi, Energy, Environment & Economics B.V., 2014.

[28] Infiniti Research Limited, "Global solar water heater market 2017-2021," Market Hub Research, Tech. Rep., 2017.

[29] J. Ondraczek, "The sun rises in the east (of africa): The development and status of the solar energy markets in kenya and tanzania," university of Hamburg, Research Unit Sustainability and Global Change.

[30] KNBS and SID, "Pulling apart or pooling together." *Exploring Kenya's inequality*, vol. 1, 2012.

[31] Y.-H. Wu, "Investigation of deforestation in east africa on regional scales," Master's thesis, Stockholm University, 2011.

[32] E. Baerbel, "Kenya: Regulation increases solar water heater uptake," April 2012. [Online]. Available: http://www.solarthermalworld.org/content/kenya-regulation-increases-solar-water-heater-uptake

[33] A. D. Laborderie, C. Puech, and N. Adra, "Environmental impacts of solar thermal systems with life cycle assessment," in *Solar Thermal Applications*. World Renewable Energy Congress 2011-Sweden, 05 2011, pp. 3678–3685.

[34] S. Sukhatme, *Solar Energy; Principles of thermal collection and storage*, 2nd ed. India, Tata McGraw-Hill.

[35] C. Marimuthu and V. Kirubakaran, "Carbon payback period and energy payback period for solar water heater," *International Research Journal of Environment Sciences*, vol. 3, no. 2, pp. 93–98, 2014.

[36] R. McCarter, "A solar hot water sizing and payback calculator: an innovation based on hot water consumption models," Solar Hot Water Sizing and Payback Calculator, Tech. Rep., 2011.

[37] P. G. N. Tiwari, "Energy payback time and life-cycle conversion efficiency of solar energy park in idian conditions," *International Journal of Low-Carbon Technologies*, vol. 4, no. 3, p. 182186, 2009.

[38] M. Nahar and H. Garg, "Free convection and shading due to gap spacing between an absorber plate and the cover glazing in solar energy flat-plate collectors," *Applied Energy*, vol. 7, pp. 129–145, 1980.

[39] M. A. R. Akhanda and F. Chowdhury, "Natural convection heat transfer from a hot rectangular and a square corrugated plate to a cold flat plate," *Journal of Thermal Science*, vol. 9, no. 3, pp. 143–248, 2000.

[40] A. K. Endalew, "Numerical modeling and experimental validation of heat pipe solar collector for water heating," Master's thesis, KTH -School of Industrial Engineering and Management, 2011.

[41] L. QinYi and C. Qun, "Application of entransy theory in the heat transfer optimization of flat-plate solar collectors," *Engineering Thermophysics*, vol. 57, no. 3, pp. 299–306, Jan. 2012.

[42] Z. Ruken, "Optimization of the geometry and material of solar water heaters," Master's thesis, The Ggraduate School of Natural and Applied Sciences of the Middle East Technical University, 2001.

[43] N. Benz and T. Beikircher, "High efficiency evacuated flat-plate solar collector for process steam production," *Solar Energy*, vol. 65, pp. 111–118, 1999.

[44] S. Exergia, "Materials used for manufacturing solar domestic hot water systems & comments on their reliability," European Commission Directorate General for Energy and Transport, Tech. Rep., 2004.

[45] J. A. Duffie and W. A. Beckman, *Solar Engineering of Thermal Processes*. USA, John Wiley and Sons, Inc.

[46] C. Flohlich, "Solar constant and total solar irradiance variation," *Encyclopedia Sustainability manuscript*, 2010.

[47] P. Burgess, "Variation in light intesity at different latitudes and seasons, effects of cloud cover, and amounts of direct and diffused light," in *Continuous Cover Forestry Group Scientific Meeting*, 2009.

[48] F. Oloo, L. Olang, and J. Strobl, "Spatial modelling of solar energy potential in kenya," *International Journal of Sustainable Energy Planning and Management*, vol. 06, pp. 17–30, 2016.

[49] I. Grigorios, "Flat plate solar collectors for water heating with improved heat transfer for application in climatic conditions of the mediterranian region," *Durham Theses, Durham University*, pp. 71–73, 2009.

[50] N. Groenhout, G. Morrison, and M. Behnia, "Design of advanced solar water heaters," *Renewable Energy Transforming Business*, pp. 295–303, 2000.

[51] New Technology Demonstration Program, "Parabolic trough solar water heating," *Federal Technology Alert*, pp. 1–39, 2000.

[52] M. Ludth, "Domestic heating with solar thermal ; studies of technology ina social context and social components in technical studies," in *Digital Comprehensive summaries of Uppsala University dissertations from the fuculity of science and technology 645*, 2009.

[53] A. N. Ogie, O. Ikponmwosa, and J. Jesumirewhe, "Design and construction of a solar water heater based on the thermosyphon principle," *Journal of Fundamentals of Renewable Energy and Applications*, vol. 3, pp. 1–8, 2013.

[54] G. Morrison and H. Tran, "Simulation of the long term performance of thermosyphon solar water heater," *Solar Energy*, vol. 33, pp. 515–526, 1984.

[55] C. Diao and L. Xiaoyang, "Solar heating industry in china and sweden," Master's thesis, University of Gavle, 2015.

[56] Z. Kaneesamkandi, "Performance evaluation of a low cost integrated collector storage solar water heater with independent plane reflectors," *Bangladesh Journal of Scientific and Industrial Research*, vol. 49, no. 3, pp. 147–154, 2014.

[57] SunMaxx Solar Inc., "Evacuated tube solar collectors," *SunMaxx Information Guide*, pp. 2–6, 2013.

[58] N. C. Tarak, "Study on testing procedure for evacuated tube solar water heater systems," Master's thesis, Jadavpur University, 2010.

[59] Federal Energy Management Program, "Solar water heating," *Federal Technology Alert*, vol. 2, pp. 1–44, 1998.

[60] Navitron LTD, "Solar evacuated tube collectors," Navitron Limited, UK, Tech. Rep., 2012.

[61] P. Sae-Jung, T. Krittayanawach, P. Deedom, and B. Limmeechokchai, "An experimental study of thermo-syphon solar water heater in thailand," *Energy Procedia*, vol. 79, p. 442 447, 2015.

[62] V. Quaschinig, "Solar thermal water heating," *Renewable Energy World*, vol. 2, pp. 90–95, 2004.

[63] F. Struckmann, "Analysis of a flat-plate solar collector," *Heat and Mass Transport*, 2008.

[64] BINE Informationsdienst, "Plastic film insulates flat plate collector," Federal Ministry for environment, Nature conservation and Nuclear Safety, Tech. Rep., 2010.

[65] J. O. Dalenback, "Flat plate solar collectors," Chalmers University of Technology, Tech. Rep., 2012.

[66] C. B. Eaton and H. A. Blum, "The use of moderate vacuum environments as a means of increasing the collection efficiencies and operating temperatures of flat-plate solar collectors," *Solar Energ*, vol. 17, pp. 151–15, 1975.

[67] S. Jaisankar, "Experimental studies on aero profile thermosyphon solar water heating system," *International Journal of Engineering Research and Technology*, vol. 9, no. 1, pp. 89–94, 2016.

[68] K. Markus, G. M. Wallner, and R. W. Lang, "Black pigmented polypropylene materials for solar absorbers," *Energy*, 2012.

[69] J. Idris, N. S. Mahat, M. Z. Ahmad, and M. M. Taheri, "Duplex coating of black ceramic coating for copper and stainless steel substrate," *Research Gate*, 2014.

[70] E. Sparrow and S. H. Lin, "Absorption of thermal radiation in a v-groove cavity," *International Journal of Heat Mass Transfer*, vol. 5, pp. 1111–1115, 1962.

[71] T. Beikirchera, P. Osgyana, M. Reuss, and G. Streiba, "Flat plate collector for process heat with full surface aluminium absorber, vacuum super insulation and front foil," in *SHC 2013, International Conference on Solar Heating and Cooling for Buildings and Industry*, 2013.

[72] A. Basharia, A. Yousef, and N. Adam, "Performance and cost analysis of double duct solar air heaters," *International Journal of Scientific and Technology Research*, vol. 1, pp. 109–116, 2012.

[73] W. Gogol and A. J. Jaworski, "Low mass flow rate in flat-plate liquid heating solar collectors," 1993, institute of Heat Engineering.

[74] R. B. Zipin, "The apparent thermal radiation properties of an isothermal v-groove with specularly reflecting walls," *JOURNAL OF RESEARCH of the National Bureau of Standards - C. Engineering and Instrumentation*, 1966.

[75] C.-L. Cheng, "Study of the inter-relationship between water use and energy conservation for a building," *Energy and Buildings*, vol. 34, no. 3, p. 261266, 07 2001.

[76] F. Rohles and S. Konz, "Showering behavior: implications for water and energy conservation," *American Society of Heating, Refrigerating, and Air Conditioning Engineers*, vol. 88, 01 1982.

[77] "Calculating system size," Consolar Thermal Heat Stores, Tech. Rep., 2012.

[78] Thermostatic Mixing Valve Manufacturers Association, "Recommended code of practice for safe water temperatures."

[79] D. M. Atia, F. H. Fahmy, N. M. Ahmed, and H. T. Dorrah, "Optimal sizing of a solar water heating system based on a genetic algorithm for an aquaculture system," *Mathematical and Computer Modelling*, vol. 55, pp. 1436–1449, 2012.

[80] R. Siegel and J. R. Howell, *Thermal Radiation Heat Transfer*, M. Prescott and carolyn V. Ormes, Eds. USA, Hemisphere Publishing Corporation.

[81] J. Psarouthakis, "Apparent Thermal Emissivity From Surfaces With Multiple V-Shaped Grooves," *AIAA Journal*, vol. 1, no. 8, pp. 1879–1882, 1963.

[82] A.Fudholi, A. Zaharim, and R. Zulkifly, "Heat transfer correlation for the v-groove solar collector," in *8th WSEAS International Conference on SIMULATION, MODELLING and OPTIMIZATION*, no. 1790-2769, 09 2008, pp. 177–182.

[83] N. Akhtar and S. C. Mullick, "Correlations for surface temperatures of the glass cover for estimation of heat- transfer coefficients in upward heat-flow in solar collectors with single glazing," *Journal of Solar Energy Engineering*, vol. 121, pp. 201–206, 11 1999.

[84] A. Naiem and S. Mullick, "Effect of absorption of solar radiation in glass-cover(s) on heat transfer coefficients in upward heat flow in single and double glazed flat-plate collectors," *International Journal of Heat and Mass Transfer*, vol. 55, pp. 125–132, 2012.

[85] A. K. Verma, *Process Modelling and Simulation in Chemical, Biochemical and Environmental Engineering*, 1st ed. USA, CRC Press, Taylor & Francis Group.

[86] J. W. Ramsey, J. T. Borzoni, and T. H. Holland, "Development of flat-plate solar collectors for the heating and cooling of buildings," National Aeronautics and Space Administration, Tech. Rep., 1975.

[87] Y. Deng, Y. Zhao, Z. Quan, and T. Zhu, "Experimental study of the thermal performance for the novel flat plate solar water heater with micro heat pipe array absorber," *Energy Procedia*, vol. 70, pp. 41–48, 2015.

[88] K. Zelzouli, A. Guizani, R. Sebai, and C. Kerkeni, "Solar thermal systems performances versus flat plate solar collectors connected in series," *Engineering*, vol. 4, pp. 881–893, 10 2012.

[89] Y. Kolipak and K. K. Guduru, "Thermal analysis of solar flat plate collector," *International Journal of Research and Computational Technology*, vol. 7, no. 5, pp. 01–05, 12 2015.

[90] Z. Ge, H. Wang, and X. Guan, "Exergy analysis of flat plate solar collectors," *Entropy*, vol. 16, pp. 2549–2567, 05 2014.

[91] A. Bejan, D. Kearney, and F. Kreith, "Second law analysis and synthesis of of solar collector systems," *Journal of Solar Energy Engineering*, vol. 103, pp. 23–28, 02 1981.

[92] D. Ammour, H. Iacovides, and T. Craft, "Model validation for buoyance driven flows inside differentially heated cavities."

[93] M. Irwanto, "Solar iirradiance and optimum tilt angle of photovoltaic module in tanjung morawa, north sumatera, indonesia," *International Journal of Research in Advanced Engineering and Technology*, vol. 1, no. 1, pp. 34–38, 2015.

[94] R. Morse and J. Czarnecki, "Flat plate solar absorbers; the effect on incident radiation of inclination and orientation," Commonwealth scientific and industrial research organization, Engineering section, Tech. Rep., 1958.

[95] J. kern and I. Harris, "On optimum tilt of a solar collector," *Solar energy*, vol. 17, 1975.

[96] C. Christensen and G. Barker, "Effects of tilt and azimuth on annula incident solar radiation for united states locations," in *roceedings of solar forum 2001: Solar Energy, The power to choose*, 2001.

[97] A. Hafez, A. Soliman, K. El-Metwally, and I. Ismael, "A review of tilt and azimuth angles in solar energy applications," *Renewable and sustainable energy reviews*, vol. 77, pp. 147–168, 2017.

[98] K. Ulgen, "Optimum tilt angles for solar collectors," *Energy sources,part A; Recovery, utilization and Environmental effects*, pp. 1171–1180, 2006.

[99] C. Stanciu and D. Stanciu, "Optimal tilt angle for flat plate collectors all over the world-a declination dependent formulae and comparisons of three solar radiation models," *Energy conversion and management*, vol. 81, pp. 133–143, 05 2014.

[100] J. Manikandan and B. Sivaraman, "Comparative studies on thermal efficiency of single and double glazed flat plate solar water heater," *ARPN Journal of engineering and applied sciences*, vol. 11, no. 9, pp. 5521–5526, 2016.

[101] N. Ihaddadene, R. Ihaddadene, and A. Mahdi, "Effect of glazing number on the performance of a solar thermal collector," *International Journal of Science and Research*, vol. 3, no. 6, pp. 1199–1203, 06 2014.

[102] R. Jain, "Parametric studies of top heat loss coefficient of double glazed solar collectors," *MIT International journal of Engineering*, vol. 1, pp. 71–78, 2011.

[103] T. Beikircher, N. Benz, and W. Spirkl, "Gas heat conduction in evacuated flat-plate solar collectors: analysis and reduction," *journal of solar energy engineering*, vol. 117, p. 229235, 1995.

[104] F. Arya, T. Hyde, P. Henshall, and S. Shire, "Current developments in flat plate vacuum solar thermal collectors," *International Journal of Chemical, Nuclear, Material and Metallurgical Engineering*, vol. 10, no. 6, pp. 715–719, 2016.

[105] ——, "Experimental measurements of evacuated enclosure thermal insulation effective for vacuum flat plate solar thermal collectors," *International Journal of Chemical, Nuclear, Material and Metallurgical Engineering*, vol. 10, no. 6, pp. 727–733, 2016.

[106] A. Bejan, *Convection Heat Transfer*, 4th ed. USA, John Wiley & Sons, Inc.

[107] P. Nag, *Heat and Mass Transfer*, 3rd ed., S. Mukherjee, Ed. USA, Tata McGraw-Hill.

[108] R. Rajput, *A textbook of Heat and Mass Transfer*, 5th ed. India, S. Chand Publishers.

[109] F. Giovannetti, S. Foste, N. Ehrmann, and G. Rockendorf, "High transmittance, low emissivity glass covers for flat plate collectors: Applications and performance," *Energy Procedia*, vol. 30, pp. 10–115, 2012.

[110] R. Bakari, J. Rwaichi, A. inja, and N. Njau, "Effect of glass thickness on performance of flat plate solar collectors for fruits drying," *Journal of Energy*, pp. 1–8, 2014.

[111] V. Nicolau and F. Maluf, "Determination of radiative properties of commercial glass," in *PLEA* $2001_T he 18th Conference of passive and low energy Architecture, Florianopolis_B razil, 092$

[112] N. AltuntoP, "The effect of obstacle geometry and position on thermal stratification in solar energy hot water storage tanks," Erciyes University of Turkey, Tech. Rep., 2008.

[113] R. Yang and N. S. Shue, "Simulation study for the effect of the storage design on the performance of a large solar hot water system," *IEEE Green Technologies*, pp. 468–472, 2013.

[114] N. J. Khalifa, T. A. Mustafa, and K. A. Khammas, "Experimental study of temperature stratification in a thermal storage tank in the static mode for different aspect ratios," *ARPN Journal of Engineering and Applied Sciences*, vol. 6, pp. 53–60, 2011.

[115] C. Bersch, M. Harvey, and B. Achhammer, "Heat and ultraviolet aging of polyvinyl chloride," *Journal of Research of the National Bureau of Standards*, vol. 60, no. 5, May 1958.

[116] D. Bouman, "Hydraulic design for gravity based water schemes. understanding gravity-flow pipelines, water flow, air locks," *AquaShareware*, 2014.

[117] N. Waziri, A. Usman, J. Enaburekhan, and A. Babakano, "Determination of optimum tilt angle and orientation of a flat plate solar water heater for different periods in kano," *Scientific research journal*, vol. 2, no. 2, pp. 34–40, 02 2014.

[118] R. P. Bevington and D. R. Keith, *Data Reduction and Error Analysis for the Physical Sciences*, 3rd ed., D. Bruflodt, Ed. USA, Kent A Peterson, McGraw Hill Higher Education.

[119] R. J. Taylor, *An Introduction to Error Analysis; The study of Uuncertainties in physical measurements*, 2nd ed., A. McGuire, Ed. USA, University Science Books.

[120] H. Dagdougui, A. Ouammi, and R. Michela, "Thermal analysis and performance optimization of a solar water heater, flat plate collector; application to ttouan morocco." *Renewable and Sustainable Energy Reviews*, vol. 15, pp. 630–638, 2011.

[121] N. Ihaddadene, R. Ihaddadene, and A. Mahdi, "Effect of glazing number on the performance of a solar thermal collector," *International Journal of Science and Research (IJSR)*, vol. 3, no. 358, pp. 1199–1203, 2012.

[122] H.Vettrivel and P.Mathiazhagan, "Comparison study of solar flat plate collector with single and double glazing systems," *INTERNATIONAL JOURNAL of RENEWABLE ENERGY RESEARCH*, vol. 7, no. 1, pp. 266–274, 2017.

[123] N. Benz, T. Beikircher, and W. Spirkl, "Gas heat conduction in evacuated flat plate solar collectors: Analysis and conduction," *Journal of Solar Energy Engineering*, vol. 117, pp. 228–235, 1995.

[124] R. Hosseini and M. Saidi, "Experimental study of air pressure effects on natural convection from a horizontal cylinder," *Heat Transfer Engineering*, vol. 33, pp. 878–884, 2012.

[125] A. Hafeza, A. Solimana, K. El-Metwally, and I. Ismaila, "Tilt and azimuth angles in solar energy applications a review," *Renewable and Sustainable Energy Reviews*, vol. 77, p. 147168, 2017.

[126] K. Ulgen, "Optimum tilt angle for solar collectors," *Energy Sources, Part A: Recovery, Utilization, and Environmental Effects*, pp. 1171–1180, 2006.

[127] V. M. Gacuca, "Design and fabrication of a solar hand washing cistern using an integrated solar collector," Master's thesis, Jomo Kenyatta University of Agriculture and Technology, 2014.

[128] D. Sarma, P. B. Barua, and D. Hatibaruah, "Optimization of glazing cover parameters of a solar flat plate collector (fpc)," *International Journal of Engineering Trends and Technology*, vol. 14, no. 2, pp. 74–80, 2014.

[129] M. Hayek, J. Assaf, and W. Lteif, "Experimental Investigation of the Performance of Evacuated- Tube Solar Collectors under Eastern Mediterranean Climatic Conditions," *Energy Procedia*, vol. 6, pp. 618–626, 2011.

[130] S. Gurveer, "Experimental investigation of the fluid temperature field and the thermal performance of insert devices in a flat-plate solar collector," Master's thesis, The School of Graduate and Postdoctoral Studies The University of Western Ontario London, Ontario, Canada, 2013.

[131] Alselectro, "K type thermocouple temperature sensor," Tech. Rep. [Online]. Available: http://www.alselectro.com/-k-type-thermocouple-temperature-sensor-with--max6675-module-for-arduino.html

[132] ThermcoProducts, "Scantemp 485 infrared thermometer," Tech. Rep. [Online]. Available: http://www.thermcoproducts.com/ACCD485IR-ScanTemp-485-Infrared-Thermometer.html

[133] *TMPV 206 Solar Irradiance Meter.*

APPENDICES

DERIVATION OF DESIGN EQUATIONS

Derivation of shape factor

Configuring absorber plate into v-groove profile allows one surface of the v-groove to radiate a given percentage of long wave radiation onto the opposite surface. This relationship is complex one and can simply be expressed by the shape factor equation

$$dF_{l-dx} = dX\left[\frac{1}{2} + \frac{cos(2\theta) - X}{2(X^2 + 1 - 2Xcos(2\theta))^{1/2}}\right] \tag{1}$$

where dF_{l-dx} represents the configuration factor one infinitely long finite surface to a differential element on the other surface at distance x from the vertex. X is the ratio of distance of the differential element from the vertex to the width of the surface,(x/l). Radiation leaving elemental area dA_1 of surface 1 that reaches dA_2 of surface 2 is given by [80]

$$d^2Q_{d1-d2} = \frac{\pi i_1 \cos(2\theta)_1 \cos(2\theta)_2}{\pi S^2} \tag{2}$$

Where S is the distance between the two surfaces and (2θ) is the angle line S makes with normal to the surface

But since both surfaces are finite and have the same width, and also have uniform emissivity at equal isothermal temperatures T_{ap}, dF_{l-dx} is redefined as a fraction of energy leaving surface A_1 and absorbed by surface A_2, i.e. dF_{1-2} and vice versa. Upon integration over both A_1 and A_2 we get,

$$F_{1-2} = \frac{\int_{A1}\int_{A2} \pi i_1 \frac{\cos(2\theta)_1 \cos(2\theta)_2}{\pi S^2} dA_1 dA_2}{\pi i_1 A_1} \tag{3}$$

where $\pi i_1 A_1$ is the total energy emitted from surface 1 at uniform intensity i_1. After simplification

$$F_{1-2} = \frac{1}{A_1}\int_{A1}\int_{A2} \frac{\cos(2\theta)_1 \cos(2\theta)_2}{\pi S^2} dA_1 dA_2 \tag{4}$$

This can be written in terms of configuration factors involving differential areas as

$$F_{1-2} = \frac{1}{A_1}\int_{A1}\int_{A2} dF_{d1-d2} dA_1 = \frac{1}{A_1}\int_{A1} F_{d1-2} dA_1 \tag{5}$$

Similary shape factor for surface 2 to surface 1 is given as

$$F_{2-1} = \frac{1}{A_2}\int_{A2}\int_{A1}\frac{\cos(2\theta)_1\cos(2\theta)_2}{\pi S^2}dA_2dA_1 \tag{6}$$

equating the two equations 4 and 6 yields the reciprocity relation 5

$$F_{1-2}A - 1 = F_{2-1}A_2 \tag{7}$$

Applying equation 7 into equation 5 results

$$F_{1-2} = \frac{A_2}{A_1}F_{2-1} = \frac{1}{A_1}\int_{A2}dF_{1-d2}A_1 = \int_{A2}dF_{1-d2} \tag{8}$$

Substituting equation 1 into equation 5 results we get

$$F_{l-l2} = \int_{x=0}^{l2}dF_{l-dx} = \int_0^{l2}\left[\frac{1}{2} + \frac{cos(2\theta) - X}{2(X^2+1-2Xcos(2\theta))^{1/2}}\right]dX \tag{9}$$

where l_2 is the width of the side having element dx. Since l=l_2, the dimensionless variable $X = \frac{x}{l} = 1$, thus

$$F_{l-l2} = \int_0^{1}\left[\frac{1}{2} + \frac{cos(2\theta) - X}{2(X^2+1-2Xcos(2\theta))^{1/2}}\right]dX \tag{10}$$

$$F_{l-l2} = F_{1-2} = 1 - \left(\frac{1-\cos(2\theta)}{2}\right)^{1/2} = 1 - \sin\theta \tag{11}$$

Derivation of Grashof's number, component D

$Gr = \left(\frac{g\rho^2\beta_t L^3(T_{ap}-T_g)}{\mu^2}\right)$

Assuming air obeys ideal gas low where $\rho = \frac{P}{R(T_{ap}+T_g)/2}$ and $\beta_t = \frac{2}{T_{ap}+T_g)}$, then

$Gr = \left(\frac{gP^2L^3(T_{ap}-T_g)}{\mu^2R^2((T_{ap}+T_g)/2)^3}\right)$

but by fitting an equation to the tabulated values of dynamic viscosity μ [66]

$\mu = 1.265\times10^{-3} + 6.734\times10^{-5}((T_{ap}+T_g)/2) + 3.348\times10^{-8}((T_{ap}+T_g)/2)^2$

Taking g=9.81m/s and R=287J/(KgK), and replacing in the grashof's number equation we get

$$Gr = \frac{(P/133.322)^2\times(100L)^3(T_{ap}-T_g)}{D} \tag{12}$$

where $\mathrm{D} = 9.4595 \times 10^{-8}(T_{ap}+T_g)^3 + 5.0356 \times 10^{-9}(T_{ap}+T_g)^4 + 6.8267 \times 10^{-11}(T_{ap}+T_g)^5 + 3.3381 \times 10^{-14}(T_{ap}+T_g)^6 + 4.1413 \times 10^{-18}(T_{ap}+T_g)^7$.

DESIGN CALCULATIONS

Design of absorber plate area and dictating heat losses

Calculation of theoretical values of parameters

Energy required to raise 100 litres of water from 20^0C to 41^0C in 5 hours is calculated using equation **??**

$$q_{required} = m \times C_w \times \frac{\Delta T}{\Delta t} \tag{13}$$

but water at 41^0C require a huge 100 liter storage tank compared to water at 80^0C. Hence setting FPSWH operating temperatures at 80^0C, we obtain mass flow rate as

$$q_{required} = \frac{100}{5} \times C_w \times (41^0C - 20^0C) = \dot{m} \times C_w \times (80^0C - 20^0C) \tag{14}$$

$$\dot{m} = \frac{20 \times 21}{60} = 7kilograms/hour = 1.944 \times 10^{-3}kg/s \tag{15}$$

but

$$mass = \rho V \tag{16}$$

hence, water volumetric flow rate is expressed as

$$V = uA = \frac{\dot{m}}{\rho} = \frac{7kg/hour}{1000kg/m^3} = 0.007m^3 = 7litres/hour \tag{17}$$

$$V = 7litres/hour = \frac{7000m^3 \times 10^{-6}}{3600seconds} = 1.9444 \times 10^{-6}m^3/s \tag{18}$$

Since thermosyphonic forces and gravity are responsible for forcing water through the FPSWH, the highest flow rate is achieved at peak operating temperature. It then becomes possible to calculate flow velocity into and out of FPSWH. Velocity of water through pipes leading into and out of FPSWH for pipe diameter of 1/2", is given from equation 18 [53]

$$u = \frac{\mu.Re}{\rho.D} \tag{19}$$

where, μ is dynamic viscosity of water at peak temperature, 80^0C, and Re is the Reynolds number for lamina flow. In FPSWHs $200 < Re < 2000$ since flow rates are

Table 1: Materials used for FPSWH fabrication

COMPONENT	MATERIAL	ATTACHING ACCESSORIES
Glazing	High iron content window glass	Silicone glue
Absorber plate	Galvanized iron sheet	MIG welding
Black painting	Black matte spray paint	-
Insulation	Fibre glass	Silicon glue
Casing	25mm thick wooden block boards	2" nails and water resistant wooden glue
Flow regulating valves	Casted brass	thread tapes
Water conveying pipes	1/2" bore PVC pipes	Clamping clips
Storage tank	Stainless steel	Arc welded
Stand	40mm x 40mm x 2mm angle bars	Arc welded
Thermocouples	Standard K-Type	Threads and glue

low in order to allow fluid to gain heat. Hence Re has an average value of 1000 [130] thus

$$u = \frac{0.9 \times 10^{-3} N/m^2.s \times 1000}{1000 kg/m^3 \times 1.27 \times 10^{-2} m} = 0.070866 m/s \tag{20}$$

assuming an efficiency of 50% absorber plate area is estimated as [53]

$$A_{ap} = \frac{\frac{7(kg)}{3600(seconds)} \times 4184(Joules/kg^0C) \times (T_{out} - T_{in})^0 C}{0.5 I\tau(watts/m^2)} \tag{21}$$

$$A_{ap} = \frac{\frac{7(kg)}{3600(seconds)} \times 4184(Joules/kg^0C) \times (80 - 25)^0 C}{0.5 \times 1000 \times 0.85(watts/m^2)} = 1.0 m^2 \tag{22}$$

Calculation of Heat losses

Parameter	Denotation	Value
Insolation	I	1000Watts/m^2
Absorber plate temperature	T_{ap}	100^0 C
Atmospheric temperature	T_a	25^0 C
Water outlet temperature	T_{out}	85^0 C
Water inlet temperature	T_{in}	25^0 C
Absorber plate absorptivity	α_{ap}	0.95
Absorber plate emissivity	ϵ_{ap}	0.95
Glazing glass absorptivity	α_g	0.11
Glazing glass emissivity	ϵ_g	0.91
Glazing glass transmittance	τ_g	0.90
Wind speed	w	2.5m/s
Air gap	L	60 mm
Flow rate	$\dot{m}$	1.944×10^{-3} kg/s

Table 2: Design parameters for calculation of A_{ap}

Using above outlined parameters

$$h_w = 5.7 + 3.8v$$

$$h_w = 5.7 + 3.8 \times 2.5 = 15.2 watts/m^2$$

Considering a single glazed FPSWH

$$T_g = \frac{fT_{ap} + T_a + \frac{\alpha_g I}{h_w+6}}{1+f}$$

Where

$$f = \frac{(12\times10^{-8}(0.2T_{ap}+T_a)^3 + h_w)^{-1}}{6\times10^{-8}((\epsilon_{ap})_a + 0.028)(T_{ap}+0.5T_a)^3 + 0.6L_{ap-g}^{-0.2}(((T_{ap}-T_a)\cos\beta)^{0.25})^{-1}}$$

$$f = \frac{(12\times10^{-8}(0.2\times373+298)^3 + 15.2)^{-1}}{6\times10^{-8}(1.00+0.028)(373+0.5\times298)^3 + 0.6\times0.06^{-0.2}(((373-298)\cos8^0)^{0.25})^{-1}}$$

$$f = \frac{0.0467128}{8.3208439 + 0.35877113} = 0.005382$$

Hence

$$T_g = \frac{0.005382 * 373 + 298 + \frac{0.11\times1000}{15.2+6}}{1+0.005382} = 303.56K$$

$$T_{Maen} = \frac{T_{ap}+T_a}{2} == \frac{373+298}{2} = 335.5k$$

Properties of air at 1 atmosphere and at T_{Maen}

$$Density = \rho = 1.0125Kg/m^3$$

$$Thermal - Conductivity = k = 0.0282625w/(mk)$$

$$Kinematic - viscosity = \nu = 1.921\times10^{-5}m^2/s$$

$$Prandtl - Number = Pr = 0.719575$$

Therefore

$$Ra_L\cos\beta = \frac{g\beta_t(\Delta T)L^3}{\nu^2}\times Pr\times\cos\beta$$

$$Ra_L\cos\beta = \frac{9.81\times\frac{1}{335.5}(373-298)\times0.06^3}{(1.921\times10^{-5})^2}\times0.719575\times\cos8^0 = 9.1467\times10^5$$

Thus using Hollands et al correlation,

$$Nu_L = \ 1+1.44\left[1-\frac{1708}{Racos\beta}\right]\times\left[1-\frac{1708(sin1.8\beta)^{1.6}}{Racos\beta}\right]+\left[\left(\frac{Racos\beta}{5830}\right)^{1/3}-1\right]; \quad 5830 < Ra_Lcos\beta < 1\times10^6 \tag{23}$$

$$Nu_L = 1 + 1.44\left[1 - \frac{1708}{9.1467\times10^5}\right] \times \left[1 - \frac{1708(sin1.8\times8^0)^{1.6}}{9.1467\times10^5}\right] + \left[\left(\frac{9.1467\times10^5}{5830}\right)^{1/3} - 1\right]$$

$$Nu_L = 6.83$$

Considering Buchberg et al,

$$Nu_L = 0.157(Ra_L cos\beta)^{0.285}; 9.23\times10^4 < Ra_L cos\beta < 10^6$$

$$Nu_L = 0.157(9.1467\times10^5)^{0.285} = 7.849826$$

Therefore convective coefficient from the absorber plate to the cover glass is calculated as

$$h_{ap-g} = \frac{Nu_L \times k}{L} \tag{24}$$

According to Hollands et al

$$h_{ap-g} = \frac{6.83\times0.0383625}{0.06} = 4.367W/(m^2K) \tag{25}$$

According to Buchberg et al

$$h_{ap-g} = \frac{7.849826\times0.0383625}{0.06} = 5.01898W/(m^2K) \tag{26}$$

Radiative heat transfer coefficient between the absorber plate and the cover glass is calculated as

$$q_{rad} = \frac{\sigma A_{ap}[(T_{ap})^4 - (T_{glass})^4]}{\left(\frac{1}{(\epsilon_{ap})_a} + \frac{1}{\epsilon_{glass}} - 1\right)} = \epsilon_{glass}\sigma A_{ap}[(T_{glass})^4 - (T_{sky})^4]$$

hence

$$h_{ap-g,rad} = \frac{\sigma[(T_{ap}^2 + T_{glass}^2)(T_{ap} + T_{glass})](F_{13}^2)}{\left(\frac{1}{\epsilon_{ap}} + \frac{1}{\epsilon_{glass}} - 1\right)}$$

$$h_{ap-g,rad} = \frac{5.67 \times 10^{-8} \times [(373^2 + 303.56^2)(373 + 303.56)]}{\left(\frac{1}{1} + \frac{1}{0.91} - 1\right)} = 2.527 W/(m^2 K)$$

Bottom heat loss coefficient is summarized as

$$\frac{1}{U_b} = \frac{q_{back}}{A_{ap}(T_{ap} - T_a)} = \frac{\delta_{fg}}{k_{fg}} + \frac{\delta_{air}}{k_{air}} + \frac{\delta_{wood}}{k_{wood}} \tag{27}$$

Therefore,

$$\frac{1}{U_b} = \frac{0.05}{0.057} + \frac{0.05}{0.03186} + \frac{0.05}{0.15} = 2.7799 \tag{28}$$

$$U_b = \frac{1}{2.7799} = 0.3597 w/(m^2 k)$$

Total heat loss coefficient,U_l, is a sum of all convective, radiative and conductive heat losses

$$U_l = h_{ap-g} + h_{ap-g,rad} + U_b$$

$$U_l = 4.367 + 2.527 + 0.3597 = 7.254 w/(m^2 k)$$

Collectors effective area

$$A_{ap} = \frac{\dot{m} \times C_w \times (T_{out} - T_{in})}{I\alpha\tau - U_l(T_{map} - T_a)} \tag{29}$$

$$A_{ap} = \frac{1.944 \times 10^{-3} \times 4184 \times (358 - 303)}{1000 \times 0.95 \times 0.9 - 7.254(335.5 - 298)} = 0.0.7674 \cong 1.0 m^2 \tag{30}$$

Instantaneous efficiency of FPSWH is calculated as a fraction of total received solar energy which is converted to useful thermal energy

$$\eta = \frac{\dot{m} \times C_w \times (T_{out} - T_{in})}{I\tau A_{ap}} \tag{31}$$

$$\eta = \frac{1.944 \times 10^{-3} \times 4184 \times (358 - 303)}{1000 \times 0.9 \times 1.0} = 0.497 \tag{32}$$

TEMPERATURE, INSOLATION AND FLOWRATE MEASUREMENTS

Instrumentation and Parameters Measurements

Temperature Measurements

Thermocouples were very crucial in this experiment since it involved temperature measurements in order to ascertain energy gain and heat losses. For this experiment, k-type thermocouples were used with both plain welded tips for fixing on to surfaces and threaded tips for ease of fitting into inlet and outlet pipes as well as in the stratification tank. To measure heat gained by circulating water in FPSWH, short threaded probe thermocouples, Figure 3, were placed in the inlet pipe of the FPSWH and in the the outlet pipe of FPSWH. Three plain welded tip thermocouples , Figure 2, were glued on to the absorber plate and three more were glued onto the glass pane for measuring their temperatures relative to water temperatures. To measure net heat gain in the storage tank, long threaded probe thermocouples , Figure 4, were placed in the inlet pipe of stratification tank and in the outlet pipe of the stratification tank. An infrared thermometer , Figure 5, was used to measure outlet temperatures of FPSWH casing as well as outer casing of stratification tank. All the thermocouples were coupled on to a digital data logger , Figure 1. Room temperature was measured using a mercury thermometer placed in a shaded place, with free air flow, next to the FPSWH.

The data logger , Figure 1, is a TDS-530 model multi-channel scanning data logger with a response time of 0.4 seconds, its accuracy is dependent on that of coupled thermocouples. Thermocouples used in this experiment, Figures 2, 3 and 4 had an accuracy of $\pm 1.5^0$C and a response time of 0.7 seconds as described by the manufacturer [131]. The infrared thermometer used, Figure 5, is a ScanTemp 485 Infrared Thermometer with a system accuracy of $\pm 0.1^0$C and response time of 0.2 seconds [132].

Figure 1: Data Logger

Figure 2: Plain welded tip K-Type thermocouple

Insolation Measurements

Solar radiation intensity was measured using a digital Insolation Meter, Figure 7, that converted solar radiation into watts/m^2 readings. The digital insolation meter is a TMPV 206 Solar Irradiance Meter with an accuracy of 0.1% at 25^{0}C with an additional temperature included error $\pm 0.38 W/m^2/^0$C from 25^{0}C, response time of 0.25 seconds and angular accuracy cosine corrected to 5% for angles up to 60^0 [133].

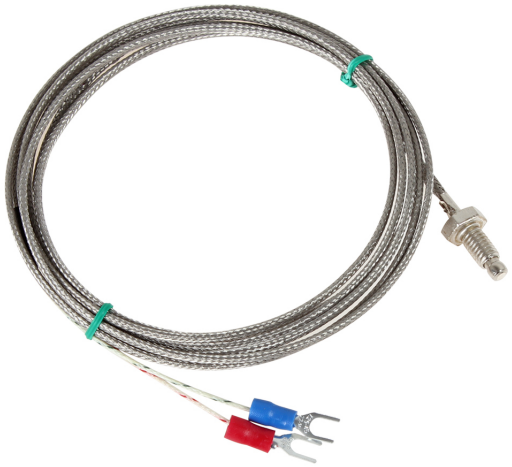

Figure 3: K-Type thermocouple with 6mm threaded probe

Figure 4: K-Type thermocouple with 100mm screwed probe

During data collection the irradiance meter was oriented in the same direction and tilt angle as the FPSWH.

Water flowrate Measurements

Water flow rate was measured using a digital Hall Effect flowmeter, Figure 7, calibrated to operate with maximum accuracy of 0.1% at flow rate of 100-300 millilitres/minute.

Figure 5: Infra red thermometer used to measure casing temperatures

Figure 6: Digital Irradiance Meter used for this experiment

Figure 7: 0.1-3.0L/Min Hall Effect water flow rate sensor with LCD read out